In-Medium Similarity Renormalization Group for Nuclear Many-Body Systems

Koshiroh Tsukiyama

Department of Physics
The University of Tokyo

January 31st, 2011

Abstract

We present a new ab-initio method that uses similarity renormalization group (SRG) techniques to continuously transform nuclear many-body Hamiltonians toward a desired form. In contrast to applications of the SRG to two- and three-nucleon interactions in free space, we perform the SRG evolution "in-medium" directly in the A-body system of interest. The in-medium approach has the advantage that one can approximately evolve $3, ..., A$-body operators using only two-body machinery based on normal-ordering techniques. The method is non-perturbative and can be tailored to a variety of problems ranging from the diagonalization of closed-shell nuclei to the construction of effective valence shell-model Hamiltonians and operators. The perturbative analysis of the IM-SRG provides the machinery to make a systematic improvement of accuracy, making the theory controllable. The analysis also shows that the solution of the IM-SRG contains the low order perturbation diagrams exactly, without encountering the divergence of the perturbation series due to the zero denominator, which pertains conventional Q-box expansion with non-degenerate model spaces. We apply the IM-SRG to nuclei and present first results for the ground-state energies of ^{4}He, ^{16}O and ^{40}Ca, which have accuracies comparable to coupled-cluster calculations. An important advantage of the (IM-)SRG is that an arbitral operator can be evolved simultaneously with a Hamiltonian. We show this feature by applying the IM-SRG to the calculation of radius. We also discuss the contamination of the spurious center of mass excitation into many-body wave functions, which general many-body methods cannot avoid. We demonstrate that the many-body wave function of the IM-SRG decouples to a large extent into its intrinsic and center of mass parts, and the obtained ground-state energy corresponds to the intrinsic energy, where non-interesting center-of-mass excitation is sufficiently eliminated. Furthermore, the flexibility of the IM-SRG will be manifested by the first application of the IM-SRG to the derivation of effective valence-shell interactions in nuclear shell model, taking ^{6}Li in p-shell as an example. The obtained spectra show the clear similarity between the IM-SRG and a non-perturbative Q-box expansion. Finally, we investigate the structure of low-lying states in drip-line oxygen isotope, to which the fully *ab-initio* description has not been reachable. The *ab-initio* description of drip-line nuclei is attended with the interplay between many-body correlations and coupling to the continuum states. We focus on the continuum effects and employ the Gamow shell model, where the coupling to the continuum is treated in a well-defined procedure and the realistic nucleon-nucleon (NN) interactions are taken. We have reached the conclusion that the continuum coupling is important for excited states but not

crucial to determine the drip line in the case of oxygen. This conclusion is consistent with the recent microscopic approach including the effects of three-nucleon forces.

Contents

Chapter 1

Introduction

1.1 Nuclear structure physics in a new stage

The nuclear physics is facing a new era. Regarding the understanding of nuclear force, the progress of the Lattice Quantum ChromoDynamics (QCD) [1, 2, 3, 4] and the chiral effective field theory (χEFT) [5,6,7,8] provide new and unified interpretations of nucleonic interactions.

In theoretical nuclear structure physics, various *ab-initio* methods have been developed, while the objects that are reachable by the large scale calculations are extending together with the growth of the computer power. To date, fully *ab-initio* description of nuclei with accurate nucleon-nucleon (NN) and/or three-nucleon (3N) forces is available up to $A = 12$. Extending the applicable region of *ab-initio* methods is an important undertaking. The Coupled-Cluster (CC) theory [9, 10, 11, 12, 13, 14, 15, 16, 17, 18, 19, 20] is one of the strong canditates along this line, but the application of the CC methods is limited to the nuclei around the closed-shell. For medium-mass or semi-closed nuclei, the many-body methods represented by the shell model, configuration interaction (CI) methods in more general word, have been developed in order to have the predictive power with controllable accuracy. Once a model space and an effective Hamiltonian in the space are defined, the shell model provides very accurate description of various observables, including low-lying energy levels, the transitions among them, the spectroscopic amplitudes and deformation of nuclei. The shell model plays a crucial role as a tool for precise investigation of fundamental physics such as isospin-symmetry breaking for nuclear observables, astrophysical reactions, or the features of neutrino [21]. At this point, a clearly important question is how to construct the effective Hamiltonians to be used for the shell-model calculations. Although there is a typical method based on the many-body perturbation theory (MBPT) [22, 23, 24], the nuclear physics has been lacking a

fully-microscopic and non-perturbative theory to derive the effective Hamiltonians for a given model space. To give a clear direction to this problem is one of the main aims of this thesis.

In the experimental side, the outstanding facilities with very high technologies over the world, including RIKEN, FAIR and FRIB, are widening the research field for unstable nuclei. In unstable nuclei, especially in exotic nuclei, where the number of protons and neutrons are highly unbalanced, there are many interesting phenomena, including the varying magic numbers, neutron halo and the island of inversion, which are known to be far from the mean-field picture. Further, the study for neutron-rich nuclei are inevitable for the reliable simulation of the supernovae in nuclear astrophysics and for the nucleosynthesis.

As mentioned above, it is true that both the purely theoretical aspect and the potential applicability for other fields are realized to be very important. Considering the expansion of the understanding of the nuclear forces, developments of *ab-initio* methods and the strong potential of the wide applicability of nuclear structure theory, it is an indispensable and challenging undertaking to understand nuclei based on the the fundamental degrees of freedom, nucleons, and their interactions, nuclear forces.

1.2 Nuclear structure from nucleonic interactions

In general, the description of physics phenomena depends on the energy scale which characterizes the system of interest. While the fundamental theory to describe the strong interactions is the QCD, in the low energy which is typical to nuclei, the details of high-energy physics, or corresponding shot-range details cannot be resolved. Effective degrees of freedom to describe the nuclear forces are not quarks and gluons, but the hadrons which are color singlet.

Regarding the nuclear forces, there exist several theories based on nucleons and mesons, including the χEFT and meson-exchange models. They are one of realistic nuclear forces in the sense that they are constructed so as to reproduce the low-energy nucleon-nucleon (NN) scattering data and deuteron properties. The realistic nuclear forces have in common a strong coupling between high- and low-momentum modes, which is responsible for the hard core if one assumes the local potentials. Due to this strong coupling, the nuclear systems are highly non-perturbative, thus one cannot directly apply perturbative methods, and *ab-initio* methods need huge computational costs. Therefore, the descriptions of the nuclear structure has been highly restricted with specific models for each mass region of interest. There have been systematic descriptions with unified methods, but in many cases, the nucleonic correlations have not been fully taken into account. The nuclear structure strongly needs microscopic

many-body methods which are non-perturbative and computationally feasible.

Tremendous progress has been made in *ab-initio* nuclear structure over the past decade, where it is now possible to calculate properties of light nuclei up to about carbon in Green's Function Monte Carlo (GFMC) [25, 26, 27, 28] and No-Core Shell Model (NCSM) calculations [29, 30, 31]. Low-lying states of medium-mass nuclei near closed shells are calculated by coupled cluster (CC) theory [32, 33] and unitary model operator approach (UMOA) [34].

A difficulty in extending this *ab-initio* frontier to heavier nuclei is the strong coupling between low and high momenta in two- and three-nucleon interactions used in these calculations. Historically, a number of methods have been tried to solve the problem caused by the strong coupling between high- and low-momentum states. Among them are G-matrix [24], Lee-Suzuki [35] transformation and unitary correlation operator method (UCOM) [36, 37].

In recent years, new approaches to nuclear forces based on renormalization group (RG) ideas have been developed that decouple high-momentum degrees of freedom by lowering the resolution (or a cutoff) scale in nuclear forces to typical nuclear structure momentum scales [38]. Such RG-evolved potentials, known generically as "low-momentum interactions," greatly simplify the nuclear many-body problem and enhance the convergence of structure and reaction calculations, while the freedom to vary the resolution scale provides a powerful tool to assess theoretical uncertainties due to truncations in the Hamiltonian and from many-body approximations [38, 39, 40, 41]. In general, many-body interactions are generated during the RG evolution. The truncation of the induced many-body interactions in many-body problems leads us to the cutoff dependence of the observables. In this thesis, we introduce a new *ab-initio* method, in-medium similarity renormalization group, which provides the ground-state energies of closed-shell nuclei and valence-shell effective Hamiltonians simultaneously, taking into account the induced many-body interactions in an efficient approximation.

1.3 The limit of the existence of matters

Although the *ab-initio* methods have been extending the region of their applications, the weakly bound systems have not yet been described by nucleonic degrees of freedom except a few applications for light nuclei [42, 43] or nuclei around the doubly magic [44]. The study of nuclei far from stability is a leading direction in nuclear physics, experimentally and theoretically. It represents a considerable intellectual challenge to our understanding of the stability of matter itself, with potential implications for the synthesis of elements. An important aspect of this research direction is to understand how magic numbers and shells appear and evolve

with increasing numbers of neutrons or protons. Except for a qualitative understanding of the neutron and proton dependence of the magic numbers in terms of mean-field models, we lack a quantitative theoretical understanding in terms of the basic constituents of the underlying nuclear many-body Hamiltonian. After more than five decades of nuclear physics research, we are not yet in a position where we can quantitatively explain how shells evolve from a fundamental point of view.

For nuclei, the interpretation of the standard magic numbers 2, 8, 20, 28, 50, 82, and 126 is linked to the interplay between the filling up of single-particle (s.p.) orbitals (s.p. picture) and the underlying interactions. The magic numbers lead to so-called shell gaps in the s.p. spectra near the Fermi energy. For various magic numbers, in particular for stable doubly magic nuclei, one can have a large number of stable isotopes (increasing number of neutrons N but fixed number of protons Z) or isotones (increasing number of protons Z and fixed N). Eventually, as one adds more neutrons or protons, namely, moving away from the valley of nuclear stability towards the drip lines, the outermost nucleons literally start to drip off the nuclei, thereby defining the very limits of stable matter. As one approaches these limits, new phenomena emerge such as halo densities, extreme matter clusterization and reorganization of shell structure, as seen in the case of $N = 20$ for nuclei around ^{32}Mg, the so-called 'island of inversion' region. Another example is the appearance of the $N = 14$ and $N = 16$ shell gaps when one moves from the $N = 20$ shell gap in ^{30}Si to ^{24}O.

From a theoretical standpoint, nuclei at their extremes are a challenging undertaking. Loosely bound or unbound nuclear states are located near the scattering threshold and should be treated as open quantum many-body systems, where coupling with the scattering continuum is explicitly taken into account. A coupling to continuum states within a traditional configuration interaction approach (shell-model), with wave functions built up from linear combinations of Slater determinants, results in prohibitively huge dimensionalities when solving the many-body Schrödinger equation. Furthermore, the necessity to include three-body interactions complicates the solution strategies of the nuclear many-body problem. Recent results from *ab-initio* methods for nuclei up to mass number $A = 12$ demonstrate the importance of such interactions. It is also not fully clear how various parts of the underlying nucleon-nucleon interaction, such as the spin-orbit force [45, 46] and the tensor force [47, 48], affect the structure of nuclei close to the drip line. In this thesis, we employ the Gamow shell model [49] and show the importance of the continuum effects on dripline nuclei, taking an example of oxygen isotopes.

1.4 Thesis organization

This thesis is organized as follows. After a brief introduction to the nuclear forces in Chapter 2, we outline the theories to renormalize strong nuclear forces to be useful for nuclear structure calculations. Especially we give an introduction to the similarity renormalization group (SRG) in Section 2.4. After emphasizing the importance to handle the many-body interactions induced in many-body theories, we formulate the SRG transformation directly in a many-body medium (In-medium SRG) in Chapter 3. Chapter 4 is devoted for the investigation of how the in-medium SRG is related to the other many-body methods, taking an example of the perturbation theory and the Q-box expansion theory. Then we show the first results for nuclei in Chapter 5 , including the ground-state energies of ^{4}He, ^{16}O and ^{40}Ca. The problem on the spurious center of mass excitation will be discussed in Section 5.3. We also discuss about the derivation of effective interactions for valence-nucleon systems in the framework of the in-medium SRG in Chapter 6. The description of neutron-rich nuclei with realistic NN interactions is discussed in Section 6.3.

Chapter 2

Nuclear forces

In this chapter, we discuss the features and effective theories of the nuclear forces, which is the most fundamental ingredient in low-energy nuclear structure.

2.1 Realistic Nucleon-Nucleon (NN) interactions

Ab-initio nuclear many-body problems start with the nucleon degrees of freedom and their interaction, nuclear forces. Nucleons are not the elemental particles but an effective degrees of freedom at low energy phenomena. The nuclear forces are therefore not the most fundamental interaction but an effective one that should be reduced from the strong interaction within quarks and gluons. The difficulty in deriving nuclear forces from QCD is that the theory is non-perturbative at the low energy regime which is typical to nuclear structure physics. A hopeful way to attack this problem is the use of Lattice QCD. The intensive studies by the Lattice QCD [1, 50, 3, 51] have explained the general behaviour of nuclear force in the form of local potential. The simulation with lighter pion mass, or closer to the real pion mass, is expected to provide more realistic description of nuclear forces. To date, an NN potential applicable for quantitative nuclear structure calculations has not been obtained.

There have been existing many phenomenological models for nuclear forces before the discovery of the QCD. The important points are that there exist a clear energy-scale separation and that a nucleon is in fact measured as a composite particle. Hence, protons and neutrons can be the most fundamental degrees of freedom in nuclear structure physics. Based on the fit of the proton-proton (pp) and proton-neutron (pn) scattering data on the assumption of various phenomenological NN potentials below the energy of the pion-production threshold, the guideline for nuclear forces was given by Taketani *et al.* in the early 50's [52], where

the long range part ($r > 2$ fm) is described by the one-pion exchange and intermediate range ($1 < r < 2$ fm) is explained by the exchange of heavier mesons, and the short range part ($r < 1$ fm) contains the details of high-energy physics thus have to be treated highly phenomenologically.

Based on the assertion, a number of meson-exchange models for nuclear forces have been constructed, improving their accuracy. The parameters in the models are fixed by the low-energy NN scattering data and the properties of the deuteron. The phase-shift analysis based on the assumption of the local potential requires the presence of strong repulsive core, which was originally pointed out by Jastrow [53], and is the common feature in most of the models of nuclear forces. Nowadays, the NN potentials $V(r)$ in coordinate space of $V(k, k')$ in momentum space with certain parametrization have been constructed by fitting the low-energy NN phase shift and the deuteron binding energy with $\chi^2/\text{dof} \sim 1$ in the range $0 - 350$ MeV in laboratory energy. These potentials are called high-precision or realistic NN potential, including the Argonne V18 [54] potential, CD-Bonn potential [55] and Nijmegen potential [56].

Since the phenomenological models are constrained by the phase shift and binding energy of the deuteron, the on-shell properties of various potential models are similar. However, the off-shell properties are highly model-dependent and does affect to few- and many-body observables. This means the three- and higher-body forces are also model dependent, and no unified conclusion about the many-body forces in nuclei has been obtained.

2.2 Chiral perturbation theory

In a couple of decades, more systematic framework for nuclear forces based on the chiral effective field theory has been developed. One can construct the low-energy effective theory of QCD by writing down the most general Lagrangian consistent with the assumed symmetry principle, as suggested by Weinberg [57]. The relevant degrees of freedom in the χEFT are pions and nucleons governed by spontaneously broken (approximate) chiral symmetry of QCD. The χEFT has a momentum scale $\Lambda_\chi \approx 1$ GeV, which is chiral symmetry breaking scale. The Λ_χ divides physics into two parts. One is long-range physics, which is resolved and treated explicitly by the low-energy degrees of freedom. The other is short-range physics, which is integrated out thus is not resolved and replaced by contact interactions. The details in high-energy physics are not resolved in the low-energy scale which is typical to the low-energy nuclear physics, and can be captured into the resolution-dependent low-energy constants.

The χEFT provides us with a systematic expansion of the nuclear amplitude in terms of

$(Q/\Lambda_\chi)^\nu$, where Q denotes a typical momentum or pion mass, m_π. There is actually another cutoff Λ to regulate the theory, thus the expansion follows $(Q/\Lambda)^\nu$ rather than $(Q/\Lambda_\chi)^\nu$ if $\Lambda < \Lambda_\chi$. Power counting determines the power $\nu(\geq 0)$ of the expansion. At a given ν, the finite number of terms are uniquely defined and one can achieve the model-independent prediction of physical amplitudes with controlled accuracy.

Another important point in χEFT is the systematic organization of many-body forces. Following the power counting by Weinberg, two-nucleon (2N) forces appear at the leading order (LO, $\nu = 0$), non-vanishing 3N forces start at the next-to-next-to leading order (NNLO, $\nu = 3$), and 4N forces at N^{3}LO with $\nu = 4$. Therefore, the χEFT naturally explains the empirically known hierarchy of many-body forces

$$V_{\rm 2N} \gg V_{\rm 3N} \gg V_{\rm 4N} \cdots . \tag{2.1}$$

There are several unsolved problems remain in χEFT, including a different way of power counting, inclusion of Δ particle, 3N forces at higher order. In this thesis, we follow Entem and Machleidt [7] and use NN only potential as a starting point of the calculations. This specific choice is not relevant to our discussion in this thesis. In ref. [7], 2N interactions are constructed up to N^{3}LO ($\nu = 4$), described with contact terms and irreducible pion-exchange processes. In order for the theory to be a low-momentum expansion, the potential is multiplied by the regulator

$$V_\Lambda(\boldsymbol{p}, \boldsymbol{p'}) = e^{-(p/\Lambda)^{2n}} V(\boldsymbol{p}, \boldsymbol{p'}) e^{-(p'/\Lambda)^{2n}}, \quad \Lambda = 500\text{MeV}, \tag{2.2}$$

and is applied to obtain T-matrix in the Lippmann-Schwinger equation. We will denote this potential as N^{3}LO(500) hereafter. The $2n$ in the regulator is chosen to be sufficiently large so that the regulator generates higher powers than those at which the expansion is terminated. Although the importance of the 3N forces is reported in various researches, including ref. [58, 28, 30], we do not include 3N forces in this thesis. At early stage of the investigation, we focus on the details of the methodology rather than the comparison to experimental data.

2.3 Effective theories of strong nuclear forces

As mentioned in the introduction, the difficulty of the *ab-initio* calculations is the common feature of nuclear forces that realistic NN interactions have strong coupling between high- and low-momentum states. Even though the nuclear force is a low-energy effective theory of

QCD, it still contains higher-momentum components compared to the energy scale of nuclear structure. This strong coupling makes many-body problems highly non-perturbative, as a consequence of which one sees very slow convergence of the *ab-initio* calculations with respect to the truncation of the Hilbert space.

There are several ways to bypass this problem. Among them is the G-matrix. The G-matrix is obtained by solving the Bethe-Goldstone equation

$$G(\omega) = V_{\rm NN} + V_{\rm NN}\frac{\mathcal{Q}_{2p}}{\omega - H_0}G(\omega), \tag{2.3}$$

where the $\mathcal{Q}_{2p}$ is the operator to project onto the state where two particles are outside the defined model space. The G-matrix is the in-medium sum of ladder diagrams to construct an effective two-body interaction starting from the NN potential. The G-matix can be understood as a special case, as specified by the $\mathcal{Q}_{2p}$, of Bloch-Horowitz (BH) equation [59,60]. The Bloch-Horowitz approach starts with the division of the Hilbert space into a model space, with the d dimension, and its complement space, specified by the projection operators

$$\mathcal{P} = \sum_{i=1}^{d} |i\rangle \langle i|, \qquad \mathcal{Q} = \sum_{i=d+1}^{\infty} |i\rangle \langle i|, \tag{2.4}$$

respectively. Here, the states $|i\rangle$ are the eigenstates of an unperturbed Hamiltonian H_0 of $H = H_0 + H_1$. The projection operators have features of completeness $\mathcal{P} + \mathcal{Q} = \mathbf{1}$, orthogonality $\mathcal{P}\mathcal{Q} = \mathcal{Q}\mathcal{P} = 0$ and idempotency $\mathcal{P}^2 = \mathcal{P}$, $\mathcal{Q}^2 = \mathcal{Q}$. The Schrödinger equation can be written in a matrix form

$$\begin{pmatrix} \mathcal{P}H\mathcal{P} & \mathcal{P}H\mathcal{Q} \\ \mathcal{Q}H\mathcal{P} & \mathcal{Q}H\mathcal{Q} \end{pmatrix} \begin{pmatrix} \mathcal{P}|\Psi\rangle \\ \mathcal{Q}|\Psi\rangle \end{pmatrix} = E \begin{pmatrix} \mathcal{P}|\Psi\rangle \\ \mathcal{Q}|\Psi\rangle \end{pmatrix}. \tag{2.5}$$

Elimination of the $\mathcal{Q}|\Psi\rangle$ in the second row in Eq. (2.5) yields the equation for the effective Hamiltonian

$$\mathcal{P}H_{\rm eff}(E)\mathcal{P}|\Psi\rangle = EP|\Psi\rangle, \tag{2.6}$$

where the effective Hamiltonian can be obtained by the Bloch-Horowitz equation

$$H_{\rm eff}(E) = H + H\mathcal{Q}\frac{1}{E - \mathcal{Q}H\mathcal{Q}}\mathcal{Q}H. \tag{2.7}$$

If one solves the BH equation for two-body system with $\mathcal{Q} = \mathcal{Q}_{2p}$, Eq. (2.7) becomes the Bethe-Goldstone equation (2.3) [*1]. The effective Hamiltonian depends on the exact energy

[*1] Note that we the relation $[\mathcal{P}, H_0] = [\mathcal{Q}, H_0] = 0$ in this case

E, which one has to solve for, therefore the BH equation should be solved self-consistently. Note that the effective Hamiltonian $H_{\rm eff}(E)$ is defined in a whole Hilbert space, while the model-space projected Hamiltonian $\mathcal{P}H_{\rm eff}(E)\mathcal{P}$ operates only on the model space, reproducing the exact d eigenenergies of H. These are important features of the G-matrix, that is energy-dependent and by construction defined in the whole Hilbert space for two body, thus the decoupling of high-momentum modes is not fully achieved. The latter can be considered to be a reason why in the nuclear matter calculations a perturbation expansion in powers of the G-matrix was not convergent and one had to do additional prescription like the hole-line expansion [61].

On the other hand, the Lee-Suzuki transformation [35,62] achieves the explicit decoupling between an arbitrary chosen model space (denoted by $\mathcal{P}$) and its complement space (denoted by $\mathcal{Q} \equiv \mathbf{1} - \mathcal{P}$). The Lee-Suzuki transformation guarantees the decoupling by constructing an appropriate similarity transformation of a Hamiltonian $\mathcal{H} = S^{-1}HS$, as a consequence of which the transformed Hamiltonian has no connection between the $\mathcal{P}$ and $\mathcal{Q}$ spaces,

$$\mathcal{Q}\mathcal{H}\mathcal{P} = 0. \tag{2.8}$$

It is easy to see that the $\mathcal{P}\mathcal{H}\mathcal{P}$ becomes an equivalent effective interaction that is operative only on the model space $\mathcal{P}$ and energy independent as long as the decoupling condition of Eq. (2.8) is satisfied. A choice of the model space,

$$\mathcal{P}_\Lambda := \int_{0\le|\boldsymbol{p}|\le\Lambda} |\boldsymbol{p}\rangle\, d\boldsymbol{p}\, \langle\boldsymbol{p}|\,, \qquad \mathcal{Q}_\Lambda = \mathbf{1} - \mathcal{P}_\Lambda = \int_{\Lambda<|\boldsymbol{p}|} |\boldsymbol{p}\rangle\, d\boldsymbol{p}\, \langle\boldsymbol{p}|\,, \tag{2.9}$$

is used for the construction of low-momentum NN interactions $V(k,k')$ defined in $k < \Lambda$ [63,64]. Another choice

$$\mathcal{P}_\rho := \sum_{e=2n+l=0}^{\rho} |n,l\rangle\, \langle n,l| \tag{2.10}$$

in Harmonic oscillator (HO) states is used to form an effective NN interactions defined in a sufficiently small model space, specified by ρ, and applied for the NCSM calculations in their early stage [65,66]. The Lee-Suzuki transformation is by construction non hermitian. Thus, if one needs a hermitian effective interaction, one has to either parametrize the unitary transformation [67] or perform additional unitary transformation for hermitization [63].

Recently, several methods based on renormalization group (RG) have been developed for nuclear forces [38,63,68,39]. One way to decouple high-momentum degrees of freedom is to integrate out the high-momentum states above a cutoff, requiring the invariance of the half

on-shell T-matrix, and renormalize the complicated physics in high momentum into effective NN interaction defined below the cutoff [63, 68]. This low-momentum interaction is known as $V_{\mathrm{low-k}}$, preserving the observables below the cutoff, and can be understood as the successive implementation of the Lee-Suzuki transformation. While the short-range behavior changes with the cutoff, the long-range parts remain unchanged. This general feature is constructively used for the investigation of the effective shell-model interactions. It is recently reported that the long-range part of the tensor force is not affected by the renormalization, nor by the in-medium correction. This non-trivial feature of tensor force via renormalization supports the robust explanation of the effective monopole interactions in the shell model [69]. So far, the $V_{\mathrm{low-k}}$ is formulated for two-nucleon system,therefore the A-body observables ($A > 2$) are Λ-dependent, although the $V_{\mathrm{low-k}}$ provides us with the accelerated convergence for many-body theories. The construction of the $V_{\mathrm{low-k}}$ in three- or higher-body systems is faced by a conceptional difficulty. In the three-body system, for instance, the T-matrix has a pole at the energy of the bound state of the deuteron and the three-body break up.

2.4 Similarity Renormalization Group (SRG)

Another path to decouple high-momentum degrees of freedom is the similarity renormalization group (SRG), which was introduced independently by Glazek and Wilson [70] and Wegner [71]. Consider a Hamiltonian that we split into diagonal and off-diagonal parts

$$H = H^{\mathrm{d}} + H^{\mathrm{od}}. \tag{2.11}$$

This could be a simple 1-body Hamiltonian, or it could be a complicate nuclear Hamiltonian with 2- and 3-body forces acting in a many-body Hilbert space. Suppose that we want to construct a unitarily equivalent Hamiltonian where the dominant piece has an operator structure given by H^{d}. The SRG consists of a continuous sequence of unitary transformations that suppress off-diagonal matrix elements, driving the Hamiltonian towards a band- or block-diagonal form. Consider the unitary transformed Hamiltonian parametrized by s,

$$H(s) = U(s)HU^{\dagger}(s) \equiv H^{\mathrm{d}}(s) + H^{\mathrm{od}}(s)\,, \tag{2.12}$$

where $H^{\mathrm{d}}(s)$ and $H^{\mathrm{od}}(s)$ are the appropriately defined "diagonal" and "off-diagonal" parts of the Hamiltonian, and $U(0) = 1, H(0) = H$. Taking the derivative with respect to s, the evolution with the flow parameter s is given by

$$\frac{dH(s)}{ds} = [\eta(s), H(s)]\,. \tag{2.13}$$

Here

$$\eta(s) \equiv \frac{dU(s)}{ds}\,U^{\dagger}(s) \tag{2.14}$$

is the anti-hermitian generator of the transformation. We can formally write the unitary transformation as an s-ordered exponential,

$$U(s) = \mathcal{T}_s \exp\left(-\int_0^s ds'\eta(s')\right). \tag{2.15}$$

The choice of the generator first suggested by Wegner,

$$\eta(s) = [H^{\rm d}(s), H(s)] = [H^{\rm d}(s), H^{\rm od}(s)]\,, \tag{2.16}$$

guarantees that the off-diagonal coupling of $H^{\rm od}$ is driven exponentially to zero with increasing s [71]. Through different choices for $H^{\rm d}$ and $H^{\rm od}$, one can tailor the SRG evolution to transform the initial Hamiltonian to a form that is most convenient for a particular problem [72, 73]. It is this flexibility, together with the fact that one never explicitly constructs and applies the unitary transformation $U(s)$ (rather it is implemented implicitly through the integration of Eq. (2.13)) that makes the SRG a powerful alternative to conventional effective interaction methods such as Lee-Suzuki similarity transformations [39, 38, 74]. To date, the SRG applications to nuclear forces have been carried out in free space to construct "soft" nucleon-nucleon (NN) and three-nucleon (3N) interactions to be used as input in ab-initio calculations [39, 74, 40].

We close this section by noting the importance of treating many-body forces in many-body problems. The general origin of many-body interactions in effective theories is a restriction of degrees of freedom. The 3N forces in Fujita-Miyazawa theory [75] arises from the elimination of Δ or anti-nucleon in the effective theory described by nucleons. Elimination of high-momentum modes with RG also generates many-body forces in the corresponding effective theory at low energy. Thus if one construct an effective Hamiltonian characterized by the cutoff Λ in a-body system and applies to A-body problem ($A > a$), one sees a Λ dependence of observables due to the induced many-body interactions, the size of which depends on the Λ. It is indeed important to manage the induced many-body interactions for a many-body theory to be useful for the nuclear structure calculations. While the free-space evolution is convenient

since it does not have to be performed for each different nucleus or nuclear matter density, it is necessary to handle 3N (and possibly higher-body) interactions to be able to lower the cutoff [*2] significantly and maintain approximate cutoff independence of $A \geqslant 3$ observables. The consistent SRG evolution of 3N operators represents a significant technical challenge that has only recently been solved in a convenient basis [40]. In the next Chapter, we will introduce a new efficient method to take into account the induced many-nucleon interactions in many-body system.

[*2] A measure of the band-diagonal width of the SRG-evolved Hamiltonian is given by the "cutoff" $\lambda \equiv s^{-1/4}$.

Chapter 3

In-medium SRG

In this Chapter, we introduce an efficient way to treat the induced many-body interactions in a relatively simple machinery. Instead of performing SRG in free space, we propose the SRG transformation directly in nuclear many-body medium [76]. The Hamiltonian is given as

$$H = \sum_{ij} T_{ij} a_i^\dagger a_j + \frac{1}{2!^2} \sum_{ijkl} V^{(2)}_{ijkl} a_i^\dagger a_j^\dagger a_l a_k + \frac{1}{3!^2} \sum_{ijklmn} V^{(3)}_{ijklmn} a_i^\dagger a_j^\dagger a_k^\dagger a_n a_m a_l + \cdots . \tag{3.1}$$

Using Wick's theorem, all operators are normal-ordered with respect to a reference state $|\Phi_0\rangle$, which can be a non-interacting Fermi sea or self-consistent mean field,

$$H = E_0 + \sum_{ij} f_{ij} \{a_i^\dagger a_j\} + \frac{1}{2!^2} \sum_{ijkl} \Gamma_{ijkl} \{a_i^\dagger a_j^\dagger a_l a_k\} + \frac{1}{3!^2} \sum_{ijklmn} W_{ijklmn} \{a_i^\dagger a_j^\dagger a_k^\dagger a_n a_m a_l\}, \tag{3.2}$$

where the coefficients of the normal-ordered operators, $E_0, f_{ij}, \Gamma_{ijkl}$ are given by

$$E_0 = \langle \Phi_0 | H | \Phi_0 \rangle = \sum_k T_{kk} n_k + \frac{1}{2} \sum_{ij} V^{(2)}_{ijij} n_i n_j + \frac{1}{6} \sum_{ijk} V^{(3)}_{ijkijk} n_i n_j n_k \tag{3.3}$$

$$f_{ij} = T_{ij} + \sum_k \{ik|V_2|jk\} n_k + \frac{1}{2} \sum_{kl} \{ikl|V_3|jkl\} n_k n_l \tag{3.4}$$

$$\Gamma_{ijkl} = V^{(2)}_{ijkl} + \frac{1}{4} \sum_m V^{(3)}_{ijmklm} n_m \tag{3.5}$$

$$W_{ijklmn} = V^{(3)}_{ijklmn}. \tag{3.6}$$

Here, the initial n-body interactions are denoted by $V^{(n)}$, and $n_i = \theta(\varepsilon_\mathrm{F} - \varepsilon_i)$ are occupation numbers in the reference state $|\Phi_0\rangle$, with Fermi energy ε_F. It is evident from Eqs. (3.3)–(3.5) that the normal-ordered terms, E_0, f and Γ, include contributions from the three-body interaction $V^{(3)}$ through sums over the occupied single-particle states in the reference

state $|\Phi_0\rangle$. Therefore, truncating the in-medium SRG equations to normal-ordered two-body operators, which we denote by IM-SRG(2), will approximately evolve induced three- and higher-body interactions through the nucleus-dependent 0-, 1-, and 2-body terms.

Using Wick's theorem to evaluate Eq. (2.13) with

$$H(s) = E_0(s) + f(s) + \Gamma(s) + W(s), \tag{3.7}$$

and

$$\eta(s) = \eta^{(1)}(s) + \eta^{(2)}(s) + \eta^{(3)}(s) \tag{3.8}$$

truncated to normal-ordered three-body operators, one obtains the coupled IM-SRG(3) flow equations (with $\bar{n}_i \equiv 1 - n_i$)

$$\frac{dH(s)}{ds} = [\eta(s), H(s)]. \tag{3.9}$$

The flow equation can be given in matrix form with the permutation operators,

$$P_{ij} f(i,j) = f(j,i), \quad P(ij/k) = 1 - P_{ik} - P_{jk}, \quad P(i/jk) = 1 - P_{ij} - P_{ik}, \tag{3.10}$$

$$\begin{aligned}
\frac{d}{ds}E_0(s) &= \sum_{ab}(n_a - n_b)\eta^{(1)}_{ab} f_{ba} + \frac{1}{2}\sum_{abcd}\eta^{(2)}_{abcd}\Gamma_{cdab}(s) n_a n_b \bar{n}_c \bar{n}_d \\
&\quad + \frac{1}{18}\sum_{abcdef}\eta^{(3)}_{abcdef} W_{defabc} n_a n_b n_c \bar{n}_d \bar{n}_e \bar{n}_f
\end{aligned} \tag{3.11}$$

$$\begin{aligned}
\frac{d}{ds}f_{ij}(s) &= \sum_a (1 + P_{ij})\eta^{(1)}_{ia} f_{aj} + \sum_{ab}(n_a - n_b)(\eta^{(1)}_{ab}\Gamma_{biaj} - f_{ab}\eta^{(2)}_{biaj}) \\
&\quad + \sum_{abc}(n_a n_b \bar{n}_c + \bar{n}_a \bar{n}_b n_c)(1 + P_{ij})\eta^{(2)}_{ciab}\Gamma_{abcj} \\
&\quad + \frac{1}{4}\sum_{abcd}(n_a n_b \bar{n}_c \bar{n}_d)(\eta^{(3)}_{abicdj}\Gamma_{cdab} - W_{abicdj}\eta^{(2)}_{cdab}) \\
&\quad + \frac{1}{12}\sum_{abcde}(n_a n_b \bar{n}_c \bar{n}_d \bar{n}_e + \bar{n}_a \bar{n}_b n_c n_d n_e)(\eta^{(3)}_{abicde} W_{cdeabj} - W_{abicde}\eta^{(3)}_{cdeabj})
\end{aligned} \tag{3.12}$$

$$\begin{aligned}
\frac{d}{ds}\Gamma_{ijkl}(s) &= \sum_a \Big\{(1 - P_{ij})(\eta^{(1)}_{ia}\Gamma_{ajkl} - f_{ia}\eta^{(2)}_{ajkl}) - (1 - P_{kl})(\eta^{(1)}_{ak}\Gamma_{ijal} - f_{ak}\eta^{(2)}_{ijal})\Big\} \\
&\quad + \frac{1}{2}\sum_{ab}(1 - n_a - n_b)(\eta^{(2)}_{ijab}\Gamma_{abkl} - \Gamma_{ijab}\eta^{(2)}_{abkl}) \\
&\quad - \sum_{ab}(n_a - n_b)\Big[(1 - P_{ij})(1 - P_{kl})\eta^{(2)}_{bjal}\Gamma_{aibk}\Big] \\
&\quad + \sum_{ab}(n_a - n_b)\left(\eta^{(3)}_{aijbkl} f_{ba} - W_{aijbkl}\eta^{(1)}_{ba}\right)
\end{aligned}$$

$$
\begin{aligned}
&+\frac{1}{2}\sum_{abc}(n_a\bar{n}_b\bar{n}_c+\bar{n}_an_bn_c)\left\{(1-P_{ik}P_{jl}P_{ij}-P_{kl}+P_{ik}P_{jl})(\eta^{(3)}_{aijbcl}\Gamma_{bcak}-W_{aijbcl}\eta^{(2)}_{bcak})\right\}\\
&+\frac{1}{6}\sum_{abcd}(n_a\bar{n}_b\bar{n}_c\bar{n}_d-\bar{n}_an_bn_cn_d)(\eta^{(3)}_{aijbcd}W_{bcdakl}-\eta^{(3)}_{bcdakl}W_{aijbcd})\\
&+\frac{1}{4}\sum_{abcd}(\bar{n}_a\bar{n}_bn_cn_d-n_an_b\bar{n}_c\bar{n}_d)(1-P_{ij})(1-P_{kl})\eta^{(3)}_{abicdl}W_{cdjabk}. \qquad (3.13)
\end{aligned}
$$

$$
\begin{aligned}
\frac{d}{ds}W_{ijklmn}(s)=&\sum_a\left\{P(i/jk)\eta^{(1)}_{ia}W_{ajklmn}-P(l/mn)\eta^{(1)}_{al}W_{ijkamn}\right\}\\
&-\sum_a\left\{P(i/jk)f_{ia}\eta^{(3)}_{ajklmn}-P(l/mn)f_{al}\eta^{(3)}_{ijkamn}\right\}\\
&+\sum_a P(ij/k)P(l/mn)(\eta^{(2)}_{ijla}\Gamma_{akmn}-\Gamma_{ijla}\eta^{(2)}_{akmn})\\
&+\frac{1}{2}\sum_{ab}(1-n_a-n_b)(P(i/jk))(\eta^{(2)}_{ijab}W_{abklmn}-\Gamma_{ijab}\eta^{(3)}_{abklmn})\\
&-\frac{1}{2}\sum_{ab}(1-n_a-n_b)(P(lm/n))(\eta^{(2)}_{ablm}W_{ijkabn}-\Gamma_{ablm}\eta^{(3)}_{ijkabn})\\
&-\sum_{ab}(n_a-n_b)P(i/jk)p(l/mn)(\eta^{(2)}_{bial}W_{ajkbmn}-\Gamma_{bial}\eta^{(3)}_{ajkbmn})\\
&+\frac{1}{6}\sum_{abc}(n_an_bn_c+\bar{n}_a\bar{n}_b\bar{n}_c)(\eta^{(3)}_{ijkabc}W_{abclmn}-W_{ijkabc}\eta^{(3)}_{abclmn})\\
&+\frac{1}{2}\sum_{abc}(n_an_b\bar{n}_c+\bar{n}_a\bar{n}_bn_c)P(ij/k)P(l/mn)(\eta^{(3)}_{abkcmn}W_{cijabl}-\eta^{(3)}_{cjkabn}W_{iablmc}).
\end{aligned}
\qquad (3.14)
$$

The commutator form of the flow equations gives a fully connected structure in which $H(s)$ has at least one contraction with η. Therefore, there are no unlinked diagrams and the flow equations are size-extensive. A theory is said to be size-extensive if the energy calculated thereby scales linearly with the number of constituent particles A. [*1]. Although it is desirable to explicitly solve the flow equations above, the treatment of the tree-body operator is very memory and time consuming in the view point of computational cost. Thus we start with the truncation of the flow equation up to the normal-ordered two-body level, denoting as IM-SRG(2).

3.1 IM-SRG(2) equations for nuclear systems

The flow equations (3.11)-(3.14) are given in arbitrary basis. In homogeneous systems like nuclear matter, a set of discretized momentum states are taken as a basis. In the application

[*1] If the method is size-extensive, then the error estimation in smaller systems can hold for heavier systems.

to nuclear many-body systems, it is convenient to employ spherical single-particle (s.p.) basis based on the spherical shell model. In the spherical shell model, nucleons are confined in a mean field, which generates spherical s.p. orbits, specified by the set of quantum numbers $a = (n_a, l_a, j_a, m_a, t_{za})$. The n, l and j correspond to the principal, orbital angular-momentum, and angular-momentum quantum numbers, respectively. The m and t_z are the projections of angular momentum and isospin onto an axis of quantization (We take z-axis for quantization). The shell model is a simple but efficient way to understand nuclei such as the magic numbers as is well known. Starting with the spherical s.p. shell-model basis, we take a doubly-magic nucleus as a reference state $|\Phi_0\rangle$. The doubly-magic nucleus in naive shell-model picture consists of nucleons that fill up to a certain s.p. orbit bellow the shell gap at the magic number. Thus, the reference state is isotropic and has the spin-parity $J^\pi = 0^+$. The reference state for ^{4}He is, for instance,

$$|\Phi_0\rangle = a^\dagger_{0s_{1/2,m=1/2,t_z=-1/2}} a^\dagger_{0s_{1/2,m=-1/2,t_z=-1/2}} a^\dagger_{0s_{1/2,m=1/2,t_z=1/2}} a^\dagger_{0s_{1/2,m=-1/2,t_z=1/2}} |0\rangle\,, \quad (3.15)$$

where the $|0\rangle$ is the vacuum. Having defined the s.p. basis, the flow equation is written by the matrix elements of the Hamiltonian and the generator with all possible many-body states in a given model space. In this first application, we truncate the flow equations Eqs (3.11-3.14) up to the normal-ordered two-body level, and call it IM-SRG(2).

3.1.1 M-scheme

With the spherical s.p. basis, many-body states, or Slater determinants, has a conserved values of the z-component of the total angular momentum J and isospin T, denoted by M and T_z, respectively. So, a state $|ab\rangle$ has $M = m_a + m_b$ and $T_z = t_{za} + t_{zb}$. Since a nuclear Hamiltonian and thus a generator of the SRG is a scalar under the rotation, all the matrix elements in the flow equation are classified according to the value of M. This way of classification is called M-scheme. The IM-SRG(2) flow equation in M-scheme representation is given as,

$$\frac{dE_0}{ds} = \sum_{ab} \eta^{(1)}_{ab}\, f_{ba}\, (n_a - n_b) + \frac{1}{2} \sum_{abcd} \eta^{(2)}_{abcd}\, \Gamma_{cdab}\, n_a n_b \bar{n}_c \bar{n}_d\,, \quad (3.16)$$

$$\begin{aligned}\frac{df_{ij}}{ds} &= \sum_a (1 + P_{ij}) \eta^{(1)}_{ia}\, f_{aj} + \sum_{ab} (n_a - n_b)(\eta^{(1)}_{ab}\, \Gamma_{biaj} - f_{ab}\, \eta^{(2)}_{biaj}) \\ &\quad + \frac{1}{2} \sum_{abc} (n_a n_b \bar{n}_c + \bar{n}_a \bar{n}_b n_c)(1 + P_{ij}) \eta^{(2)}_{ciab} \Gamma_{abcj}\,, \end{aligned} \quad (3.17)$$

$$\frac{d\Gamma_{ijkl}}{ds} = \sum_a (1 - P_{ij})(\eta^{(1)}_{ia}\, \Gamma_{ajkl} - f_{ia}\, \eta^{(2)}_{ajkl}) - \sum_a (1 - P_{kl})(\eta^{(1)}_{ak}\, \Gamma_{ijal} - f_{ak}\, \eta^{(2)}_{ijal})$$

$$+\frac{1}{2}\sum_{ab}(1-n_a-n_b)\Big[\eta^{(2)}_{ijab}\,\Gamma_{abkl}+\Gamma_{ijab}\,\eta^{(2)}_{abkl}\Big]$$
$$-\sum_{ab}(n_a-n_b)(1-P_{ij})(1-P_{kl})\eta^{(2)}_{bjal}\Gamma_{aibk}\,. \tag{3.18}$$

Note that the condition for the conservation of M and T_z is implicit. While the IM-SRG equations are of second order in the interactions, the flow equations build up non perturbative physics via the interference between the particle-particle and the two particle-hole channels for Γ, Eq. (3.18), and between the two-particle–one-hole and two-hole–one-particle channels for f, Eq. (3.17). Note that the terms with $n_a - n_b$ in the flow equation only survive if the intermediate states a and b are particle and hole states, observing that $n_a - n_b = -(\bar{n}_a n_b - n_a \bar{n}_b)$. Similarly, the terms proportional to $1 - n_a - n_b$ $(= \bar{n}_a \bar{n}_b - n_a n_b)$ only survive if their intermediate states are two-particle (pp) or two-hole (hh) states. As we will later prove, the IM-SRG(2) level is third-order exact. In addition, the numerical scaling with the number of single-particle orbitals is approximately of order N^6, which makes the method suitable for medium-mass nuclei.

3.1.2 J-coupled scheme

So far, the flow equation for the IM-SRG has been obtained in M-scheme that is a reducible representation under rotation group. It is, however, very convenient to represent the flow equation in irreducible basis of rotation group when the assumption of the spherical symmetry makes sense.

We here re-introduce the quantum numbers $a = (n_a, l_a, j_a, t_{za})$ and $\omega_a = (l_a, j_a, t_{za}, m_a)$. M-scheme matrix elements and those of J-coupled scheme are related as bellow

$$f_{im_ijm_j} = \delta_{\omega_i\omega_j} f_{ij} \tag{3.19}$$

$$\begin{aligned}\Gamma_{im_ijm_jkm_klm_l} &= \sqrt{(1+\delta_{ij})(1+\delta_{kl})}\sum_{JM}(j_im_ij_jm_j|JM)(j_km_kj_lm_l|JM)\Gamma^J_{ijkl}\\ &\equiv \sum_{JM}(j_im_ij_jm_j|JM)(j_km_kj_lm_l|JM)\tilde{\Gamma}^J_{ijkl}\end{aligned} \tag{3.20}$$

In the same way , the J-coupled matrix elements of the generator are given by

$$\eta^{(1)}_{im_ijm_j} = \delta_{\omega_i\omega_j}\eta^{(1)}_{ij} \tag{3.21}$$
$$\eta^{(2)}_{im_ijm_jkm_klm_l} = \sum_{JM}(j_im_ij_jm_j|JM)(j_km_kj_lm_l|JM)\tilde{\eta}^{(2),J}_{ijkl} \tag{3.22}$$

The J-scheme representation of the flow equation can be derived from the M-scheme representation. We give the derivation in Section A.2. Here we just show the final expression,

$$\frac{d}{ds}E_0 = \frac{1}{2}\sum_{ijkl}\sum_{J}(2J+1)\tilde{\eta}^{2b,J}_{ijkl}\tilde{\Gamma}^{2b,J}_{ijkl}n_i n_j \bar{n}_k \bar{n}_l + \sum_{ij}(2j_i+1)\eta^{(1)}_{ij}g^{od}_{ij}(n_i-n_j) \tag{3.23}$$

$$\begin{aligned}\frac{d}{ds}f_{ij} = &\sum_a \left(\eta^{(1)}_{ia}f_{aj} - f_{ia}\eta^{(1)}_{aj}\right) \\ &+ \frac{1}{(2j_i+1)}\sum_J(2J+1)\left[\sum_{ab}(n_a-n_b)\left\{\eta^{1b}_{ab}\tilde{\Gamma}^J_{biaj} - f^{od}_{ab}\tilde{\eta}^{(2),J}_{biaj}\right\}\right. \\ &\left.\frac{1}{2}\sum_{abc}\tilde{\eta}^{(2),J}_{ciab}\tilde{\Gamma}^J_{abcj}\left(\bar{n}_a\bar{n}_b n_c + n_a n_b \bar{n}_c\right) + (i\leftrightarrow j)\right]\end{aligned} \tag{3.24}$$

$$\begin{aligned}\frac{d}{ds}\tilde{\Gamma}^J_{ijkl} = &\sum_a\left[\left(\eta^{(1)}_{ia}\tilde{\Gamma}^J_{ajkl} - f_{ia}\tilde{\eta}^{(2),J}_{ajkl}\right) - (i\leftrightarrow j)\right] - \sum_a\left[\left(\eta^{(1)}_{ak}\tilde{\Gamma}^J_{ijal} - f_{ak}\tilde{\eta}^{(2),J}_{ijal}\right) - (k\leftrightarrow l)\right] \\ &+ \frac{1}{2}\sum_{ab}(1-n_a-n_b)\left[\left(\tilde{\eta}^{(2),J}_{ijab}\tilde{\Gamma}^J_{abkl}\right) + (i,j\leftrightarrow k,l)\right] \\ &- \sum_{ab}(n_a-n_b)(1-(-1)^{j_i+j_j-J+1}P_{ij})(1-(-1)^{j_k+j_l-J+1}P_{kl}) \\ &\cdot\sum_{J_1J_2}(2J_1+1)(2J_2+1)(-1)^{j_i+j_k+J_1-J_2+J}\begin{Bmatrix} j_a & j_l & J_1 \\ j_i & J & j_j \\ J_2 & j_k & j_b\end{Bmatrix}\tilde{\eta}^{(2),J_1}_{bjal}\tilde{\Gamma}^{J_2}_{aibk}\end{aligned} \tag{3.25}$$

The most complicated and costly part of the flow equation is the one with particle-hole intermediate states, which appears in the last terms in the two-body sectors. These terms can be simplified by making use of the Racah's algebra. Following the ref [77], we introduce the cross-coupled matrix elements in which single-particle angular momenta from the bra and ket vectors are coupled, given as

$$\langle \overset{\star}{a}\overset{\star}{b}|\tilde{\chi}|\overset{\circ}{c}\overset{\circ}{d}\rangle_J := (-1)^{j_a+j_d+J}\sum_{J'}(2J'+1)(-1)^{J'}\begin{Bmatrix} j_c & j_a & J \\ j_b & j_d & J'\end{Bmatrix}\tilde{\chi}^J_{abcd}, \tag{3.26}$$

where the coupling order in the cross-coupled matrix elements is given by the symbols, "$\circ \rightarrow \star$", while $\tilde{\chi}^J_{abcd}$ denotes the standard coupling matrix elements.

$$\tilde{\chi}^J_{abcd} = \sum_{m_a m_b m_c m_d}(j_a m_a j_b m_b|JM)(j_c m_c j_d m_d|JM)\left\langle j_a m_a, j_b m_b\right|\chi\left|j_c m_c j_d m_c\right\rangle \tag{3.27}$$

Using the angular-re-coupling technique [77], the last term in Eq (3.25) can be simplified as

$$-\sum_{ab}(n_a-n_b)(1-(-1)^{j_i+j_j-J+1}P_{ij})(1-(-1)^{j_k+j_l-J+1}P_{kl})$$

$$\cdot \sum_{J'} (-1)^{j_i+j_l+J'+j_a+j_b+1} \begin{Bmatrix} j_k & j_l & J \\ j_j & j_i & J' \end{Bmatrix} \left(\langle \overset{\star}{b} j | \tilde{\eta}^{(2)} | \overset{\circ}{a} l \rangle_{J'} \langle \overset{\star}{b} j | \tilde{\Gamma} \overset{\circ}{a} l \rangle_{J'} \right). \tag{3.28}$$

This representation is computationally efficient because once the cross-coupled matrix elements are calculated and stored, only a single summation over J' is required, whereas the original flow equation needs a summation over three J's, considering that 9j symbol can be expanded over a single-J' summation with three 6j symbols. Moreover, with the use of the cross-coupling of the J-coupled matrix elements, one can recast Eq. (3.28) in the flow equation in terms of the matrix multiplication, which makes the numerical calculations significantly fast.

3.2 Decoupling and generator choices

In this initial study, we restrict our attention to the ground states of doubly-magic nuclei and define $H^{\mathrm{od}}(s) = f^{\mathrm{od}}(s) + \Gamma^{\mathrm{od}}(s)$, with

$$f^{\mathrm{od}}(s) = \sum_{ph} f_{ph}(s) \{a_p^\dagger a_h\} + \mathrm{h.c.}\,, \tag{3.29}$$

$$\Gamma^{\mathrm{od}}(s) = \sum_{pp'hh'} \Gamma_{pp'hh'}(s) \{a_p^\dagger a_{p'}^\dagger a_{h'} a_h\} + \mathrm{h.c.}\,, \tag{3.30}$$

where p, p' and h, h' denote unoccupied (particle) and occupied (hole) Hartree-Fock orbitals, respectively. We consider three different cases for the generator, Wegner's choice (η^{I}), White's choice (η^{II}) and Heidbrink's choice (η^{III}) in order to achieve the suppression of the off-diagonal part of the Hamiltonian H^{od}.

3.2.1 Wegner's choice

The Wegner's original choice for the generator is

$$\eta = [H^{\mathrm{d}}, H], \tag{3.31}$$

making the off-diagonal part of the Hamiltonian decay during the flow. If the diagonal matrix elements of a (finite) Hamiltonian are denoted by ε_i $(i = 1, \cdots N)$, the generator is

$$\eta_{ij} = (\varepsilon_i - \varepsilon_j) H_{ij}. \tag{3.32}$$

This yields,

$$\frac{d}{ds} H_{ij}(s) = \sum_k (\varepsilon_i + \varepsilon_j - 2\varepsilon_k) H_{ik}(s) H_{kj}(s). \tag{3.33}$$

One can show the measure of the off-diagonal coupling, $\mathrm{Tr}[(H^{\mathrm{od}})^\dagger(H^{\mathrm{od}})]$ can be suppressed during the flow. In fact, the following two relations

$$0 = \frac{d}{ds}\mathrm{Tr}[H^\dagger H] = \frac{d}{ds}\sum_i \varepsilon_i^2 + \frac{d}{ds}\sum_{i\neq j} H_{ij}^{\mathrm{od}} H_{ji}^{\mathrm{od}}, \tag{3.34}$$

and

$$\frac{d}{ds}\sum_i \varepsilon_i^2 = 2\sum_{ij}(\varepsilon_i - \varepsilon_j)H_{ij}^{\mathrm{od}} H_{ji}^{\mathrm{od}} \geq 0 \quad \text{(by Eq. (3.33))} \tag{3.35}$$

guarantee the suppression of the off-diagonal matrix elements

$$\frac{d}{ds}\mathrm{Tr}[(H^{\mathrm{od}})^\dagger(H^{\mathrm{od}})] = \frac{d}{ds}\sum_{i\neq j} H_{ij}^{\mathrm{od}} H_{ji}^{\mathrm{od}} \leq 0. \tag{3.36}$$

The suppression can be demonstrated by an approximate solution of Eq. (3.33). Assuming that the ε_i is s-independent,

$$\frac{d}{ds}H_{ij}(s) = -(\varepsilon_i - \varepsilon_j)^2 H_{ij}(s) + \mathcal{O}(H^2). \tag{3.37}$$

Thus, the off-diagonal elements decay as

$$H_{ij}(s) \cong H_{ij}(0)e^{-(\varepsilon_i-\varepsilon_j)^2 s}. \tag{3.38}$$

One clearly sees that the large energy difference terms are eliminated with higher priority. In another words, different off-diagonal matrix elements have their own decaying speeds $e^{-(\varepsilon_i-\varepsilon_j)^2 s}$, which in general makes the flow equation difficult to solve in numerical calculations. In our application for nuclei, we take

$$\eta^{\mathrm{I}}(s) = [H^{\mathrm{d}}(s), H^{\mathrm{od}}(s)], \tag{3.39}$$

which doesn't exactly follow the Wegner's original one because the $H^{\mathrm{d}}(s)$ is not diagonal in its matrix form, but rather the form to which we make the initial Hamiltonian drive. At least, the flow stops when the $\eta(s)$ vanishes, which means there is a common basis set of H^{d} and H. We will explicitly demonstrate the suppression of the off-diagonal matrix elements later.

For the case of nuclear system, Using the commutation relations in Eqs. (A.5), the generator is obtained as

$$\eta = \eta^{(1)} + \eta^{(2)}, \tag{3.40}$$

$$\text{with} \qquad \eta^{(1)} = \sum_{ij}\{a_i^\dagger a_j\}\eta_{ij}^{(1)}, \quad \eta^{(2)} = \frac{1}{4}\sum_{ijkl}\{a_i^\dagger a_j^\dagger a_l a_k\}\eta_{ijkl}^{(2)}, \tag{3.41}$$

where

$$\eta^{(1)}_{ij} = \sum_a (1-P_{ij}) f^{\mathrm{d}}_{ia} f^{\mathrm{od}}_{aj} - \sum_{ab} (n_a - n_b) f^{\mathrm{od}}_{ab} \Gamma^{\mathrm{d}}_{biaj} + \frac{1}{2} \sum_{abc} (\bar{n}_a \bar{n}_b n_c + n_a n_b \bar{n}_c)(1+P_{ij}) \Gamma^{\mathrm{d}}_{ciab} \Gamma^{\mathrm{od}}_{abcj} \tag{3.42}$$

$$\begin{aligned}\eta^{(2)}_{ijkl} = &\sum_a \left\{ (1-P_{ij}) \left(f^{\mathrm{d}}_{ia} \Gamma^{\mathrm{od}}_{ajkl} - f^{\mathrm{od}}_{ia} \Gamma^{\mathrm{d}}_{ajkl} \right) - (1-P_{kl}) \left(f^{\mathrm{d}}_{ak} \Gamma^{\mathrm{od}}_{ijal} - f^{\mathrm{od}}_{ak} \Gamma^{\mathrm{d}}_{ijal} \right) \right\} \\ &+ \frac{1}{2} \sum_{ab} \left(\Gamma^{\mathrm{d}}_{ijab} \Gamma^{\mathrm{od}}_{abkl} - \Gamma^{\mathrm{od}}_{ijab} \Gamma^{\mathrm{d}}_{abkl} \right) (1 - n_a - n_b) \\ &- \sum_{ab} (n_a - n_b)(1-P_{ij})(1-P_{kl}) \Gamma^{\mathrm{d}}_{bjal} \Gamma^{\mathrm{od}}_{aibk}. \end{aligned} \tag{3.43}$$

3.2.2 White's choice

White's choice [73] is also designed to suppress the off-diagonal part of a Hamiltonian, making numerical approaches much more efficient. First, consider the general expression of a Hamiltonian

$$H(s) = \sum_\alpha a_\alpha(s) h_\alpha, \tag{3.44}$$

where each h_α is a product of creation and annihilation operators, and $a_\alpha(s)$ is the corresponding coefficient.

Original definition

According to White, the generator for the flow equations is generally written as

$$\eta(s) = \sum_\alpha \eta_\alpha(s) h^{\mathrm{od}}_\alpha(s), \quad \text{where} \quad \eta_\alpha(s) = x_\alpha(s) a_\alpha(s). \tag{3.45}$$

The h^{od}_α is the operators that we want to eliminate.

As seen in the previous section, the flow by the Wegner's generator gives widely varying decaying speeds for different h^{od}_α, indicating that the flow equation becomes a stiff coupled differential equations, where one needs very large number of integration steps. In order to avoid this problem, White suggested a choice

$$x_\alpha(s) = (E^\alpha_L - E^\alpha_R)^{-1}, \tag{3.46}$$

with

$$E^\alpha_L = \langle L^\alpha | \, H \, | L^\alpha \rangle, \quad E^\alpha_R = \langle R^\alpha | \, H \, | R^\alpha \rangle. \tag{3.47}$$

Choosing the x_α as Eq (3.46), different operator terms h_α have similar decaying speed, therefore the flow equation is no longer stiff, making the convergence of the equation very first.

The left and right states, $|L^\alpha\rangle$ and $|R^\alpha\rangle$, are defined as follows. Considering the particle-hole transformation, we introduce a quasi-particle operators d and $d^\dagger$, which satisfy $d\,|\Phi_0\rangle = 0$. This operators by definition have the structure that $d_i^\dagger = a_i^\dagger$ for an unoccupied state i, and $d_i^\dagger = a_i$ for an occupied state i. Although large number of pairs of states $\langle L^\alpha|$ and $|R^\alpha\rangle$ can be connected by an operator term h_α , such that $\langle L|\, h_\alpha\, |R\rangle \neq 0$, we consider the pair of states that is closest to the reference state $|\Phi_0\rangle$, namely, is created by the fewest number operation of $d^\dagger$ on $|\Phi_0\rangle$. As a specific example, consider the h_α

$$h_\alpha = d_i^\dagger d_j d_k d_m, \tag{3.48}$$

then the most important pairs of states are

$$|R^\alpha\rangle = d_m^\dagger d_k^\dagger d_j^\dagger\, |\Phi_0\rangle\,, \quad |L^\alpha\rangle = d_i^\dagger\, |\Phi_0\rangle\,. \tag{3.49}$$

Note that the creation operators $d^\dagger$ in the interaction term are assigned for the left states, and annihilation operators d are assigned for the right states.

For nuclear system

We apply the White's definition to our case, nuclei. The operators which we want eliminate are

$$h_\alpha = \{p^\dagger h\}, \{h^\dagger p\}, \{p_1^\dagger p_2^\dagger h_2 h_1\} \text{ and } \{h_1^\dagger h_2^\dagger p_2 p_1\}. \tag{3.50}$$

These are divided into two classes. The $\{p^\dagger h\}$ and $\{p_1^\dagger p_2^\dagger h_2 h_1\}$ are products of $d^\dagger$-type operators, so assigned to the left state. On the other hand, the $\{h^\dagger p\}$ and $\{h_1^\dagger h_2^\dagger p_2 p_1\}$ are products of d-type operators, so assigned to the right state.

One-body generator: η_{ph} and η_{hp}

In this case the left and right states are defined as

$$|R\rangle = |\Phi_0\rangle \tag{3.51}$$

$$|L\rangle = \{p^\dagger h\}\, |\Phi_0\rangle\,, \quad \langle L| = \langle \Phi_0|\, \{h^\dagger p\}, \tag{3.52}$$

giving

$$E_{ph}^R(s) = \langle R|\, H\, |R\rangle = E_0(s) \tag{3.53}$$

$$E^L_{ph}(s) = \langle L| H |L\rangle \tag{3.54}$$
$$= E_0(s) + \sum_{ij} f_{ij} \langle \Phi_0| \{h^\dagger p\}\{i^\dagger j\}\{p^\dagger h\} |\Phi_0\rangle \tag{3.55}$$
$$+ \frac{1}{4}\sum_{ijkl} \Gamma_{ijkl} \langle \Phi_0| \{h^\dagger p\}\{i^\dagger j^\dagger lk\}\{p^\dagger h\} |\Phi_0\rangle \tag{3.56}$$
$$= E_0(s) + f_{pp} - f_{hh} - \Gamma_{phph}. \tag{3.57}$$

Hence, the energy denominator is $E^{\text{den}}_{ph} = E^L_{ph} - E^R_{ph} = f_{pp} - f_{hh} - \Gamma_{phph}$. Therefore, the generator is

$$\eta_{ph} = \frac{1}{f_{pp} - f_{hh} - \Gamma_{phph}} f_{ph}. \tag{3.58}$$

In the same manner, the generator η_{hp} can be written as

$$\eta_{hp} = \frac{1}{f_{hh} - f_{pp} + \Gamma_{phph}} f_{hp}. \tag{3.59}$$

Two-body generator: $\eta_{pp'hh'}$ and $\eta_{hh'pp'}$

The left and right states are defined as

$$|R\rangle = 0 \tag{3.60}$$
$$|L\rangle = \{p^\dagger p'^\dagger h' h\} |\Phi_0\rangle, \quad \langle L| = \langle \Phi_0| \{h^\dagger h'^\dagger p' p\}. \tag{3.61}$$

Therefore,

$$E^R_{pp'hh'}(s) = \langle R| H |R\rangle = E_0(s) \tag{3.62}$$
$$E^L_{pp'hh'}(s) = \langle L| H |L\rangle \tag{3.63}$$
$$= E_0(s) + \sum_{ij} f_{ij} \langle \Phi_0| \{h^\dagger h'^\dagger p' p\}\{i^\dagger j\}\{p^\dagger p'^\dagger h' h\} |\Phi_0\rangle \tag{3.64}$$
$$+ \frac{1}{4}\sum_{ijkl} \Gamma_{ijkl} \langle \Phi_0| \{h^\dagger h'^\dagger p' p\}\{i^\dagger j^\dagger lk\}\{p^\dagger p'^\dagger h' h\} |\Phi_0\rangle \tag{3.65}$$
$$= E_0(s) + f_{pp} + f_{p'p'} - f_{hh} - f_{hh'} \tag{3.66}$$
$$+ \Gamma_{pp'pp'} + \Gamma_{hh'hh'} \underline{- \Gamma_{phph} - \Gamma_{ph'ph'} - \Gamma_{p'hp'h} - \Gamma_{p'h'ph}}. \tag{3.67}$$
$$\equiv E_0(s) + f_{pp} + f_{p'p'} - f_{hh} - f_{h'h'} + \underline{A_{pp'hh'}} \tag{3.68}$$

Thus, the generator is

$$\eta_{pp'hh'} = \frac{1}{f_{pp} + f_{p'p'} - f_{hh} - f_{h'h'} + A_{pp'hh'}} \Gamma_{pp'hh'} \tag{3.69}$$

Similarly, the generator $\eta_{hh'pp'}$ is

$$\eta_{hh'pp'} = \frac{1}{-f_{pp} - f_{p'p'} + f_{hh} + f_{h'h} - A_{hh'pp'}} \Gamma_{hh'pp'} = -\eta_{pp'hh'}. \tag{3.70}$$

In the end, the White's generator is written as

$$\eta^{\mathrm{II}} = \sum_{ph} \frac{f_{ph}\,\{a_p^\dagger a_h\}}{f_p - f_h - \Gamma_{phph}} - \text{h.c.} + \sum_{pp'hh'} \frac{\Gamma_{pp'hh'}\,\{a_p^\dagger a_{p'}^\dagger a_{h'} a_h\}}{f_p + f_{p'} - f_h - f_{h'} + A_{pp'hh'}} - \text{h.c.}\,, \tag{3.71}$$

where

$$A_{pp'hh'} = \Gamma_{pp'pp'} + \Gamma_{hh'hh'} - \Gamma_{phph} - \Gamma_{p'h'p'h'} - \Gamma_{ph'ph'} - \Gamma_{p'hp'h} \tag{3.72}$$

and $f_p \equiv f_{pp}$ (the s-dependence is suppressed for simplicity).

In J-coupled scheme

In White's generator, matrix elements of the two-body operators appear in the denominators. It is not so clear that these matrix elements can be written in J-coupled scheme. One can in fact define the White's generator in the J-coupled scheme, by introducing the monopole term of the interaction matrix elements. We re-write the energy denominator in the generator $E_\alpha^{\mathrm{den}} = E_\alpha^L - E_\alpha^R$, as

$$E_{ph}^{\mathrm{den}} = \frac{1}{(2j_p+1)(j_h+1)} \sum_{m_p m_h} E_{ph}^{\mathrm{den}}, \tag{3.73}$$

$$E_{pp'hh'}^{\mathrm{den}} = \frac{1}{(2j_p+1)(2j_{p'}+1)(2j_h+1)(2j_{h'}+1)} \sum_{m_p m_{p'} m_h m_{h'}} E_{pp'hh'}^{\mathrm{den}}. \tag{3.74}$$

These energy denominators can be expressed by the monopole matrix element of operators. For example, Eq. (3.73) can be written

$$E_{ph}^{\mathrm{den}} = g_{pp} - g_{hh} - \frac{1}{(2j_p+1)(2j_h+1)} \sum_{m_p m_h} \sum_{JM} (j_p m_p j_h m_h | JM)^2 \tilde{\Gamma}^J_{phph} \tag{3.75}$$

$$= g_{pp} - g_{hh} - \tilde{\Gamma}^{\mathrm{m}}_{ph}, \tag{3.76}$$

where

$$\tilde{\Gamma}^{\mathrm{m}}_{ph} := \frac{\sum_J (2J+1)\tilde{\Gamma}^J_{phph}}{\sum_J (2J+1)}. \tag{3.77}$$

3.2.3 Heidbrink's choice

Heidbrink's choice [78] is designed for a Hamiltonian which has block-band structure with respect to a certain counting operator q. The counting operator means that the eigenvalues of the operator q are non-negative integers. We consider the operator q which counts the number of excitation from the reference state $|\Phi_0\rangle$, *i.e.*, the number of particles above the Fermi sea and holes bellow the Fermi sea,

$$q = \sum_i q_i \{a_i^\dagger a_i\} = \sum_{i \in \mathcal{M}_p} a_i^\dagger a_i + \sum_{i \in \mathcal{M}_h} a_h a_h^\dagger, \tag{3.78}$$

where $\mathcal{M}_p$ and $\mathcal{M}_h$ denote the whole of particle and hole state, respectively, and $q_i = \mathrm{sign}(\varepsilon_i - \varepsilon_F)$. A general nuclear Hamiltonian H has this block-diagonal structure, observing that the H changes the eigenvalue of q at maximum by a finite value $M < \infty$. The H connects two eigenstates of q, $|i\rangle$ and $|j\rangle$, only if the difference between their eigenvalues is at most M, *i.e.* $|q_i - q_j| < M$. For instance, the one-body part of H changes the eigenvalue of q by at most 2, so $M = 2$. Likewise, two-body part has $M = 4$ with Γ_{pphh} and Γ_{hhpp}.

We then define the generator in the form of the matrix elements as

$$\eta_{ij}^{III}(a) := \mathrm{sign}(q_i(s) - q_j(s)) H_{ij}(s). \tag{3.79}$$

The state $|i\rangle$ denotes either one- or two-body state. With this definition the flow equation becomes

$$\frac{d}{ds} H_{ij} = -\mathrm{sign}(q_i - q_j)(H_{ii} - H_{jj}) H_{ij} + \sum_{a \neq i,j} \{\mathrm{sign}(q_i - q_a) + \mathrm{sign}(q_j - q_a)\} H_{ia} H_{aj}. \tag{3.80}$$

This generator preserves the block-band structure as observed in the flow equation. It is shown in ref [79] that this generator drives the Hamiltonian toward the block diagonal $[q, H(\infty)] = 0$ as long as the spectrum of the finite (or semi-infinite) Hamiltonian is bounded from the below.

3.2.4 Decoupling of the ground state

All generators introduced in the previous sections suppress off-diagonal ($1p1h$ and $2p2h$) couplings and drive the Hamiltonian towards diagonal form,

$$H(\infty) = E_0(\infty) + f^{\mathrm{d}}(\infty) + \Gamma^{\mathrm{d}}(\infty)\,, \tag{3.81}$$

but White's generator (η^{II}) is significantly more efficient, because the flow equations are less stiff in this case and the evaluation of η at each step is significantly faster. The evolved

Hamiltonians using η^{I}, η^{II} and η^{III} are unitarily equivalent if no truncations are made. Any differences in energy eigenvalues therefore provide a measure of the truncation error resulting from neglected three- and higher-body normal-ordered terms in our calculations.

At the end of the flow, the reference state becomes the ground state of $H(\infty)$, with fully interacting ground-state energy $E_0(\infty)$, and $|\Phi_0\rangle$ decouples from the rest of the Hilbert space ($1p1h, 2p2h, \ldots, ApAh$ sectors),

$$QH(\infty)P = 0 \quad \text{and} \quad PH(\infty)Q = 0\,, \tag{3.82}$$

where $P = |\Phi_0\rangle\langle\Phi_0|$ and $Q = 1 - P$. This decoupling follows from the observation that all other normal-ordered couplings annihilate the reference state, $(f^{\mathrm{d}}(s) + \Gamma^{\mathrm{d}}(s))|\Phi_0\rangle = 0$. Combined with $f^{\mathrm{od}}(\infty)$ and $\Gamma^{\mathrm{od}}(\infty)$ being driven to zero, this implies the block-diagonal structure of Eq. (3.82). This can be understood in a different way by the counting operator defined in Eq. (3.78). If it is true that

$$[q, H(\infty)] = 0, \tag{3.83}$$

then it means the evolved Hamiltonian is block diagonal with respect to the ph excitation for the reference state. In the current case, Eq (3.83) is no longer true, but one can derive

$$\forall n > 0; \langle npnh|\, H(\infty)\, |\Phi_0\rangle = 0, \tag{3.84}$$

by showing the relation

$$\begin{aligned} qH(\infty)\,|\Phi_0\rangle &= [q, H(\infty)]\,|\Phi_0\rangle \\ &= \left(2\sum_{ph} f_{ph}(\infty)a_p^\dagger a_h + \sum_{pp'hh'} \Gamma_{pp'hh'}(\infty)a_p^\dagger a_{p'}^\dagger a_{h'} a_h\right)|\Phi_0\rangle = 0, \end{aligned} \tag{3.85}$$

since the f_{ph} and $\Gamma_{pp'hh'}$ belong to the H^{od}, thus are eliminated during the flow by construction.

If one chooses more strict generator, namely defines more terms as H^{od} and makes then suppressed during the flow, then in some cases Eq (3.83) can be satisfied, meaning

$$\forall m, n\ (m \neq n); \langle npnh|\, H(\infty)\, |mpmh\rangle = 0. \tag{3.86}$$

In such cases, the evolved Hamiltonian has much simpler structure and the following many-body problem is easier to solve. However, this kind of stringent choice of the generator,

or "large-angle" rotation in the language of White, may generate larger amount of three- and higher-body interactions, making the truncation error larger. Our current choice of the generator is the minimal possible condition under which the Eq. (3.84) is achieved. The IM-SRG is very flexible and alternative choices of $H^{\rm od}$ (and η) can be used to target excited states, single-particle properties, and to construct effective valence shell-model Hamiltonians and operators for open-shell systems [72, 73].

Chapter 4

Comparison of the IM-SRG to other many-body methods

In this chapter, we investigate the perturbative solutions for the IM-SRG flow equations in order to discuss the connection to the other many-body theories and make a systematic improvement of the IM-SRG flow equation. We first briefly explain typical many-body methods successfully applied in nuclear physics, including the coupled-cluster (CC) theories [9, 10, 11, 12, 13, 14, 15, 16, 17, 18, 19, 20] and the many-body perturbation theory (MBPT) [22, 23, 24]. Then we demonstrate the connection between the IM-SRG and the many-body methods, by solving the IM-SRG flow equation perturbatively.

4.1 Coupled-Cluster theory

We give a brief outline of the coupled-cluster (CC) method for ground-state of the close-shell nuclei. The nuclear many-body problems start from the Schrödinger equation

$$H|\Psi_\lambda\rangle = E_\lambda|\Psi_\lambda\rangle. \tag{4.1}$$

The CC method starts with the assumption for the ground-state eigenfunction of the full problem Eq. (4.1) with mass number A as

$$|\Psi_0\rangle = e^T\,|\Phi_0\rangle\,, \tag{4.2}$$

where the particle-hole cluster operator

$$T = \sum_{k=1}^{A} T_k \tag{4.3}$$

$$T_k = \frac{1}{(k!)^2} \sum_{i_1 \cdots i_k; a_1 \cdots a_k} t_{i_1 \cdots i_k}^{a_1 \cdots a_k} a_{a_1}^\dagger \cdots a_{a_k}^\dagger a_{i_k} \cdots a_{i_1}. \tag{4.4}$$

The indices $i, j, \cdots$ denote the occupied s.p. orbitals and the $a, b, \cdots$ denote the unoccupied s.p. orbitals. Therefore, the operator T_k generates kp-kh excited state with respect to the reference state $|\Phi_0\rangle$. The ground-state energy and the cluster operators are obtained by operating the inverse of the exponential operator e^{-T} on the Schrödinger equation of Eq. (4.1) and multiplying, from the left, the reference state $\langle\Phi_0|$, and the kp-kh excited states $\left\langle \Phi_{i_1 \cdots i_k}^{a_i \cdots a_k} \right|$, respectively.

$$\langle\Phi_0| e^{-T} H e^T |\Phi_0\rangle = E_0 \tag{4.5}$$

$$\left\langle \Phi_{i_1 \cdots i_k}^{a_1 \cdots a_k} \right| e^{-T} H e^T |\Phi_0\rangle = 0 \quad (k = 1, \cdots, A). \tag{4.6}$$

Note that $\langle\Phi_0|\Phi_0\rangle = 1$ and $\left\langle \Phi_{i_1 \cdots i_k}^{a_1 \cdots a_k} | \Phi_0 \right\rangle = 0$. As seen in Eq. (4.6), one can understand that what the CC method does is to obtain the similarity transformation of the Hamiltonian $\bar{H} = e^{-T} H e^T$, as a consequence of which the transformed Hamiltonian has vanishing coupling between the reference state and kp-kh excited states. This is quite similar to the decoupling condition that is introduced in the IM-SRG in Chapter 3.2.

Usually, the cluster operator (4.3) is truncated at single- and double-excitation operator level, *i.e.*, $T \cong T_1 + T_2$, and this approximation is called CCSD. Similarly, the truncation up to the triple-excitation operators is called the CCSDT. The similarity transformed Hamiltonian $\bar{H}$ can be calculated with Campbell-Baker-Hausdorff expansion,

$$\bar{H} = e^{-T} H e^T = H + [H, T] + \frac{1}{2!}[[H, T], T] + \frac{1}{3!}[[[H, T], T], T] + \cdots. \tag{4.7}$$

This expansion in fact terminates exactly at finite terms because the commutator between Hamiltonian and a cluster operator eliminates one of the creation or annihilation operator in the Hamiltonian, and the cluster operators commute with each other. For example, if the Hamiltonian contains at most two-body interactions, then the Hausdorff expansion terminates at fourfold-nested commutators. Similarly, the expansion terminates at sixfold-nested commutators for three-body Hamiltonians.

Due to this convenient feature, one obtains analytic expressions for the CC energy and amplitude equations Eq. (4.5) and (4.6). The commutator form of the equation guarantee that every cluster operators are connected to the Hamiltonian, therefore the CC theory is intrinsically size-extensive. This is also the similar point to the IM-SRG, where the flow equation is constructed by commutator form.

The inclusion of the triple-excitation operator, that is CCSDT, makes the CC equations unfeasible in the viewpoint of the computational costs, thus the triple corrections are included perturbatively. This is called the CCSD(T), where the perturbative triple correction is constructed so that it can contain the fourth and higher-order perturbation terms for the ground state. Along this line, the most accurate approximation so far is the Λ-CCSD(T).

4.2 Many-body perturbation theory

The many-body perturbation theory starts with an arbitral mean field, by writing the Hamiltonian in Eq. (4.1) as

$$H = T + V = (T + U) + (V - U) \equiv H_0 + H_1. \tag{4.8}$$

T is the kinetic energy and V a nucleon-nucleon interaction. The eigenfunctions Φ_i of H_0 are used, as a basis, for the expansion of the eigenfunction $|\Psi_\lambda\rangle$ of H. Thus, it is conventional to choose an arbitrary auxiliary one-body potential U which has an convenient mathematical form, typically harmonic oscillator potential is used.

4.2.1 Ground state

We first outline the perturbative expansion for the ground state.

The Gell-Mann and Low theorem [80] results in the expression of the ground state of the system E_0, as

$$E_0 - W_0 = \frac{\langle\Phi_0|\, H_1\, |\Psi_0\rangle}{\langle\Phi_0|\Psi_0\rangle} = \lim_{\varepsilon\to 0} \frac{\langle\phi_0|\, H_1 U_\varepsilon(0,-\infty)\, |\Phi_0\rangle}{\langle\Phi_0|\, U_\varepsilon(0,-\infty)\, |\Phi_0\rangle}, \tag{4.9}$$

where the time-development operator $U_\varepsilon(t,t')$ is defined as

$$U_\varepsilon(t,t') = \sum_{n=0}^{\infty} \left(\frac{-1}{\hbar}\right)^n \frac{1}{n!} \int_{t'}^{t} dt_1 \cdots \int_{t'}^{t} dt_n e^{-\varepsilon(|t_1|+\cdots|t_n|)} T[H_1(t_1)\cdots H_1(t_n)], \tag{4.10}$$

and the W_n are the eigenvalue of unperturbed state, $H_0\,|\Phi_n\rangle = W_n\,|\Phi_n\rangle$. Goldstone proved [81] that the disconnected diagrams, which diverges like ε^{-1} as $\varepsilon \to 0$, exactly cancel between the denominator and the numerator in Eq. (4.9), and derived the energy shift as

$$E_0 - W_0 = \sum_{n=0}^{\infty} \langle\Phi_0|\, H_1 \left(\frac{1}{W_0 - H_1} H_1\right)^n |\Phi_0\rangle_L\,, \tag{4.11}$$

known as the Goldstone's theorem or the linked-cluster expansion. By inserting the complete set of the eigenstates of the unperturbed Hamiltonian H_0, the theorem (4.11) can be understood as a restatement of the Rayleigh-Schrödinger perturbation theory for the ground state $|\Phi_0\rangle$,

$$E_0 - W_0 = \langle\Phi_0| H_1 |\Phi_0\rangle + \sum_{n\neq 0} \frac{\langle\Phi_0| H_1 |\Phi_n\rangle \langle\Phi_n| H_1 |\Phi_0\rangle}{W_0 - W_n} + \cdots . \tag{4.12}$$

This will be compared to the result of the IM-SRG later.

4.2.2 Effective interactions for a model space

We briefly explain a typical method that is widely used to construct effective interactions for nucleon in a given model space [22, 82, 23, 24].

Since only a few low-lying states are generally of physical interest, we formulate the problem in terms of an effective Hamiltonian acting in a strongly truncated Hilbert space, i.e. a model space with a finite number of states. We define projection operators P which project the complete Hilbert space onto the model space, and its complement Q.

$$P = \sum_{i=1}^{d} |\Phi_i\rangle\langle\Phi_i|, \quad Q = \sum_{i=d+1}^{\infty} |\Phi_i\rangle |\Phi_i\rangle , \tag{4.13}$$

where $H_0 |\Phi_i\rangle = \varepsilon_i |\Phi_i\rangle$. Using P, one can formally reduce the original eigenvalue problem in Eq. (4.1) to that in the model space, such as

$$PH_{\text{eff}}P|\Psi_\lambda\rangle = E_\lambda P|\Psi_\lambda\rangle. \tag{4.14}$$

Now we define the projection of the exact eigenstate onto the model space state as $P|\Psi_\lambda\rangle = |\phi_\lambda\rangle$. At the same time, we define the wave operator Ω, which transforms the model-space projection $|\phi_\lambda\rangle$ back into the original state $|\Psi_\lambda\rangle$, namely, $|\Psi_\lambda\rangle = \Omega|\phi_\lambda\rangle$. In order for this to be possible, it should be assumed that there is a one-to-one correspondence between the states $|\Psi_\alpha\rangle$ and $|\phi_\lambda\rangle$. Assuming that the wave operator has an inverse, one can construct a similarity transformation of the Hamiltonian $\mathcal{H} = \Omega^{-1}H\Omega$ so that

$$\Omega^{-1}H\Omega\Omega^{-1}|\Psi_\lambda\rangle = E_\lambda\Omega^{-1}|\Psi_\lambda\rangle . \tag{4.15}$$

This can be re-written by using $\mathcal{H} = P\mathcal{H}P + P\mathcal{H}Q + Q\mathcal{H}P + Q\mathcal{H}Q$ as,

$$(P\mathcal{H}P + Q\mathcal{H}P)|\phi_\lambda\rangle = E_\lambda|\phi_\lambda\rangle . \tag{4.16}$$

If the relation

$$Q\mathcal{H}P = 0 \tag{4.17}$$

is satisfied, then the Eq. (4.16) is defined purely in the model space as $P\mathcal{H}P\,|\phi_\lambda\rangle = E_\lambda\,|\phi_\lambda\rangle$. This means that one can define a model-space effective Hamiltonian as

$$H_{\text{eff}} = P\mathcal{H}P = P\Omega^{-1}H\Omega P. \tag{4.18}$$

Therefore, what one has to do is to obtain a proper Ω which satisfies the condition (4.17). One typical way to obtain Ω is to assume it as

$$\Omega = 1 + \chi. \tag{4.19}$$

The χ is known as the correlation operator. Since $P\Omega P = P$, the χ has properties as below,

$$P\chi P = 0, \quad Q\Omega P = Q\chi P. \tag{4.20}$$

Since the wave operator Ω only acts on the model-space state from the left, the ΩQ does not appear, thus one can add $Q\chi Q = P\chi Q = 0$. In the end, the correlation operator has the property

$$\chi = Q\chi P. \tag{4.21}$$

Inserting the Ω into Eq. (4.17) yields

$$QHP - \chi HP + QH\chi - \chi H\chi = 0 \tag{4.22}$$

In most of the theories for an effective interaction in nuclear physics, the model space is considered to be degenerate,

$$PH_0P = \omega P, \tag{4.23}$$

where ω is the eigenvalue of the unperturbed states in the model space. Then Eq. (4.22) becomes

$$(\omega - QH_0Q - QH_1Q)\chi = QH_1P - \chi PH_1P - \chi PH_1Q\chi. \tag{4.24}$$

The effective Hamiltonian can be written (considering $\Omega^{-1} = 1 - \chi$),

$$H_{\text{eff}} = P(1-\chi)H(1+\chi) = PHP + PH\xi =: PH_0P + V_{\text{eff}}(\chi), \tag{4.25}$$

where $V_{\rm eff}(\chi) = PH_1P + PHQ\chi P$. Using the $V_{\rm eff}(\chi)$, Eq. (4.24) can be written as

$$V_{\rm eff}(\chi) = Q(\omega) - PH_1\frac{1}{\omega - QHQ}\chi V_{\rm eff}(\chi). \tag{4.26}$$

Here, we the $Q(\omega)$ is called the Q-box and defined as

$$Q(\omega) := PH_1P + PH_1Q\frac{1}{\omega - QHQ}QH_1P. \tag{4.27}$$

The projection operator Q should be distinguished from the Q-box. The Q-box can be understood as the sum of all the diagrams that have at least one H_1-vertex and are irreducible (i.e. contain at least one passive line(Q-space state) between two successive vertices) and valence-linked (i.e. have all the vertices linked to at least one valence line). Clearly, this is a non-linear equation for χ and there are several ways to solve Eq. (4.22). In fact, many iterative scheme have been developed [35,23]. We here follow the scheme by Kuo and Krenciglowa [23]. The structure of the effective interaction can be written as

$$V_{\rm eff} = \hat{Q} - \hat{Q}'\int\hat{Q} + \hat{Q}'\int\hat{Q}\int\hat{Q} - \cdots. \tag{4.28}$$

$\hat{Q}'$ is at least second order in the interaction H_1, while $\hat{Q}$ starts with first order terms. The $\int$ signs represent the folding operation[*1] and this operation can be described in terms of the energy derivative of $\hat{Q}$-box, like

$$-\hat{Q}'\int\hat{Q} = \frac{d\hat{Q}(\omega)}{d\omega}\hat{Q}(\omega), \tag{4.29}$$

where ω is a starting energy, that is, the sum of the energies of incoming particles. The general expression for an n-folded $\hat{Q}$-box is

$$\hat{Q} - \hat{Q}'\int\hat{Q} + \hat{Q}'\int\hat{Q}\int\hat{Q} - \cdots = \sum_{k_1\cdots k_n}\frac{1}{k_1!}\frac{d^{k_1}\hat{Q}'}{d\omega^{k_1}}P\frac{1}{k_2!}\frac{d^{k_2}\hat{Q}}{d\omega^{k_2}}P\cdots\frac{1}{k_n!}\frac{d^{k_n}\hat{Q}}{d\omega^{k_n}}P\hat{Q}, \tag{4.30}$$

under the constraint

$$k_1 + \cdots k_n = n, \quad k_1 \geq 1, \quad k_l \leq n - l + 1. \tag{4.31}$$

One possible solution can be obtained by the iteration

$$V_{\rm eff}^{(n)} = \hat{Q} + \sum_{k=1}^{\infty}\frac{1}{k!}\frac{d^k\hat{Q}'}{d\omega^k}\left\{V_{\rm eff}^{(n-1)}\right\}^k, \qquad V_{\rm eff}^{(0)} = \hat{Q}. \tag{4.32}$$

This expansion is used in our calculations. Note that even if a non-folded Q-box itself has only include low-order terms, like second or third, the expansion in terms of the Q-box generates higher-order terms in principle to infinite order through the resummation of interaction vertices by folded diagrams.

[*1] $\hat{Q}$-boxes and the folding operation are introduced in the context of the decomposition procedure.

4.3 Perturbative solution of the IM-SRG

In this section, we perturbatively solve the IM-SRG flow equation by expanding the Hamiltonian in terms of the bare coupling of interaction in the initial Hamiltonian. The perturbative solutions in each order are compared to the many-body perturbation theory (MBPT). We apply the generator

$$\eta(s) = [f^d(s), H(s)] = [f^d(s), f^{od}(s) + \Gamma(s) + W(s)], \tag{4.33}$$

which by definition is supposed to eliminate the energy off-diagonal interactions during the flow. Although this choice is different from the one we will apply for realistic cases, the generator (4.33) still provides the general structure of the flow equation, therefore is enough to demonstrate the connection to the MBPT. The matrix elements of the generator are given by

$$\eta^{(1)}_{ij}(s) = \sum_a (1 - P_{ij}) f^d_{ia} f^{od}_{aj} - \sum_{ab} (n_a - n_b) f_{ab} \Gamma_{biaj} \tag{4.34}$$

$$\begin{aligned} \eta^{(2)}_{ijkl}(s) = &\sum_a \left[(1 - P_{ij}) f_{ia} \Gamma_{ajkl} - (1 - P_{kl}) f_{ak} \Gamma_{ijal} \right] \\ &+ \sum_{ab} (n_a - n_b) f_{ab} W_{bijakl} \end{aligned} \tag{4.35}$$

$$\eta^{(3)}_{ijklmn}(s) = \sum_a \{ P(i/jk) f_{ia} W_{ajklmn} - P(l/mn) f_{al} W_{ijkamn} \} \tag{4.36}$$

We make a perturbative expansion for the Hamiltonian in terms of the bare coupling g as

$$E_0(s) = E_0^{[0]}(s) + g E_0^{[1]}(s) + g^2 E_0^{[2]}(s) + g^3 E_0^{[3]}(s) + \cdots \tag{4.37}$$

$$f_{ij}(s) = f_{ij}^{[0]}(s) + g f_{ij}^{[1]}(s) + g^2 f_{ij}^{[2]}(s) + g^3 f_{ij}^{[3]}(s) + \cdots \tag{4.38}$$

$$\Gamma_{ijkl}(s) = g \Gamma_{ijkl}^{[1]} + g^2 \Gamma_{ijkl}^{[2]} + g^3 \Gamma_{ijkl}^{(3)} + \cdots . \tag{4.39}$$

$$W_{ijklmn}(s) = g^2 W_{ijklmn}^{[2]} + g^3 W_{ijklmn}^{[3]} + \cdots \tag{4.40}$$

We use the square parenthesis at the superscript to denote the order of perturbation with respect to the bare coupling, while we use the normal parenthesis $X^{(i)}$ to denote that the operator X is i-body one. Thus, $X^{(i)[j]}$ means that the operator X is i-body and j-th order in the bare coupling. Regarding the power of the three-body interactions, it is naturally understood that it starts with the $\mathcal{O}(g^3)$ term if the initial Hamiltonian contains up to two-body interaction. If one also considers three-body interactions for the initial Hamiltonian,

this counting may not be the case. However, At least modern theories for three-nucleon forces have shown the hierarchy of the strength that three-body forces are one order weaker than two-body forces, including χEFT [7] and the three-body forces used for *ab-initio* calculations [27, 28, 29, 30, 31]. Thus the assumption of the order for the three-body terms is reasonable. We assume that the one-body terms in the initial Hamiltonian are diagonal at the leading order,

$$f_{ij}^{[0]}(s) = \delta_{ij}\varepsilon_i, \tag{4.41}$$

namely, we start with the self-consistent mean field like Hartree-Fock. The boundary condition for the differential equation is given as

$$E_0^{[0]}(0) = E^{\mathrm{HF}}, \qquad E_0^{[n]}(0) = 0 \quad (n \geq 1) \tag{4.42}$$

$$f_{ij}^{[0]}(0) = \delta_{ij}\varepsilon_i, \qquad f_i^{[n]}(0) = 0 \quad (n \geq 1) \tag{4.43}$$

$$\Gamma_{ijkl}^{[1]}(0) = V_{ijkl}, \qquad \Gamma_{ijkl}^{[n]}(0) = 0 \quad (n \geq 1). \tag{4.44}$$

By solving the flow equation order-by-order, one gets the perturbative solution for the in-medium SRG.

4.3.1 The flow equation at $\mathcal{O}(1)$

Since the zeroth-order generator is zero

$$\eta^{[0]}(s) = 0, \tag{4.45}$$

the flow equation is trivially given by

$$\dot{H} = 0. \tag{4.46}$$

Therefore

$$E_0(s) = E^{\mathrm{HF}}, \qquad f_{ij}^{[0]}(s) = \delta_{ij}\varepsilon_i, \qquad \Gamma^{[0]}(s) = W^{[0]}(s) = 0. \tag{4.47}$$

4.3.2 The flow equation at $\mathcal{O}(g)$

The first-order generator is given by

$$\eta_{ij}^{(1)[1]}(s) = \Delta_{ij} f_{ij}^{od,[1]}(s), \qquad \eta_{ijkl}^{(2)[1]}(s) = \Delta_{ijkl}\Gamma_{ijkl}^{[1]}(s)\,, \text{ and} \qquad \eta^{(3)[1]}(s) = 0, \tag{4.48}$$

where the Δ's denote the energy difference of the s.p. energy,

$$\begin{aligned}\Delta_{ij} &:= \varepsilon_i - \varepsilon_j \\ \Delta_{ijkl} &:= \varepsilon_i + \varepsilon_j - \varepsilon_k - \varepsilon_l \\ \Delta_{ijklmn} &:= \varepsilon_i + \varepsilon_j + \varepsilon_k - \varepsilon_l - \varepsilon_m - \varepsilon_n.\end{aligned} \tag{4.49}$$

Therefore, the flow equation becomes

$$\dot{E}_0^{[1]}(s) = 0, \quad \Rightarrow \quad E_0^{[1]}(s) = 0 \tag{4.50}$$

$$\dot{f}_{ij}^{[1]}(s) = \begin{cases} 0 & (i=j) \\ -\Delta_{ij}^2 f_{ij}^{od,[1]} & (i \neq j) \end{cases} \Rightarrow f_i^{[1]}(s) = \begin{cases} 0 & (i=j) \\ f_{ij}^{od,[1]}(0) e^{-\Delta_{ij}^2 s} = 0 & (i \neq j) \end{cases}. \tag{4.51}$$

Thus

$$f^{[1]}(s) = 0, \quad \eta^{(1)[1]}(s) = 0, \tag{4.52}$$

meaning there is no non-vanishing one-body term at the order $\mathcal{O}(g)$.

$$\dot{\Gamma}_{ijkl}^{[1]}(s) = -\Delta_{ijkl}^2 \Gamma_{ijkl}^{[1]}(s),$$

which simply gives

$$\Gamma_{ijkl}^{[1]}(s) = \Gamma_{ijkl}^{[1]}(0) e^{-\Delta_{ijkl}^2 s} = V_{ijkl} e^{-\Delta_{ijkl}^2 s}. \tag{4.53}$$

The Eq. (4.53) shows that the energy off-diagonal interaction terms decay according to the exponential with the speed of Δ_{ijkl}. This also demonstrates that the far off-diagonal terms are eliminated with higher priority as anticipated for the Wegner's generator.

4.3.3 The flow equation at $\mathcal{O}(g^2)$

The constant term

We start with the constant term in the Hamiltonian.

$$\begin{aligned}\dot{E}_0^{[2]}(s) &= \frac{1}{2} \sum_{ijkl} n_i n_j \bar{n}_k \bar{n}_l \Delta_{ijkl} |\Gamma_{ijkl}^{[1]}(s)|^2 \\ &= \frac{1}{2} \sum_{ijkl} n_i n_j \bar{n}_k \bar{n}_l \Delta_{ijkl} |V_{ijkl}|^2 e^{-2\Delta_{ijkl}^2 s} \qquad (4.54) \\ \Rightarrow E_0^{[2]}(s) &= \frac{1}{4} \sum_{ijkl} n_i n_j \bar{n}_k \bar{n}_l \frac{|V_{ijkl}|^2}{\Delta_{ijkl}} \left\{ 1 - e^{-2\Delta_{ijkl}^2 s} \right\}. \qquad (4.55)\end{aligned}$$

The limit of $s \to \infty$ of Eq. (4.55) exactly corresponds to the many-body perturbation theory at the second order.

The one-body terms

Using the relation

$$\eta_{ij}^{(1)[2]} = \Delta_{ij} f_{ij}^{od,[2]} = \Delta_{ij} f_{ij}^{[2]} \tag{4.56}$$

the one-body flow equation is

$$\begin{aligned}\dot{f}_{ij}^{[2]}(s) &= -\Delta_{ij}^2 f_{ij}^{[2]} + \frac{1}{2}\sum_{abc}(\bar{n}_a\bar{n}_b n_c + n_a n_b \bar{n}_c)(\eta_{ciab}^{(2)[1]}\Gamma_{abcj}^{[1]} - \Gamma_{ciab}\eta_{abcj}^{(2)}) \\ &= -\Delta_{ij}^2 f_{ij}^{[2]} + \frac{1}{2}\sum_{abc}(\bar{n}_a\bar{n}_b n_c + n_a n_b \bar{n}_c)(\Delta_{ciab} + \Delta_{cjab})V_{ciab}V_{abcj}e^{-(\Delta_{ciab}^2+\Delta_{abcj}^2)s}\end{aligned} \tag{4.57}$$

With the aid of the well-known expression for a general solution of an ordinary differential equation (ODE),

$$\dot{y}(t) + P(t)y(t) = Q(t) \tag{4.58}$$

$$\Rightarrow y(t) = \left[y(0) + \int_0^t Q(t')e^{\int_0^{t'} P(t'')dt''}dt'\right] e^{-\int_0^t P(t')dt'}, \tag{4.59}$$

the one-body terms can be integrated as

$$\begin{aligned}f_{ij}^{[2]}(s) &= e^{-\Delta_{ij}^2 s}\left[f_{ij}^{[2]}(0) + \int_0^\infty e^{\Delta_{ij}^2 z}\frac{1}{2}\sum_{abc}(\bar{n}_a\bar{n}_b n_c + n_a n_b\bar{n}_c)(\Delta_{ciab}+\Delta_{cjab})V_{ciab}V_{abcj}e^{-(\Delta_{ciab}^2+\Delta_{abcj}^2)z}dz\right] \\ &= \frac{1}{2}e^{-\Delta_{ij}^2 s}\sum_{abc}(\bar{n}_a\bar{n}_b n_c + n_a n_b\bar{n}_c)(\Delta_{ciab}+\Delta_{cjab})V_{ciab}V_{abcj}\int_0^\infty e^{-2\Delta_{ciab}\Delta_{cjab}z}dz \\ &= \frac{1}{2}e^{-\Delta_{ij}^2 s}\sum_{abc}(\bar{n}_a\bar{n}_b n_c + n_a n_b\bar{n}_c)V_{ciab}V_{abcj} \\ &\quad\cdot\left[\Delta_{ij}s\,(-\delta_{ciab}+\delta_{cjab}) + \frac{\bar{\delta}_{ciab}\bar{\delta}_{cjab}}{2}\left(\frac{1}{\Delta_{ciab}}+\frac{1}{\Delta_{cjab}}\right)(1-e^{-2\Delta_{ciab}\Delta_{cjab}s})\right],\end{aligned} \tag{4.60}$$

where, we define

$$\delta_X := \begin{cases}1 & \text{if} \quad \Delta_X = 0 \\ 0 & \text{others}\end{cases} \quad \text{and} \quad \bar{\delta}_X = 1 - \delta_X, \tag{4.61}$$

and the relation

$$\Delta_{ij}^2 - \Delta_{ciab}^2 - \Delta_{cjab}^2 = -2\Delta_{ciab}\Delta_{cjab} \tag{4.62}$$

is used. The Eq. (4.60) clearly show that the off-diagonal parts get suppressed exponentially as the flow parameter s increases. In the $s \to \infty$ limit, one gets

$$\lim_{s\to\infty} f_{ij}^{[2]}(s) = \begin{cases}0 & (\varepsilon_i \neq \varepsilon_j) \\ \frac{1}{2}\sum\limits_{abc;\Delta_{ciab}\neq 0}(\bar{n}_a\bar{n}_b n_c + n_a n_b\bar{n}_c)\dfrac{V_{ciab}V_{abcj}}{\Delta_{ciab}} & (\varepsilon_i = \varepsilon_j)\end{cases}. \tag{4.63}$$

The second line in the Eq. (4.63) is the 2p1h and 1p2h contribution for the single-particle energy in the second-order non-folded Q-box $Q^{(2)}(\omega)$.

The two-body terms

Since the three-body operators $\eta^{(3)}$ and W are at least the second order in the bare coupling, $\mathcal{O}(g^2)$, these terms don't contribute to the flow equation. Using that $\eta^{(2)[2]}_{ijkl} = \Delta_{ijkl}\Gamma^{[2]}_{ijkl}$, the flow equation at this order is given as follows

$$\begin{aligned}
\dot{\Gamma}^{[2]}_{ijkl}(s) &= -\Delta^2_{ijkl}\Gamma^{[2]}_{ijkl} \\
&+ \frac{1}{2}\sum_{ab}(\bar{n}_a\bar{n}_b - n_a n_b)(\Delta_{ijab} + \Delta_{klab})\Gamma^{[1]}_{ijab}\Gamma^{[1]}_{abkl} \\
&+ \sum_{ab}(\bar{n}_a n_b - n_a\bar{n}_b)\left[(\Delta_{bjal} + \Delta_{bkai})\Gamma^{[1]}_{bjal}\Gamma^{[1]}_{aibk} - (\Delta_{bial} + \Delta_{bkaj})\Gamma^{[1]}_{bial}\Gamma^{[1]}_{ajbk}\right]. \quad (4.64) \\
&=: -\Delta^2_{ijkl}\Gamma^{[2]}_{ijkl}(s) + Q^{[2],pp}_{ijkl}(s) + Q^{[2],hh}_{ijkl}(s) + Q^{[2],ph}_{ijkl}(s). \quad (4.65)
\end{aligned}$$

The $\Gamma^{[2]}_{ijkl}(s)$ can be given by

$$\Gamma^{[2]}_{ijkl}(s) = \Gamma^{[2],pp}_{ijkl}(s) + \Gamma^{[2],hh}_{ijkl}(s) + \Gamma^{[2],ph}_{ijkl}(s)., \quad (4.66)$$

where the three terms in Eq. (4.66) corresponds to the terms which have pp, hh and ph intermediate states in (4.65), respectively.

$$\Gamma^{[2],pp}_{ijkl}(s) = e^{-\Delta^2_{ijkl}s}\int_0^s Q^{[2],pp}_{ijkl}(z)e^{\Delta^2_{ijkl}z}dz \quad (4.67)$$

$$\Gamma^{[2],hh}_{ijkl}(s) = e^{-\Delta^2_{ijkl}s}\int_0^s Q^{[2],hh}_{ijkl}(z)e^{\Delta^2_{ijkl}z}dz \quad (4.68)$$

$$\Gamma^{[2],ph}_{ijkl}(s) = e^{-\Delta^2_{ijkl}s}\int_0^s Q^{[2],ph}_{ijkl}(z)e^{\Delta^2_{ijkl}z}dz. \quad (4.69)$$

In the following calculations, we frequently use the relations

$$\Delta^2_{ijkl} - \Delta^2_{ijab} - \Delta^2_{abkl} = -2\Delta_{abkl}\Delta_{abij} \quad (4.70)$$

$$\Delta^2_{ijkl} - \Delta^2_{bjal} - \Delta^2_{aibk} = -2\Delta_{albj}\Delta_{aibk} \quad (4.71)$$

$$\Delta^2_{ijkl} - \Delta^2_{bial} - \Delta^2_{ajbk} = -2\Delta_{albi}\Delta_{ajbk}. \quad (4.72)$$

The pp ladder First let's see the pp term,

$$\Gamma^{[2],pp}_{ijkl}(s) = \frac{1}{2}e^{-\Delta^2_{ijkl}s}\sum_{pp'}V_{ijpp'}V_{pp'kl}(\Delta_{ijpp'} + \Delta_{klpp'})\int_0^s dz e^{-2\Delta_{ijpp'}\Delta_{klpp'}z}$$

$$= \frac{1}{2} e^{-\Delta_{ijkl}^2 s} \sum_{pp'} \Big[\underline{\Delta_{ijkl}\ s(-\delta_{ijpp'} + \delta_{pp'kl})} + \frac{\bar{\delta}_{ijpp'}\bar{\delta}_{pp'kl}}{2} \left(\frac{1}{\Delta_{ijpp'}} + \frac{1}{\Delta_{klpp'}} \right) \left(1 - e^{-2\Delta_{ijpp'}\Delta_{klpp'} s} \right) \Big] \tag{4.73}$$

$$\to \frac{1}{4} \sum_{pp';\Delta_{ijpp'}\Delta_{pp'kl}\neq 0} \left(\frac{V_{klpp'}V_{pp'ij}}{\Delta_{ijpp'}} + \frac{V_{ijpp'}V_{pp'kl}}{\Delta_{klpp'}} \right) \quad (s \to \infty). \tag{4.74}$$

$$\equiv \frac{1}{2}(X_{ijkl}^{[2],pp} + X_{klij}^{[2],pp}) \tag{4.75}$$

The terms with underlines vanish when taking $s \to \infty$ since only the terms with $\Delta_{ijkl=0}$ survive. The final result is nothing but the hermitized second-order pp-ladder diagram, where $X_{ijkl}^{[2],pp}$ is a non-hermitized pp-ladder diagram in Fig. 4.1. One should note that the intermediate summation over particles, pp', is restricted under the condition

$$\Delta_{ijpp'}\Delta_{pp'kl} \neq 0. \tag{4.76}$$

Thus, the problem of zero denominator which may occur for the conventional perturbation theory never occurs.

The hh-ladder Similarly, the terms that have intermediate 2h states can be calculated as

$$\Gamma_{ijkl}^{[2],hh}(s) = -\frac{1}{2} e^{-\Delta_{ijkl}^2 s} \sum_{hh'} V_{ijhh'}V_{hh'kl}(\Delta_{ijhh'} + \Delta_{klhh'}) \int_0^s dz e^{-2\Delta_{ijhh'}\Delta_{klhh'}z}$$

$$= -\frac{1}{2} e^{-\Delta_{ijkl}^2 s} \sum_{hh'} \Big[\underline{\Delta_{ijkl}\ s(-\delta_{ijhh'} + \delta_{hh'kl})} + \frac{\bar{\delta}_{ijhh'}\bar{\delta}_{hh'kl}}{2} \left(\frac{1}{\Delta_{ijhh'}} + \frac{1}{\Delta_{klhh'}} \right) \left(1 - e^{-2\Delta_{ijhh'}\Delta_{klhh'} s} \right) \Big] \tag{4.77}$$

$$\to \frac{1}{4} \sum_{pp';\Delta_{ijhh'}\Delta_{hh'kl}\neq 0} \left(\frac{V_{klhh'}V_{hh'ij}}{\Delta_{hh'ij}} + \frac{V_{ijhh'}V_{hh'kl}}{\Delta_{hh'kl}} \right) \quad (s \to \infty). \tag{4.78}$$

$$\equiv \frac{1}{2}(X_{ijkl}^{[2],hh} + X_{klij}^{[2],hh}). \tag{4.79}$$

Again, the second-order hh-ladder diagram is obtained, where $X_{ijkl}^{[2],hh}$ is a non-hermitized hh-ladder diagram in Fig. 4.1.

The core polarization Finally, the ph terms can be calculated as

$$\Gamma_{ijkl}^{[2],ph}(s) = e^{-\Delta_{ijkl}^2 s} \sum_{ab} (\bar{n}_a n_b - n_a \bar{n}_b) \Big[(\Delta_{bjal} + \Delta_{bkai}) V_{bjal}V_{aibk} \int_0^s e^{-2\Delta_{bjal}\Delta_{bkai}z} dz + (\Delta_{bial} + \Delta_{bkaj}) V_{bial}V_{ajbk} \int_0^s e^{-2\Delta_{bial}\Delta_{bkaj}z} dz \Big]$$

$$
\begin{aligned}
&= e^{-\Delta^2_{ijkl}s} \sum_{ab} (\bar{n}_a n_b - n_a \bar{n}_b) \\
&\cdot V_{bjal} V_{aibk} \left[\underline{\Delta_{ijkl}\ s(-\delta_{bjal} + \delta_{bkai})} + \frac{\bar{\delta}_{bjal}\bar{\delta}_{bkai}}{2} \left(\frac{1}{\Delta_{bjal}} + \frac{1}{\Delta_{bkai}} \right) \left(1 - e^{-2\Delta_{bjal}\Delta_{bkai}s} \right) \right] \\
&- V_{bial} V_{ajbk} \left[\underline{\Delta_{ijkl}\ s(-\delta_{bial} + \delta_{bkaj})} + \frac{\bar{\delta}_{bial}\bar{\delta}_{bkaj}}{2} \left(\frac{1}{\Delta_{bial}} + \frac{1}{\Delta_{bkaj}} \right) \left(1 - e^{2\Delta_{bial}\Delta_{bkaj}s} \right) \right].
\end{aligned}
\tag{4.80}
$$

In the limit, $s \to \infty$, four terms with the underline vanish, then one gets

$$
\begin{aligned}
\Gamma^{[2],ph}_{ijkl}(\infty) &= \frac{1}{2} \sum_{ab;\Delta_{bjal}\Delta_{bkai}\neq 0} (\bar{n}_a n_b - n_a \bar{n}_b) \left(\frac{V_{bjal}V_{aibk}}{\Delta_{bkai}} + \frac{V_{bkai}V_{albj}}{\Delta_{bjal}} \right) \\
&\quad - \frac{1}{2} \sum_{ab;\Delta_{bial}\Delta_{bkaj}\neq 0} (\bar{n}_a n_b - n_a \bar{n}_b) \left(\frac{V_{bial}V_{ajbk}}{\Delta_{bkaj}} + \frac{V_{bkaj}V_{albi}}{\Delta_{bial}} \right) \qquad (4.81) \\
&= \frac{1}{2} \sum_{ph;\Delta\neq 0} \left\{ (1 + P_{ik}P_{jl})(1 - P_{ij})(1 - P_{kl}) \frac{V_{hjpl}V_{pihk}}{\Delta_{hkpi}} \right\} \\
&= \frac{1}{2} \left(X^{[2],ph}_{ijkl} + X^{[2],ph}_{klij} \right), \qquad (4.82)
\end{aligned}
$$

where the summation $\sum_{\Delta\neq 0}$ means that no denominator vanishes. What is obtained is nothing but the hermitized second-order core-polarization diagrams.

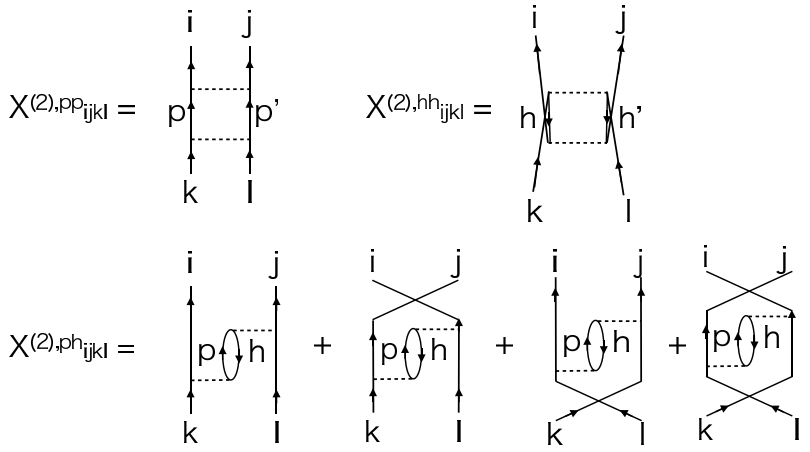

Figure 4.1: The second-order diagrams for two-body interactions which appear in the second-order Q-box $Q^{(2)}$. These diagrams are in general not hermitian. The perturbative solution of the IM-SRG(2) corresponds to the simply hermitized interaction.

The three-body term

The second-order flow equation for the three-body terms is given by

$$\begin{aligned}\frac{d}{ds}W^{[2]}_{ijklmn} &= -\Delta_{ijklmn}\eta^{(3)[2]}_{ijklmn} + P(ij/k)P(l/mn)\sum_a(\eta^{(2)[1]}_{ijla}\Gamma^{[1]}_{akmn} - \Gamma^{[1]}_{ijla}\eta^{(2)[1]}_{akmn}) \\ &= -\Delta^2_{ijklmn}W^{[2]}_{ijklmn} + P(ij/k)P(l/mn)\sum_a(\Delta_{ijla}+\Delta_{mnak})V_{ijla}V_{akmn}e^{-(\Delta^2_{ijla}+\Delta^2_{mnak})s},\end{aligned} \tag{4.83}$$

where the second-order three-body generator is

$$\eta^{(3)[2]}_{ijklmn}(s) = \Delta_{ijklmn}W^{[2]}_{ijklmn}. \tag{4.84}$$

The Eq. (4.83) can be easily solved as

$$\begin{aligned}W^{[2]}_{ijklmn}(s) &= e^{-\Delta^2_{ijklmn}s}\Big[W^{[2]}_{ijklmn}(0) \\ &\quad + P(ij/k)P(l/mn)\sum_a(\Delta_{ijla}+\Delta_{mnak})V_{ijla}V_{akmn}\int_0^s e^{(\Delta^2_{ijklmn}-\Delta^2_{ijla}+\Delta^2_{mnak})z}dz\Big] \\ &= e^{-\Delta^2_{ijklmn}s}P(ij/k)P(l/mn)V_{ijla}V_{akmn} \\ &\quad \cdot\left[\Delta_{ijklmn}\ s(-\delta_{ijla}+\delta_{akmn}) + \frac{\bar{\delta}_{ijal}\bar{\delta}_{akmn}}{2}\left(\frac{1}{\Delta_{ijla}}+\frac{1}{\Delta_{mnak}}\right)\left(1-e^{-2\Delta_{ijla}\Delta_{mnak}s}\right)\right].\end{aligned} \tag{4.85}$$

Here, the relation

$$\Delta^2_{ijklmn} - \Delta^2_{ijla} - \Delta^2_{mnak} = -2\Delta_{ijla}\Delta_{mnak} \tag{4.86}$$

is used. Therefore

$$\lim_{s\to\infty} W^{[2]}_{ijklmn}(s) = \begin{cases} 0 & (\Delta_{ijklmn}\neq 0) \\ \displaystyle\sum_{a;\Delta_{ijla}\neq 0}\frac{V_{ijla}V_{akmn}}{\Delta_{ijla}} & (\Delta_{ijklmn}=0)\end{cases}. \tag{4.87}$$

The Eq. (4.87) shows that the off-diagonal part is suppressed during the flow, and the diagonal part is nothing but the tree-level diagram that appears in the second-order three-body Q-box $Q^{(3)}_{3N}$ [24]. So far, we have shown that the perturbative solutions for the IN-SRG(2) give, in the $s\to\infty$ limit, the second order perturbation diagram exactly.

4.3.4 The flow equation at $\mathcal{O}(g^3)$

The constant term

Here we show the third order solution for the ground state energy.

$$\dot{E}_0^{[3]}(s) = \sum_{ijkl} n_i n_j \bar{n}_k \bar{n}_l \Delta_{ijkl} \Gamma^{[1]}_{ijkl}(s) \Gamma^{[2]}_{ijkl}(s). \tag{4.88}$$

$$= \sum_{hh'pp'} \Delta_{hh'pp'} V_{hh'pp'} e^{-\Delta^2_{hh'pp'} s} \left(\Gamma^{[2],pp}_{hh'pp'}(s) + \Gamma^{[2],hh}_{hh'pp'}(s) + \Gamma^{[2],ph}_{hh'pp'}(s) \right) \tag{4.89}$$

$$=: \dot{E}_0^{[3],pp}(s) + \dot{E}_0^{[3],hh}(s) + \dot{E}_0^{[3],ph}(s). \tag{4.90}$$

The three vertex functions $\Gamma^{[2],X}_{hh'pp'}(s)$, $X = pp, hh, ph$, are defined in Eq. (4.67-4.69), and the $\dot{E}_0^{[3],X}(s)$ are defined as

$$\dot{E}_0^{[3],pp}(s) := \sum_{hh'pp'} \Delta_{hh'pp'} V_{hh'pp'} e^{-\Delta^2_{hh'pp'} s} \Gamma^{[2],pp}_{hh'pp'}(s) \tag{4.91}$$

$$\dot{E}_0^{[3],hh}(s) := \sum_{hh'pp'} \Delta_{hh'pp'} V_{hh'pp'} e^{-\Delta^2_{hh'pp'} s} \Gamma^{[2],hh}_{hh'pp'}(s) \tag{4.92}$$

$$\dot{E}_0^{[3],ph}(s) := \sum_{hh'pp'} \Delta_{hh'pp'} V_{hh'pp'} e^{-\Delta^2_{hh'pp'} s} \Gamma^{[2],ph}_{hh'pp'}(s) \tag{4.93}$$

From now on, we use the indices $pp'qq'$ for unoccupied states, and $hh'll'$ for occupied states.

Contribution from pp-ladder

$$\dot{E}_0^{[3],pp}(s) = \frac{1}{2} \sum_{hh'pp'} \Delta_{hh'pp'} V_{hh'pp'} e^{-2\Delta^2_{hh'pp'} s} \left[\sum_{qq';\Delta_{qq'pp'}=0} \Delta_{hh'pp'} V_{hh'qq'} V_{qq'pp'} s \right.$$
$$\left. + \frac{1}{2} \sum_{\Delta_{qq'pp'} \neq 0} \left(\frac{1}{\Delta_{hh'qq'}} + \frac{1}{\Delta_{pp'qq'}} \right) V_{hh'qq'} V_{qq'pp'} s \left(1 - e^{-2\Delta_{hh'qq'} \Delta_{pp'qq'} s} \right) \right]. \tag{4.94}$$

Integrating from $s = 0$ to ∞, together with the initial condition $E_0^{[3],pp}(0) = 0$, and the relation,

for $\forall \alpha \in \boldsymbol{R}_{>0}$;

$$\int_0^s z e^{-\alpha z} dz = \alpha^{-2} \left\{ 1 - (1 + s\alpha) e^{-\alpha s} \right\} \to \alpha^{-2} (s \to \infty) \tag{4.95}$$

one gets

$$E_0^{[3],pp}(\infty) = \frac{1}{2}\sum_{hh'pp'qq'} V_{hh'pp'}V_{hh'qq'}V_{pp'qq'}$$
$$\left[\frac{\delta_{qq'pp'}}{4\Delta^2_{hh'pp'}} + \frac{\bar{\delta}_{qq'pp'}}{4}\left(\frac{1}{\Delta_{hh'qq'}} + \frac{1}{\Delta_{pp'qq'}}\right)\left(\frac{1}{\Delta^2_{hh'pp'}} - \frac{1}{\Delta^2_{hh'pp'} + \Delta_{hh'qq'}\Delta_{pp'qq'}}\right)\Delta_{hh'pp'}\right]$$
$$= \frac{1}{8}\sum_{hh'pp'qq'} \frac{V_{hh'pp'}V_{hh'qq'}V_{pp'qq'}}{\Delta_{hh'pp'}\Delta_{hh'qq'}} + R^{[3],pp}, \tag{4.96}$$

where $R^{[3],pp}$ is given by

$$R^{[3],pp} = \frac{1}{8}\sum_{hh'pp'qq';\Delta_{qq'pp'}\neq 0}\left[\frac{1}{\Delta_{pp'qq'}\Delta^2_{hh'pp'}} - \frac{\Delta_{pp'qq'} + \Delta_{hh'qq'}}{\Delta_{pp'qq'}\Delta_{hh'qq'}(\Delta^2_{hh'pp'} + \Delta_{pp'qq'}\Delta_{hh'qq'})}\right]$$
$$\times \Delta_{hh'pp'}V_{hh'pp'}V_{hh'qq'}V_{pp'qq'}. \tag{4.97}$$

In fact, the $R^{[3],pp}$ can be shown to be zero as follows,

$$R^{[3],pp} = \frac{1}{8}\sum_{hh'pp'qq';\Delta_{qq'pp'}\neq 0} \frac{\Delta_{hh'qq'}(\Delta^2_{hh'pp'} + \Delta_{hh'qq'}\Delta_{pp'qq'}) - (\Delta_{pp'qq'} + \Delta_{hh'qq'})\Delta^2_{hh'pp'}}{\Delta_{pp'qq'}\Delta_{hh'pp'}\Delta_{hh'qq'}(\Delta^2_{hh'pp'} + \Delta_{hh'qq'}\Delta_{pp'qq'})}$$
$$\times V_{hh'pp'}V_{hh'qq'}V_{pp'qq'}$$
$$= \frac{1}{8}\sum_{hh'pp'qq';\Delta_{qq'pp'}\neq 0} \frac{(\Delta^2_{hh'qq'} - \Delta^2_{hh'pp'})V_{hh'pp'}V_{hh'qq'}V_{pp'qq'}}{\Delta_{hh'pp'}\Delta_{hh'qq'}\left\{\Delta^2_{hh'pp'} + \Delta_{hh'qq'}(\Delta_{pp'hh'} + \Delta_{hh'qq'})\right\}}$$
$$= \frac{1}{8}\sum_{hh'pp'qq';\Delta_{qq'pp'}\neq 0} \frac{(\Delta^2_{hh'qq'} - \Delta^2_{hh'pp'})V_{hh'pp'}V_{hh'qq'}V_{pp'qq'}}{\Delta_{hh'pp'}\Delta_{hh'qq'}(\Delta^2_{hh'pp'} + \Delta^2_{hh'qq'} - \Delta_{hh'pp'}\Delta_{hh'qq'})}$$
$$= 0. \tag{4.98}$$

In the last line of the above equation, only the part in blue is antisymmetric under the exchange of pp' and qq', therefore the summation over $pp'qq'$ vanishes.

Contribution from hh-ladder

$$\dot{E}_0^{[3],hh}(s) = \frac{1}{2}\sum_{hh'pp'}\Delta_{hh'pp'}V_{hh'pp'}e^{-2\Delta^2_{hh'pp'}s}\left[\sum_{ll';\Delta_{ll'hh'}=0}\Delta_{pp'hh'}V_{hh'll'}V_{ll'pp's}\right.$$
$$\left. + \frac{1}{2}\sum_{\Delta_{ll'hh'}\neq 0}\left(\frac{1}{\Delta_{hh'll'}} + \frac{1}{\Delta_{pp'll'}}\right)V_{hh'll'}V_{ll'pp's}\left(1 - e^{-2\Delta_{hh'll'}\Delta_{pp'll'}s}\right)\right]. \tag{4.99}$$

Integrating from $s = 0$ to ∞, together with the initial condition $E_0^{[3],hh}(0) = 0$ and the relation in Eq. (4.95), one gets

$$E_0^{[3],hh}(\infty) = -\frac{1}{2}\sum_{hh'pp'll'} V_{hh'pp'}V_{hh'll'}V_{ll'pp'}$$

$$\left[\frac{\delta_{ll'hh'}}{4\Delta^2_{hh'pp'}} + \frac{\bar{\delta}_{ll'hh'}}{4}\left(\frac{1}{\Delta_{pp'll'}} + \frac{1}{\Delta_{hh'll'}}\right)\left(\frac{1}{\Delta^2_{hh'pp'}} - \frac{1}{\Delta^2_{hh'pp'} + \Delta_{hh'll'}\Delta_{pp'll'}}\right)\Delta_{hh'pp'}\right]$$
$$= \frac{1}{8}\sum_{hh'pp'll'} \frac{V_{hh'pp'}V_{hh'll'}V_{pp'll'}}{\Delta_{hh'pp'}\Delta_{ll'pp'}} + R^{[3],hh}, \tag{4.100}$$

where $R^{[3],hh}$ is given by

$$R^{[3],hh} = -\frac{1}{8}\sum_{hh'pp'hh';\Delta_{hh'll'}\neq 0}\left[\frac{1}{\Delta_{pp'qq'}\Delta_{hh'pp'}} - \frac{\Delta_{pp'll'} + \Delta_{hh'll'}}{\Delta_{pp'll'}\Delta_{hh'll'}(\Delta^2_{hh'pp'} + \Delta_{pp'll'}\Delta_{hh'll'})}\right]$$
$$\times V_{hh'pp'}V_{hh'qq'}V_{pp'qq'}. \tag{4.101}$$

Like in the case of pp contribution, the $R^{[3],hh}$ can be shown to be zero as following.

$$R^{[3],hh} = \frac{1}{8}\sum_{hh'pp'll';\Delta_{ll'hh'}\neq 0} \frac{\Delta_{pp'll'}(\Delta^2_{hh'pp'} + \Delta_{hh'll'}\Delta_{pp'll'}) - (\Delta_{pp'll'} + \Delta_{hh'll'})\Delta^2_{hh'pp'}}{\Delta_{pp'll'}\Delta_{hh'pp'}\Delta_{hh'll'}(\Delta^2_{hh'pp'} + \Delta_{hh'll'}\Delta_{pp'll'})}$$
$$\times V_{hh'pp'}V_{hh'qq'}V_{pp'qq'}$$
$$= \frac{1}{8}\sum_{hh'pp'll';\Delta_{ll'hh'}\neq 0} \frac{(\Delta^2_{ll'pp'} - \Delta^2_{hh'pp'})V_{hh'pp'}V_{hh'qq'}V_{pp'qq'}}{\Delta_{hh'pp'}\Delta_{ll'pp'}\left\{\Delta^2_{hh'pp'} + \Delta_{pp'll'}(\Delta_{hh'pp'} + \Delta_{pp'll'})\right\}}$$
$$= \frac{1}{8}\sum_{hh'pp'll';\Delta_{ll'hh'}\neq 0} \frac{(\Delta^2_{ll'pp'} - \Delta^2_{hh'pp'})V_{hh'pp'}V_{hh'qq'}V_{pp'qq'}}{\Delta_{hh'pp'}\Delta_{ll'pp'}(\Delta^2_{hh'pp'} + \Delta^2_{ll'pp'} - \Delta_{hh'pp'}\Delta_{ll'pp'})}$$
$$= 0. \tag{4.102}$$

In the last line of the above equation, only the part in blue is antisymmetric under the exchange of hh' and ll', therefore the summation over $hh'll'$ vanishes.

Contribution from ph

$$\dot{E}_0^{[3],ph}(s) = \sum_{pp'hh'ab}(\bar{n}_a n_b - n_a\bar{n}_b)\Delta_{hh'pp'}V_{hh'pp'}e^{-2\Delta^2_{hh'pp's}}$$
$$\cdot V_{bh'ap'}V_{ahbp}\left[\Delta_{pp'hh'}\ s(\delta_{bh'ap'} - \delta_{bpah}) + \frac{\bar{\delta}_{bh'ap'}\bar{\delta}_{bpah}}{2}\left(\frac{1}{\Delta_{bh'ap'}} + \frac{1}{\Delta_{bpah}}\right)\left(1 - e^{-2\Delta_{bh'ap'}\Delta_{bpah}s}\right)\right]$$
$$- \cdot V_{bhap'}V_{ah'bp}\left[\Delta_{pp'hh'}\ s(\delta_{bhap'} - \delta_{bpah'}) + \frac{\bar{\delta}_{bhap'}\bar{\delta}_{bpah'}}{2}\left(\frac{1}{\Delta_{bhap'}} + \frac{1}{\Delta_{bpah'}}\right)\left(1 - e^{-2\Delta_{bhap'}\Delta_{bpah'}s}\right)\right] \tag{4.103}$$

Integrating from $s = 0$ to ∞, one gets

$$E_0^{[3],ph}(\infty) = \sum_{hh'pp'lq} V_{hh'pp'}V_{lh'qp'}V_{qhlp}$$

$$\cdot \left[4\frac{\delta_{lpqh}}{4\Delta^2_{hh'pp'}} + \bar{\delta}_{lpqh} \left(\frac{1}{\Delta_{lh'qp'}} + \frac{1}{\Delta_{lpqh}} \right) \left(\frac{1}{\Delta^2_{hh'pp'}} - \frac{1}{\Delta^2_{hh'pp'} + \Delta_{lh'qp'}\Delta_{lpqh}} \right) \right]$$
$$= \sum_{hh'pp'lq} \frac{V_{hh'pp'}V_{lh'qp'}V_{qhlp}}{\Delta_{hh'pp'}\Delta_{lh'qp'}} + R^{[3],ph}. \tag{4.104}$$

One can again show that $R^{[3],ph} = 0$ as

$$\begin{aligned} R^{[3],ph} &= \sum_{hh'pp'lq;\Delta_{lp'qh'}\neq 0} V_{hh'pp'}V_{lh'qp'}V_{qhlp} \frac{\Delta_{lh'qp'}(\Delta^2_{hh'pp'} + \Delta_{lh'qp'}\Delta_{lpqh}) - \Delta^2_{hh'pp'}(\Delta_{lh'qp'} + \Delta_{lpqh})}{\Delta_{lpqh}\Delta_{hh'pp'}\Delta_{lh'qp'}(\Delta^2_{hh'pp'} + \Delta_{lh'qp'}\Delta_{lpqh})} \\ &= \sum_{hh'pp'lq;\Delta_{lp'qh'}\neq 0} V_{hh'pp'}V_{lh'qp'}V_{qhlp} \frac{\Delta^2_{lh'qp'} - \Delta^2_{hh'pp'}}{\Delta_{hh'pp'}\Delta_{lh'qp'}\left\{\Delta^2_{hh'pp'} + \Delta_{lh'qp'}(\Delta_{lh'qp'} + \Delta_{pp'hh'})\right\}} \\ &= \sum_{hh'pp'lq;\Delta_{lp'qh'}\neq 0} V_{hh'pp'}V_{lh'qp'}V_{qhlp} \frac{\Delta^2_{lh'qp'} - \Delta^2_{hh'pp'}}{\Delta_{hh'pp'}\Delta_{lh'qp'}(\Delta^2_{hh'pp'} + \Delta^2_{lh'qp'} - \Delta_{lh'qp'}\Delta_{pp'hh'}))} \\ &= 0. \end{aligned} \tag{4.105}$$

Only the factor in blue is antisymmetric under the exchange between lq and hp, therefore the summation over l, q, h, p vanishes.

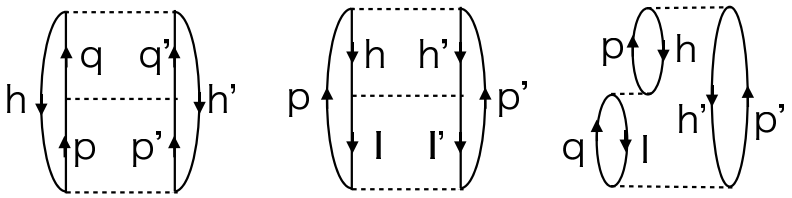

Figure 4.2: The third-order diagrams for the ground state.

Therefore, $E_0^{[3]}(\infty)$ is obtained as

$$E_0^{[3]}(\infty) = \frac{1}{8} \sum_{hh'pp'qq'} \frac{V_{hh'pp'}V_{hh'qq'}V_{pp'qq'}}{\Delta_{hh'pp'}\Delta_{hh'qq'}} + \frac{1}{8} \sum_{hh'pp'll'} \frac{V_{hh'pp'}V_{hh'll'}V_{pp'll'}}{\Delta_{hh'pp'}\Delta_{ll'pp'}} + \sum_{hh'pp'lq} \frac{V_{hh'pp'}V_{lh'qp'}V_{qhlp}}{\Delta_{hh'pp'}\Delta_{lh'qp'}}. \tag{4.106}$$

This is exactly the third-order contribution of the Goldstone expansion for the ground-state energy. The perturbative solution for the in-medium SRG has been investigated up to the third order in the bare coupling strength. Regarding the ground-state energy, the perturbative solution includes exact MBPT(3).

One-body terms

The third-order flow equation for one-body terms is given by

$$\begin{aligned}\dot{f}_{ij}^{[3]}(s) &= \sum_a (1+P_{ij})\eta_{ia}^{(1)[3]} f_{aj}^{[0]} + \sum_{ab}(n_a - n_b)\left(\eta_{ab}^{(1)[2]}\Gamma_{biaj}^{[1]} - f_{ab}^{[2]}\eta_{biaj}^{(2)[1]}\right) \\ &+ \sum_{abc}(n_a n_b \bar{n}_c + \bar{n}_a\bar{n}_b n_c)(1+P_{ij})\left(\eta_{ciab}^{(2)[2]}\Gamma_{abcj}^{[1]} + \Gamma_{ciab}^{[1]}\eta_{abcj}^{(2)[2]}\right) \\ &+ \frac{1}{4}\sum_{abcd}(n_a n_b \bar{n}_c \bar{n}_d - \bar{n}_a\bar{n}_b n_c n_d)\left(\eta_{abijcd}^{(3)[2]}\Gamma_{cdab}^{[1]} - W_{abijcd}^{[2]}\eta_{cdab}^{(2)[1]}\right) \\ &= -\Delta_{ij}^2 f_{ij}^{[3]}(s) + Q_{ij}^{(1)[3],I}(s) + Q_{ij}^{(1)[3],II}(s) + Q_{ij}^{(1)[3],III}(s), \end{aligned} \tag{4.107}$$

where

$$Q_{ij}^{(1)[3],I}(s) = \sum_{ab}(n_a - n_b)\left(\eta_{ab}^{(1)[2]}\Gamma_{biaj}^{[1]} - f_{ab}^{[2]}\eta_{biaj}^{(2)[1]}\right) \tag{4.108}$$

$$Q_{ij}^{(1)[3],II}(s) = \sum_{abc}(n_a n_b \bar{n}_c + \bar{n}_a\bar{n}_b n_c)(1+P_{ij})\left(\eta_{ciab}^{(2)[2]}\Gamma_{abcj}^{[1]} + \Gamma_{ciab}^{[1]}\eta_{abcj}^{(2)[2]}\right) \tag{4.109}$$

$$Q_{ij}^{(1)[3],II}(s) = \frac{1}{4}\sum_{abcd}(n_a n_b \bar{n}_c \bar{n}_d - \bar{n}_a\bar{n}_b n_c n_d)\left(\eta_{abijcd}^{(3)[2]}\Gamma_{cdab}^{[1]} - W_{abijcd}^{[2]}\eta_{cdab}^{(2)[1]}\right) \tag{4.110}$$

This can be integrated as

$$f_{ij}^{[3]}(s) = e^{-\Delta_{ij}^2 s}\left\{f_{ij}^{[3]}(0) + \int_0^s e^{\Delta_{ij}^2 z}\left(Q_{ij}^{(1)[3],I}(z) + Q_{ij}^{(1)[3],II}(z) + Q_{ij}^{(1)[3],III}(z)\right)dz\right\} \tag{4.111}$$

$$=: f_{ij}^{[3]I}(s) + f_{ij}^{[3]II}(s) + f_{ij}^{[3]III}(s), \tag{4.112}$$

where

$$f_{ij}^{[3],I}(s) := e^{-\Delta_{ij}^2 s}\int_0^s Q_{ij}^{[3],I}(z)e^{\Delta_{ij}z}dz \tag{4.113}$$

$$f_{ij}^{[3],II}(s) := e^{-\Delta_{ij}^2 s}\int_0^s Q_{ij}^{[3],II}(z)e^{\Delta_{ij}z}dz \tag{4.114}$$

$$f_{ij}^{[3],III}(s) := e^{-\Delta_{ij}^2 s}\int_0^s Q_{ij}^{[3],III}(z)e^{\Delta_{ij}z}dz. \tag{4.115}$$

The $f_{ij}^{[3],I}(s)$ can be given with Eq. (4.108) as

$$f_{ij}^{[3],I}(s) = e^{-\Delta_{ij}^2 s}\sum_{ab}(n_a - n_b)2\Delta_{ab}\int_0^s f_{ab}^{[2]}(z)\Gamma_{biaj}^{[1]}(z)e^{\Delta_{ij}^2 z}dz. \tag{4.116}$$

This can be calculated with Eq. (4.60),

$$f_{ij}^{[3],I}(s) = \frac{1}{4}e^{-\Delta_{ij}^2 s}\sum_{abdef}(\bar{n}_a n_b - n_a\bar{n}_b)(\bar{n}_d\bar{n}_e n_f + n_d n_e \bar{n}_f)V_{fade}V_{defb}V_{biaj}$$

$$\cdot \left[\frac{\delta_{fade} - \delta_{fbde}}{\Delta^2_{ajbi}} \left\{ 1 - (1 + 2\Delta_{ab}\Delta_{ajbi}) e^{-2\Delta_{ab}\Delta_{ajbi}s} \right\} \right.$$
$$\left. -\bar{\delta}_{fade}\bar{\delta}_{fbde}\Delta_{ab} \left(\frac{1}{\Delta_{fade} + \Delta_{fbde}} \right) \left(\frac{1 - e^{-2\Delta_{ab}\Delta_{ajbi}s}}{\Delta_{ab}\Delta_{ajbi}} - \frac{1 - e^{2(\Delta_{ab}\Delta_{bjai} + \Delta_{fade}\Delta_{fbde})s}}{\Delta_{ab}\Delta_{bjai} + \Delta_{fade}\Delta_{fbde}} \right) \right]. \tag{4.117}$$

In the $s \to \infty$ limit, only the energy-diagonal terms, $\Delta_{ij} = 0$ survive, and the solution is

$$f^{[3],I}_{ij}(\infty) = -\frac{1}{4} \sum_{abcdx} (n_a n_b \bar{n}_c \bar{n}_d \bar{n}_x - n_a n_x \bar{n}_b \bar{n}_c \bar{n}_d + \bar{n}_a \bar{n}_x n_b n_c n_d - \bar{n}_a \bar{n}_b n_x n_c n_d) V_{axcd} V_{cdab} V_{bixj}$$
$$\cdot \left[\frac{\delta_{axcd} + \delta_{abcd}}{\delta_{xb}\Delta_{abcd}} + \Delta_{xb} \left(\frac{1}{\Delta_{axcd}} + \frac{1}{\Delta_{abcd}} \right) \left(\frac{1}{\Delta_{xb}\Delta_{xjbi}} - \frac{1}{\Delta_{xb}\Delta_{xjbi} + \Delta_{axcd}\Delta_{abcd}} \right) \right]. \tag{4.118}$$

Similarly, the other terms can be obtained as

$$f^{[3],II}_{ij}(s) = \frac{1}{2} \sum_{abc} (n_a n_b \bar{n}_c + \bar{n}_a \bar{n}_b n_c)(1 + P_{ij})(\Delta_{ciab} + \Delta_{cjab}) \int_0^s \Gamma^{[2]}_{ciab} \Gamma^{[1]}_{abcj} e^{\Delta^2_{ij} z} dz \tag{4.119}$$
$$= f^{[3],II\text{pphh}}_{ij}(s) + f^{[3],II\text{ph}}_{ij}(s). \tag{4.120}$$

The pphh term is

$$f^{[3],II\text{pphh}}_{ij}(s) = \frac{1 + P_{ij}}{16} e^{-\Delta^2_{ij}s} \sum_{abcde} (n_a n_b \bar{n}_c + \bar{n}_a \bar{n}_b n_c)(\bar{n}_d \bar{n}_e - n_d n_e) V_{abcj} V_{cide} V_{deab}$$
$$\bar{\delta}_{ciab} \left[(-\delta_{cide} + \delta_{deab}) \frac{\Delta_{ciab}(\Delta_{ciab} + \Delta_{cjab})}{\Delta^2_{ciab}\Delta^2_{cjab}} \left\{ 1 - (1 + 2\Delta_{ciab}\Delta_{cjab}s) e^{-2\Delta_{ciab}\Delta_{cjab}s} \right\} \right.$$
$$\bar{\delta}_{cide}\bar{\delta}_{abde}(\Delta_{ciab} + \Delta_{cjab}) \left(\frac{1}{\Delta_{cide}} + \frac{1}{\Delta_{abde}} \right)$$
$$\left. \cdot \left(\frac{1 - e^{-2\Delta_{ciab}\Delta_{cjab}s}}{\Delta_{ciab}\Delta_{cjab}} - \frac{1 - e^{-2(\Delta_{ciab}\Delta_{cjab} + \Delta_{cide}\Delta_{abde})s}}{\Delta_{ciab}\Delta_{cjab} + \Delta_{cide}\Delta_{abde}} \right) \right]. \tag{4.121}$$

This survives only when $\Delta_{ij} = 0$ in the limit of $s \to \infty$,

$$f^{[3],II\text{pphh}}_{ij}(\infty) = \frac{1 + P_{ij}}{8} \sum_{abcde} (n_a n_b \bar{n}_c + \bar{n}_a \bar{n}_b n_c)(\bar{n}_d \bar{n}_e - n_d n_e) V_{abcj} V_{cide} V_{deab}$$
$$\bar{\delta}_{ciab} \cdot \left[\frac{-\delta_{cide} + \delta_{deab}}{\Delta^2_{ciab}} + \bar{\delta}_{cide}\bar{\delta}_{abde}\Delta_{ciab} \left(\frac{1}{\Delta_{cide}} + \frac{1}{\Delta_{abde}} \right) \right.$$
$$\left. \cdot \left(\frac{1}{\Delta_{ciab}\Delta_{cjab}} - \frac{1}{\Delta_{ciab}\Delta_{cjab} + \Delta_{cide}\Delta_{abde}} \right) \right]. \tag{4.122}$$

This can be divided into five different terms as

$$f^{[3],II\text{pphh}}_{ij}(\infty) = \frac{1}{8} \sum_{abcdx} n_a n_b \bar{n}_c \bar{n}_d \bar{n}_x V_{abxj} V_{xicd} V_{cdab} \bar{\delta}_{xiab} \left[-\frac{\delta_{xicd}}{\Delta^2_{xiab}} \right.$$

$$+\bar{\delta}_{xicd}\bar{\delta}_{abcd}\Delta_{xiab}\left(\frac{1}{\Delta_{xicd}}+\frac{1}{\Delta_{abcd}}\right)\left(\frac{1}{\Delta_{xiab}^2}-\frac{1}{\Delta_{xiab}^2+\Delta_{xicd}\Delta_{abcd}}\right)\Bigg] \tag{4.123}$$

$$+\frac{1}{8}\sum_{abcdx}\bar{n}_a\bar{n}_b\bar{n}_x n_c n_d V_{cdxi}V_{xjab}V_{abcd}\bar{\delta}_{xicd}\Bigg[-\frac{\delta_{xiab}}{\Delta_{xicd}^2}$$
$$+\bar{\delta}_{xiab}\bar{\delta}_{abcd}\Delta_{xicd}\left(\frac{1}{\Delta_{xiab}}+\frac{1}{\Delta_{cdab}}\right)\left(\frac{1}{\Delta_{xicd}^2}-\frac{1}{\Delta_{xicd}^2+\Delta_{xiab}\Delta_{cdab}}\right)\Bigg] \tag{4.124}$$

$$-\frac{1}{8}\sum_{abcdx}\bar{n}_a\bar{n}_b n_c n_d n_x V_{abxj}V_{xicd}V_{cdab}\bar{\delta}_{xiab}\Bigg[-\frac{\delta_{xicd}}{\Delta_{xiab}^2}$$
$$+\bar{\delta}_{xicd}\bar{\delta}_{abcd}\Delta_{xiab}\left(\frac{1}{\Delta_{xicd}}+\frac{1}{\Delta_{abcd}}\right)\left(\frac{1}{\Delta_{xiab}^2}-\frac{1}{\Delta_{xiab}^2+\Delta_{xicd}\Delta_{abcd}}\right)\Bigg] \tag{4.125}$$

$$-\frac{1}{8}\sum_{abcdx}n_a n_b\bar{n}_c\bar{n}_d n_x V_{cdxi}V_{xjab}V_{abcd}\bar{\delta}_{xicd}\Bigg[-\frac{\delta_{xiab}}{\Delta_{xicd}^2}$$
$$+\bar{\delta}_{xiab}\bar{\delta}_{abcd}\Delta_{xicd}\left(\frac{1}{\Delta_{xiab}}+\frac{1}{\Delta_{cdab}}\right)\left(\frac{1}{\Delta_{xicd}^2}-\frac{1}{\Delta_{xicd}^2+\Delta_{xiab}\Delta_{cdab}}\right)\Bigg] \tag{4.126}$$

$$+\frac{1+P_{ij}}{8}\sum_{abcde}(\bar{n}_a\bar{n}_b\bar{n}_d\bar{n}_e n_c - n_a n_b n_d n_e\bar{n}_c)V_{abcj}V_{cide}V_{deab}\bar{\delta}_{ciab}$$
$$\Bigg[\frac{-\delta_{cide}+\delta_{deab}}{\Delta_{ciab}^2}$$
$$+\bar{\delta}_{cide}\bar{\delta}_{abde}\Delta_{ciab}\left(\frac{1}{\Delta_{cide}}+\frac{1}{\Delta_{abde}}\right)\left(\frac{1}{\Delta_{ciab}^2}-\frac{1}{\Delta_{ciab}^2+\Delta_{cide}\Delta_{abde}}\right)\Bigg]. \tag{4.127}$$

In the same way, the ph term $f_{ij}^{[3],II\mathrm{ph}}(s)$ only survives if $\Delta_{ij}=0$ for $s\to\infty$ limit,

$$f_{ij}^{[3],II\mathrm{ph}}(\infty)=\frac{1+P_{ij}}{2}\sum_{abcde}n_a n_b\bar{n}_c\bar{n}_d n_e V_{abcj}V_{ciab}V_{dcea}\bar{\delta}_{ciab}$$
$$\left[-\frac{\delta_{cidb}}{\Delta_{ciab}^2}+\bar{\delta}_{cidb}\Delta_{ciab}\left(\frac{1}{\Delta_{eidb}}+\frac{1}{\Delta_{eadc}}\right)\left(\frac{1}{\Delta_{ciab}^2}-\frac{1}{\Delta_{ciab}^2+\Delta_{eidb}\Delta_{eadc}}\right)\right] \tag{4.128}$$

$$-\frac{1+P_{ij}}{2}\sum_{abcde}n_a n_b\bar{n}_c\bar{n}_d n_e V_{abcj}V_{diea}V_{dcdb}\bar{\delta}_{ciab}$$
$$\left[+\frac{-\delta_{ecdb}+\delta_{eadi}}{\Delta_{ciab}^2}+\bar{\delta}_{ecdb}\Delta_{eadi}\left(\frac{1}{\Delta_{ecdb}}+\frac{1}{\Delta_{eadi}}\right)\left(\frac{1}{\Delta_{ciab}^2}-\frac{1}{\Delta_{ciab}^2+\Delta_{ecdb}\Delta_{eadi}}\right)\right] \tag{4.129}$$

$$- \frac{1+P_{ij}}{2} \sum_{abcde} \bar{n}_a \bar{n}_b n_c n_d \bar{n}_e V_{abcj} V_{ciab} V_{dcea} \bar{\delta}_{ciab}$$
$$\left[-\frac{\delta_{cidb}}{\Delta^2_{ciab}} + \bar{\delta}_{cidb} \Delta_{ciab} \left(\frac{1}{\Delta_{eidb}} + \frac{1}{\Delta_{eadc}} \right) \left(\frac{1}{\Delta^2_{ciab}} - \frac{1}{\Delta^2_{ciab} + \Delta_{eidb}\Delta_{eadc}} \right) \right] \tag{4.130}$$

$$+ \frac{1+P_{ij}}{2} \sum_{abcde} \bar{n}_a \bar{n}_b n_c n_d \bar{n}_e V_{abcj} V_{diea} V_{dcdb} \bar{\delta}_{ciab}$$
$$\left[+ \frac{-\delta_{ecdb} + \delta_{eadi}}{\Delta^2_{ciab}} + \bar{\delta}_{ecdb} \Delta_{eadi} \left(\frac{1}{\Delta_{ecdb}} + \frac{1}{\Delta_{eadi}} \right) \left(\frac{1}{\Delta^2_{ciab}} - \frac{1}{\Delta^2_{ciab} + \Delta_{ecdb}\Delta_{eadi}} \right) \right]. \tag{4.131}$$

Lastly, the $f^{[3],III}(s)$ can be given as

$$f^{[3],III}_{ij}(s) = \frac{1}{4} e^{-\Delta^2_{ij} s} \sum_{abcdx} (n_a n_b \bar{n}_c \bar{n}_d - \bar{n}_a \bar{n}_b n_c n_d)(2\Delta_{abcd} + \Delta_{ij}) V_{cdab} \int_0^s e^{-2\Delta_{abcd}(\Delta_{abcd}+\Delta_{ij})z}$$
$$\cdot P(ab/i) P(j/cd) V_{abjx} V_{xicd} \left[(\Delta_{abcd} + \Delta_{ij})(-\delta_{abjx} + \delta_{xicd}) z \right.$$
$$\left. \frac{1}{2} \bar{\delta}_{abjx} \bar{\delta}_{cdxi} \left(\frac{1}{\Delta_{abjx}} + \frac{1}{\Delta_{cdxi}} \right) \left(1 - e^{-2\Delta_{abjx}\Delta_{cdxi} z} \right) \right] dz. \tag{4.132}$$

The permutation operators in Eq. (4.132) can be simplified as

$$P(ab/i)P(j/cd) = 1 - 2(1+P_{ij})P_{ai} + 4P_{ai}P_{jc}. \tag{4.133}$$

Following the above relation, the $f^{[3],III}(s)$ can be given as

$$f^{[3],III}(s) = f^{[3],IIIa}(s) + f^{[3],IIIb}(s) + f^{[3],IIIc}(s). \tag{4.134}$$

In the $s \to \infty$ limit for $\Delta_{ij} = 0$, each term is given by

$$f^{[3],IIIa}_{ij}(\infty) = \frac{1}{8} \sum_{abcdx} (n_a n_b \bar{n}_c \bar{n}_d n_x - \bar{n}_a \bar{n}_b n_c n_d n_x + n_a n_b \bar{n}_c \bar{n}_d \bar{n}_x - \bar{n}_a \bar{n}_b n_c n_d \bar{n}_x) V_{cdab} V_{abjx} V_{xicd}$$
$$\bar{\delta}_{abcd} \left[\frac{-\delta_{abjx} + \delta_{xicd}}{\Delta^2_{abcd}} \right.$$
$$\left. \bar{\delta}_{abjx} \bar{\delta}_{xicd} \Delta_{abcd} \left(\frac{1}{\Delta_{abjx}} + \frac{1}{\Delta_{cdxi}} \right) \left(\frac{1}{\Delta^2_{abcd}} - \frac{1}{\Delta^2_{abcd} + \Delta_{abjx}\Delta_{cdxi}} \right) \right]. \tag{4.135}$$

$$f^{[3],IIIb}_{ij}(\infty) = -\frac{1+P_{ij}}{4} \sum_{abcdx} (n_a n_b \bar{n}_c \bar{n}_d n_x - \bar{n}_a \bar{n}_b n_c n_d n_x + n_a n_b \bar{n}_c \bar{n}_d \bar{n}_x - \bar{n}_a \bar{n}_b n_c n_d \bar{n}_x) V_{cdab} V_{ibjx} V_{xacd}$$
$$\bar{\delta}_{abcd} \left[\frac{-\delta_{bx} + \delta_{xacd}}{\Delta^2_{abcd}} \right.$$
$$\left. + \bar{\delta}_{bx} \bar{\delta}_{cdxa} \Delta_{abcd} \left(\frac{1}{\Delta_{bx}} + \frac{1}{\Delta_{cdxa}} \right) \left(\frac{1}{\Delta^2_{abcd}} - \frac{1}{\Delta^2_{abcd} + \Delta_{bx}\Delta_{cdxa}} \right) \right]. \tag{4.136}$$

$$f_{ij}^{[3],IIIc}(\infty) = -\frac{1}{2}\sum_{abcdx}(n_a n_b \bar{n}_c \bar{n}_d n_x - \bar{n}_a \bar{n}_b n_c n_d n_x + n_a n_b \bar{n}_c \bar{n}_d \bar{n}_x - \bar{n}_a \bar{n}_b n_c n_d \bar{n}_x) V_{cdab} V_{ibcx} V_{xajd}$$
$$\bar{\delta}_{abcd}\left[\frac{-\delta_{ibcx}+\delta_{xajd}}{\Delta_{abcd}^2}\right.$$
$$\left.+\bar{\delta}_{ibcx}\bar{\delta}_{xaid}\Delta_{abcd}\left(\frac{1}{\Delta_{ibcx}}+\frac{1}{\Delta_{idxa}}\right)\left(\frac{1}{\Delta_{abcd}^2}-\frac{1}{\Delta_{abcd}^2+\Delta_{ibcx}\Delta_{idxa}}\right)\right]. \tag{4.137}$$

Here, we demonstrate how the contributions from $[\eta^{(1)},\Gamma]$, $[\eta^{(3)},\Gamma]$ and $[\eta^{(2)},W]$ are superposed to reproduce the many-body perturbation theory. In doing so, it is convenient to divide the total contribution to the effective one-body interactions $H_{ij}^{(1)[3]}$ to the three different classes.

$$H_{ij}^{(1)[3]} = H_{ij}^{(1)[3]\text{class1}} + H_{ij}^{(1)[3]\text{class2}} + H_{ij}^{(1)[3]\text{class3}}. \tag{4.138}$$

The Class 1 diagrams

$$H_{ij}^{(1)[3]\text{class1}} := f_{ij}^{[3],I}(\infty) + f_{ij}^{[3],IIIb}(\infty)$$
$$= -\frac{1}{4}\sum_{abcdx}(n_a n_b \bar{n}_c \bar{n}_d \bar{n}_x - \bar{n}_a \bar{n}_b n_c n_d n_x) V_{axcd} V_{cdab} V_{ibjx} \bar{\delta}_{bx}$$
$$\left[\frac{2\delta_{axcd}}{\Delta_{xb}\Delta_{abcd}} + \bar{\delta}_{axcd}\left\{\frac{2}{\Delta_{xb}\Delta_{abcd}} + \frac{\Delta_{abcd}^2-\Delta_{xb}^2}{\Delta_{xb}\Delta_{abcd}}\left(\frac{1}{\underline{\Delta_{xb}^2+\Delta_{axcd}\Delta_{abcd}}} - \frac{1}{\Delta_{abcd}^2+\Delta_{xb}\Delta_{axcd}}\right)\right\}\right]$$
$$+\frac{1}{4}\sum_{abcdx}(n_a n_x \bar{n}_b \bar{n}_c \bar{n}_d - \bar{n}_a \bar{n}_x n_b n_c n_d) V_{axcd} V_{cdab} V_{ibjx} \bar{\delta}_{bx}$$
$$\left[\frac{2\delta_{abcd}}{\Delta_{xb}\Delta_{abcd}} + \bar{\delta}_{abcd}\left\{\frac{2}{\Delta_{xb}\Delta_{axcd}} + \frac{\Delta_{axcd}^2-\Delta_{xb}^2}{\Delta_{xb}\Delta_{axcd}}\left(\frac{1}{\underline{\Delta_{xb}^2+\Delta_{axcd}\Delta_{abcd}}} - \frac{1}{\Delta_{axcd}^2-\Delta_{xb}\Delta_{abcd}}\right)\right\}\right]$$
$$-\frac{1}{4}\sum_{abcdx}(n_a n_b \bar{n}_c \bar{n}_d n_x - \bar{n}_a \bar{n}_b n_c n_d \bar{n}_x) V_{ibjx} V_{xacd} V_{cdab}$$
$$\left[\frac{1}{\Delta_{abcd}\Delta_{cdxa}} + \frac{\Delta_{cdxa}^2-\Delta_{abcd}^2}{\Delta_{cdxa}\Delta_{abcd}}\left(\frac{1}{\underline{\Delta_{abcd}^2+\Delta_{bx}\Delta_{cdxa}}} - \frac{1}{\Delta_{cdxa}^2+\Delta_{abcd}\Delta_{bx}}\right)\right]. \tag{4.139}$$

The terms in the underlines in Eq. (4.139) are zero due to the relation

$$\Delta_{bx} - \Delta_{abcd} = \Delta_{cdxa}. \tag{4.140}$$

Finally, one obtains

$$f_{ij}^{[3],I}(\infty) + f_{ij}^{[3],IIIb}(\infty)$$
$$= \frac{1}{2}\sum_{abcdx}(n_a n_b \bar{n}_c \bar{n}_d \bar{n}_x - \bar{n}_a \bar{n}_b n_c n_d n_x)\frac{V_{xacd} V_{cdba} V_{ibjx}}{\Delta_{bx}\Delta_{cdab}} \tag{4.141a}$$

$$+\frac{1}{2}\sum_{abcdx}(n_a n_x \bar{n}_b \bar{n}_c \bar{n}_d - \bar{n}_a \bar{n}_x n_b n_c n_d)\frac{V_{ibx}V_{cdab}V_{axcd}}{\Delta_{xb}\Delta_{axcd}} \tag{4.141b}$$

$$-\frac{1}{2}\sum_{abcdx}(n_a n_b n_x \bar{n}_c \bar{n}_d - \bar{n}_a \bar{n}_b \bar{n}_x n_c n_d)\frac{V_{ibjx}V_{xacd}V_{cdba}}{\Delta_{abcd}\Delta_{xacd}}. \tag{4.141c}$$

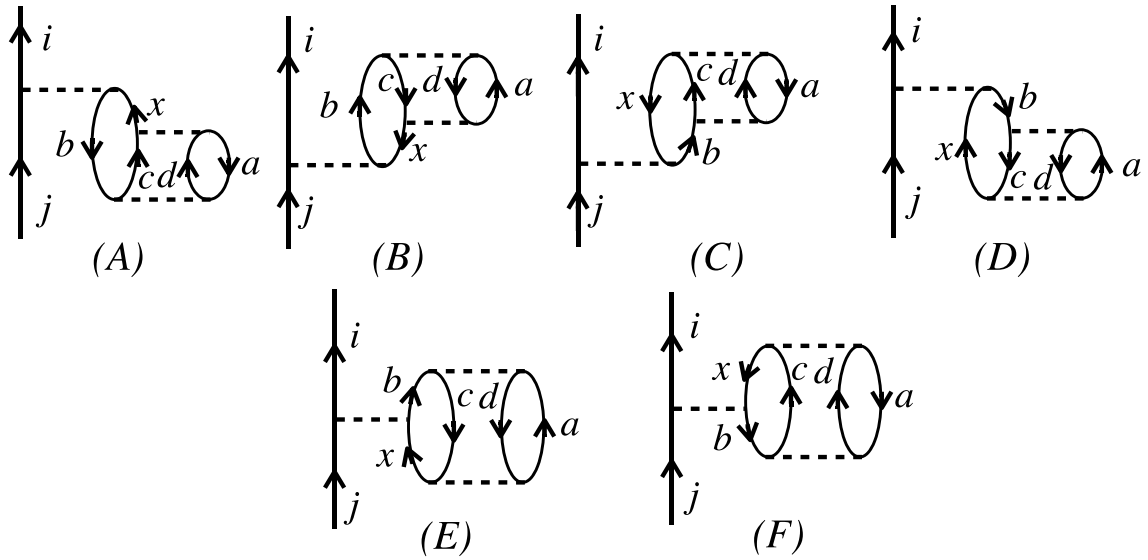

Figure 4.3: The third-order diagrams in $Q^{(3)}$ that are reproduced by the perturbative solution of the IM-SRG(3).

The two terms in Eq. (4.141a) correspond to the diagrams (A) and (B) in Fig. 4.3. In the same way, Eq. (4.141b) are identical to (C) and (D), and Eq. (4.141c) correspond to (E) and (F). As shown above, there is a complicated superposition between different contributions.

The class 2 diagrams

$$H_{ij}^{(1)[3]\text{class2}} := f_{ij}^{[3],II\text{pphh}}(\infty) + f_{ij}^{[3],IIIa}(\infty)$$

$$= \frac{1}{4}\sum_{abcdx;\Delta\neq 0} n_a n_b \bar{n}_c \bar{n}_d \bar{n}_x \frac{V_{cdab}V_{abjx}V_{xicd}}{\Delta_{abix}\Delta_{abcd}} + \frac{1}{4}\sum_{abcdx;\Delta\neq 0} \bar{n}_a \bar{n}_b n_c n_d \bar{n}_x \frac{V_{cdab}V_{abjx}V_{xicd}}{\Delta_{cdxi}\Delta_{cdab}} \tag{4.142a}$$

$$-\frac{1}{4}\sum_{abcdx;\Delta\neq 0} \bar{n}_a \bar{n}_b n_c n_d n_x \frac{V_{cdab}V_{abjx}V_{xicd}}{\Delta_{ixab}\Delta_{cdab}} - \frac{1}{4}\sum_{abcdx;\Delta\neq 0} n_a n_b \bar{n}_c \bar{n}_d n_x \frac{V_{cdab}V_{abjx}V_{xicd}}{\Delta_{xicd}\Delta_{abcd}} \tag{4.142b}$$

$$+\frac{1}{4}\sum_{abcdx;\Delta\neq 0} \bar{n}_a \bar{n}_b \bar{n}_c \bar{n}_d n_x \frac{V_{abjx}V_{xicd}V_{dcab}}{\Delta_{xiab}\Delta_{xicd}} - \frac{1}{4}\sum_{abcdx;\Delta\neq 0} n_a n_b n_c n_d \bar{n}_x \frac{V_{abjx}V_{xicd}V_{dcab}}{\Delta_{abxi}\Delta_{cdxi}} \tag{4.142c}$$

$$+ C_{ij}^{(1)[3]\text{class2}}. \tag{4.142d}$$

The $C_{ij}^{(1)[3]\mathrm{class2}}$ in the above equation is given by

$$C_{ij}^{(1)[3]\mathrm{class1}} = -\frac{1+P_{ij}}{2}\frac{1}{4}\sum_{abcdx;\Delta\neq 0} n_a n_b \bar{n}_c \bar{n}_d \bar{n}_x \delta_{xiab} \frac{V_{cdab}V_{abjx}V_{xicd}}{\Delta_{xicd}\Delta_{abcd}} \tag{4.143a}$$

$$+\frac{1+P_{ij}}{2}\frac{1}{4}\sum_{abcdx;\Delta\neq 0} \bar{n}_a \bar{n}_b n_c n_d n_x \delta_{xiab} \frac{V_{cdab}V_{abjx}V_{xicd}}{\Delta_{cdxi}\Delta_{cdab}} \tag{4.143b}$$

$$+\frac{1+P_{ij}}{2}\frac{1}{4}\sum_{abcdx;\Delta\neq 0} \bar{n}_a \bar{n}_b \bar{n}_c \bar{n}_d n_x \delta_{xicd} \frac{V_{abjx}V_{xicd}V_{dcab}}{\Delta_{xiab}\Delta_{abcd}} \tag{4.143c}$$

$$-\frac{1+P_{ij}}{2}\frac{1}{4}\sum_{abcdx;\Delta\neq 0} n_a n_b n_c n_d \bar{n}_x \delta_{xicd} \frac{V_{abjx}V_{xicd}V_{dcab}}{\Delta_{xiab}\Delta_{abcd}}. \tag{4.143d}$$

The terms in Eq. (4.142a-4.142c) are identical to the corresponding MBPT(3), while the correction terms belonging to the $C_{ij}^{(1)[3]\mathrm{class2}}$ give non-zero contribution only when a denominator in the former terms in Eq. (4.142a-4.142c) becomes zero. When one drives an effective interaction based on the perturbation theory, a model space is assumed, where the unperturbed single-particle energy of valence particles is typically considered to be degenerate in order to prevent the divergence due to the zero denominator. It is important to note that in the perturbative solution of the IM-SRG(3), all the denominators that are zero are excluded from the intermediate summation. Therefore, there is no diverging term. The additional term, $C_{ij}^{(1)[3]\mathrm{class2}}$, is in fact the correction to the ordinary many-body perturbation theory. All the terms in the $C_{ij}^{(1)[3]\mathrm{class2}}$ vanishes when one goes to the degenerate many-body perturbation theory for valence nucleons. Here I show a couple of examples. The correction at the first term in Eq. (4.143a) only appears when a denominator Δ_{xiab} in the original diagrams in the first term of Eq. (4.142a), or Fig. 4.4(A), becomes zero. Since $\Delta_{xiab} = \varepsilon_x + \varepsilon_i - \varepsilon_a - \varepsilon_b \neq 0$ as long as the state i belongs to particle state, this term does not contribute to the valence-nucleon interactions. Next, the correction at the first term of Eq. (4.143c), which is the complement of the first term of Eq. (4.142b), only contributes when $\Delta_{xiab} = 0$. The $\Delta_{xiab} < 0$ as long as the state i belongs to hole state. If one assumes the degenerate model space with the single-particle energy is ω, then $\Delta_{xiab} < \varepsilon_x - \omega < 0$. Thus, the Δ_{xiab} does not equal zero when one employs the degenerate model space, and this term does not contribute for the effective one-body interactions for valence nucleons. In the same manner, one can easily show that the correction terms in $C_{ij}^{(1)[3]\mathrm{class2}}$ vanish for the degenerate model space.

The class 3 diagrams

$$H_{ij}^{(1)[3]\mathrm{class3}} := f_{ij}^{[3],II\mathrm{ph}}(\infty) + f_{ij}^{[3],IIIc}(s)$$

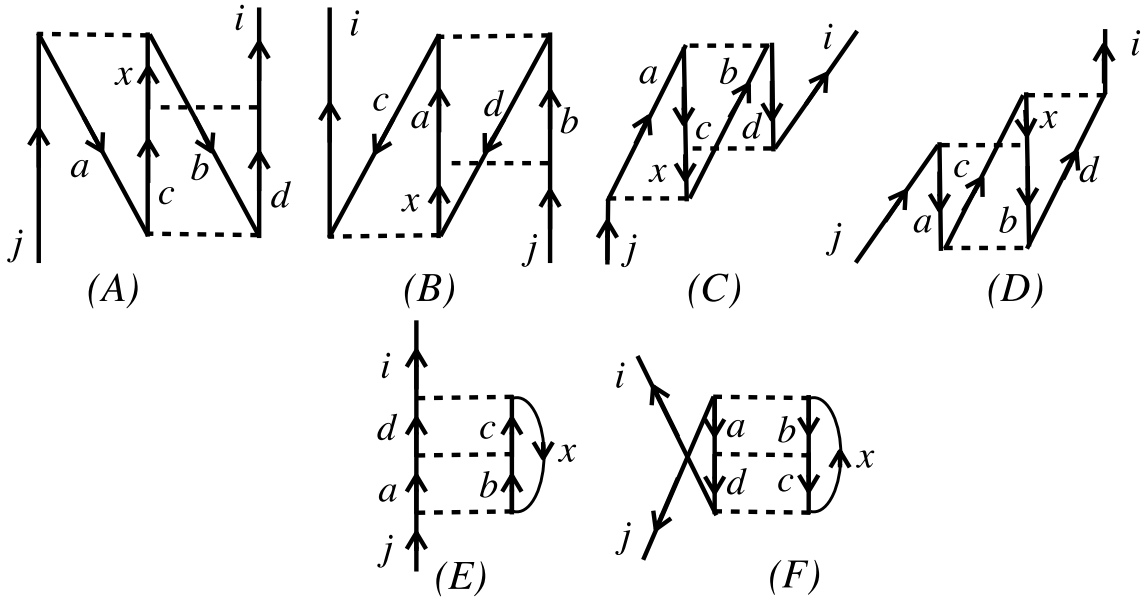

Figure 4.4: The third-order perturbation diagrams in $Q^{(3)}$ that can be obtained by the perturbative solution of IM-SRG(3).

$$= -\sum_{abcdx;\Delta\neq 0} n_a n_b \bar{n}_c \bar{n}_d n_x \frac{V_{axdj} V_{bicx} V_{cdba}}{\Delta_{axdi} \Delta_{abcd}} - \sum_{abcdx;\Delta\neq 0} \bar{n}_a \bar{n}_b n_c n_d n_x \frac{V_{axdj} V_{bicx} V_{cdba}}{\Delta_{cxbi} \Delta_{cdab}} \tag{4.144a}$$

$$+ \sum_{abcdx;\Delta\neq 0} \bar{n}_a \bar{n}_b n_c n_d \bar{n}_x \frac{V_{axdj} V_{bicx} V_{cdba}}{\Delta_{diax} \Delta_{cdab}} + \sum_{abcdx;\Delta\neq 0} n_a n_b \bar{n}_c \bar{n}_d \bar{n}_x \frac{V_{djax} V_{cxbi} V_{abdc}}{\Delta_{bicx} \Delta_{abcd}} \tag{4.144b}$$

$$- \sum_{abcdx;\Delta\neq 0} n_a n_b n_x \bar{n}_c \bar{n}_d \frac{V_{bxcj} V_{acdb} V_{diax}}{\Delta_{bxci} \Delta_{xadi}} + \sum_{abcdx;\Delta\neq 0} \bar{n}_a \bar{n}_b n_c n_d \bar{n}_x \frac{V_{bxcj} V_{acdb} V_{diax}}{\Delta_{cixb} \Delta_{diax}} \tag{4.144c}$$

$$+ C_{ij}^{(1)[3]\text{class3}}, \tag{4.144d}$$

where the correction term $C_{ij}^{(1)[3]\text{class3}}$ can be given by

$$C_{ij}^{(1)[3]\text{class3}} = \frac{1+P_{ij}}{2} \sum_{abcdx;\Delta\neq 0} n_a n_b \bar{n}_c \bar{n}_d n_x \delta_{diax} \frac{V_{axdj} V_{bicx} V_{cdba}}{\Delta_{bicx} \Delta_{abcd}} \tag{4.145a}$$

$$- \frac{1+P_{ij}}{2} \sum_{abcdx;\Delta\neq 0} \bar{n}_a \bar{n}_b n_c n_d \bar{n}_x \delta_{xaid} \frac{V_{axdj} V_{bicx} V_{cdba}}{\Delta_{cxbi} \Delta_{cdab}} \tag{4.145b}$$

$$+ \frac{1+P_{ij}}{2} \sum_{abcdx;\Delta\neq 0} n_a n_b n_x \bar{n}_c \bar{n}_d \delta_{diax} \frac{V_{bxcj} V_{acdb} V_{diax}}{\Delta_{xbci} \Delta_{dbac}} \tag{4.145c}$$

$$- \frac{1+P_{ij}}{2} \sum_{abcdx;\Delta\neq 0} \bar{n}_a \bar{n}_b n_c n_d \bar{n}_x \delta_{diax} \frac{V_{bxcj} V_{acdb} V_{diax}}{\Delta_{cixb} \Delta_{dbac}} \tag{4.145d}$$

The terms in Eqs. (4.144a-4.144b) correspond to the third-order screening effects, and the terms in Eq. (4.144c) correspond to the Tamm-Dancoff diagrams in the same order. The

correction terms in Eqs. (4.145) do not appear in the third order perturbation theory explicitly. They do not vanish only when the denominators (Δ's) in the corresponding perturbation contributions become zero as shown in the case of the class 2 terms. Likewise, the discussion

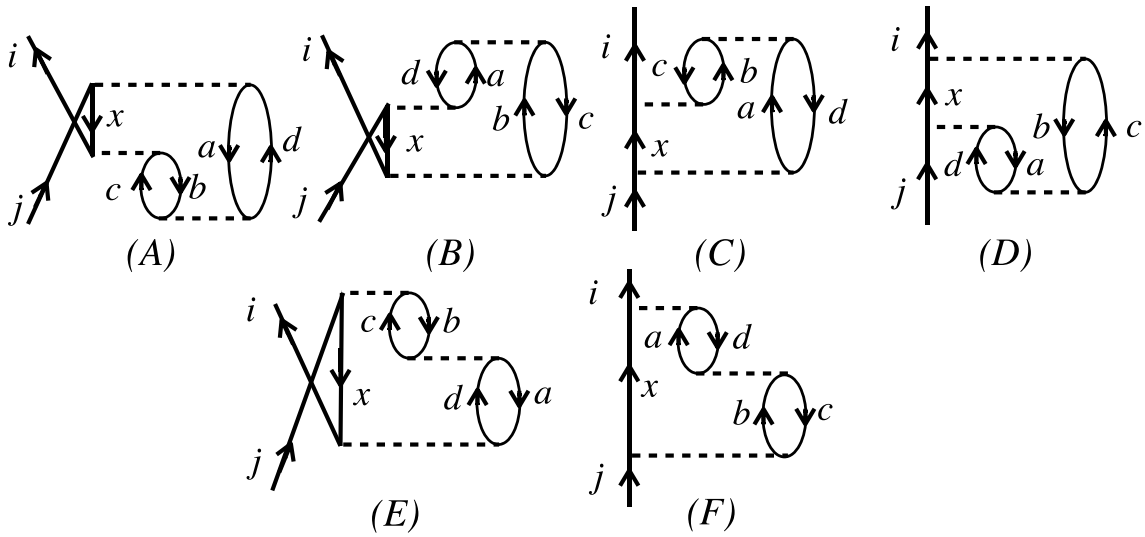

Figure 4.5: The third-order perturbation diagrams in $Q^{(3)}$ obtained by the perturbative solution of the IM-SRG(3).

for the one-body terms $f^{[3]}$ holds for the two-body terms $\Gamma^{[3]}$ as well. An important consequence is that the IM-SRG by construction does not contain zero denominator in the final results. This means that the application of the IM-SRG to the derivation of effective valence shell-model interactions can be flexible since one does not have to restrict the model space for valence shell nucleons to one major shell and can consider the multi-major shells, for which the ordinary perturbation theory diverges due to the zero denominator. This flexibility is quite important for the description of island of inversion, for which the shell model with two major shells is indispensable.

4.4 Truncation scheme of the IM-SRG flow equation

The previous section shows the clear connection to the many-body perturbation theory. In addition to that, one can see an interesting structure of the flow equation. The perturbative analysis tells us

$$f_{ii} = \mathcal{O}(1), \qquad f_{ij} = \mathcal{O}(g^2) \quad (i \neq j), \tag{4.146}$$

$$\Gamma = \mathcal{O}(g), \qquad W = \mathcal{O}(g^2), \tag{4.147}$$

$$\eta^{(1)} = \mathcal{O}(g^2), \qquad \eta^{(2)} = \mathcal{O}(g), \qquad \eta^{(3)} = \mathcal{O}(g^2). \tag{4.148}$$

Thus, the each term in the flow equation can be classified in terms of the power of the bare coupling, k of g^k. The classified flow equation is given by

$$\frac{d}{ds}E_0(s) = \underline{[\eta^{(2)}, \Gamma]^{[2]}} + [\eta^{(1)}, f]^{[4]} + [\eta^{(3)}, W]^{[4]} \tag{4.149}$$

$$\frac{d}{ds}f(s) = \underline{[\eta^{(1)}, f]^{[2]} + [\eta^{(2)}, \Gamma]^{[2]}} + [\eta^{(1)}, \Gamma]^{[3]} + [\eta^{(2)}, f]^{[3]} + [\eta^{(2)}, W]^{[3]} + [\eta^{(3)}, \Gamma]^{[3]} + [\eta^{(3)}, W]^{[4]} \tag{4.150}$$

$$\begin{aligned}\frac{d}{ds}\Gamma(s) = {} & \underline{[\eta^{(2)}, f]^{[1]} + [\eta^{(2)}, \Gamma]^{[2]}} + [\eta^{(1)}, \Gamma]^{[3]} + [\eta^{(2)}, W]^{[3]} + [\eta^{(3)}, \Gamma]^{[3]} \\ & + [\eta^{(1)}, W]^{[4]} + [\eta^{(3)}, f]^{[4]} + [\eta^{(3)}, W]^{[4]}\end{aligned} \tag{4.151}$$

$$\frac{d}{ds}W(s) = \underline{[\eta^{(3)}, f]^{[2]} + [\eta^{(2)}, \Gamma]^{[2]}} + [\eta^{(2)}, W]^{[3]} + [\eta^{(3)}, \Gamma]^{[3]} + [\eta^{(1)}, W]^{[4]} + [\eta^{(3)}, f]^{[4]}. \tag{4.152}$$

The superscript $[k]$ of the commutator $[X, Y]^{[k]}$ denotes the power in the bare coupling which the term at least contains, while the superscript with the parenthesis $X^{(n)}$ means that the operator X is a n-body operator. The terms in the same order should be treated consistently at least to reproduce the perturbation theory. In fact, the perturbative solution showed the very complicated superposition among the third-order terms in the one-body sector of the flow equation. The important point is that one-, two- and three-body operators contribute to the same order in the flow equation. This means that the truncation of the flow equation in terms of the n-body operators cannot be the relevant scheme. Of course, the SRG is non-perturbative and thus in principle contains higher-order terms in the bare coupling. But the truncation by n of n-body operator sums inconsistent contributions to infinite order, making the evolution in the wrong direction. Therefore, we only keep the terms with the under lines in the flow equation. One has to include the three-body operators, $\eta^{(3)}$ and W, when going to one higher order in the flow equation. The excluded $\mathcal{O}(g^3)$ terms in one- and two-body

sectors in the flow equation mainly contribute to the E_0 of $\mathcal{O}(g^4)$ correction as simultaneous 3p3h excitations for the reference state. But this doesn't mean IM-SRG(2) does not contain intermediate 3p3h-excited determinants since they are generated during the flow. In the case of CC, on the other hand, CCSD energy lacks triple excitation, which is mostly improved by (T) correction.

It should be noted that the IM-SRG has the machinery for the systematic improvement.

Chapter 5

Numerical results

In this Chapter, we show the application of the IM-SRG to doubly-magic nuclei. For all cases the flow equations, Eqs. (3.16)–(3.18), were solved in a J-coupled basis. All the flow equations are solved in truncated subspace of the Hilbert space, or model space. The model space is specified by the single-particle energy cutoff $e_{\max} = \max(2n + l)$, where the n and l are the quantum numbers of the underlying oscillator orbits. The actual form of the flow equation is a simultaneous ordinary differential equations (SODE) which are to be solved numerically,

$$\frac{d}{ds}\boldsymbol{a}(s) = \beta(\boldsymbol{a}, s), \tag{5.1}$$

where the $\boldsymbol{a}$ is the vector whose components are the coefficients of the normal-ordered Hamiltonian, and the $\beta(\boldsymbol{a}, s)$ is a function of $\boldsymbol{a}$ and s determined by the flow equation (3.74). Table 5.1 shows the number of the single-particle orbits and the length of the vector $\boldsymbol{a}$, $M = \dim(\boldsymbol{a})$, *i.e.*, the numbers of the components in the SODE, at each model space defined by $e_{\max}$. One should note that our truncation scheme for the model space does not guarantee the decoupling of the A-body Hamiltonian into its intrinsic and center of mass (c.m.) part. Therefore, the IM-SRG is not free from the contamination of the excitations of the c.m. motion, which we are not interested in. We will clearly show in the later section that the decoupling of the c.m. motion is in fact achieved in the IM-SRG solution.

5.1 ^{4}He

We start with the results for ^{4}He in order to demonstrate the solution of the flow equation in detail. Figure 5.1(a) shows the evolution of the ground-state energy of ^{4}He calculated in different sizes of the model spaces with $\hbar\omega = 36$ MeV. We employ the Wegner's choice for

model space ($e_{\max}$)	number of the s.p. orbits	$M = \dim(\boldsymbol{a})$ in the SODE
3	20	6,599
4	30	34,365
5	42	139,111
6	56	467,133
7	72	1,358,427
8	90	3,526,815

Table 5.1: The counts of the possible single-particle orbits and the length of the vector to be solved in the flow equation. The numbers are counted for the spherical Harmonic oscillator basis.

the generator, $\eta^{\rm I}(s)$, and the initial NN interaction is the N^{3}LO ($\Lambda = 500\,$MeV) potential of Ref. [7]. The initial values, $E_0(s=0)$ correspond to the Hartree-Fock energies, while the evolution by the IM-SRG(2) obtains the correlation energy by about 20–25 MeV. At each model space, the convergence with respect to the flow parameter s is clearly confirmed, and the convergence with respect to the size of the model space is also demonstrated for $E_0(\infty)$ values.

The convergence with respect to the basis parameter is demonstrated in Fig. 5.1(b). We start with the same NN interaction and solve the flow equation in the model spaces, $e_{\max} = 8$, where the ground-state energy is essentially converged. The figure shows the dependence of $E_0(\infty)$ on the value of $\hbar\omega$ of the underlying harmonic oscillator (HO). The $\hbar\omega$-dependence seen at the Hartree-Fock level disappears after the evolution.

Figure 5.2 shows the IM-SRG(2) ground-state energy $E_0(\infty)$ for ^{4}He calculated in increasing spaces defined by the single-particle $e_{\max} \equiv \max(2n+l)$ with the two different choices of the generators, $\eta^{\rm I}$ and $\eta^{\rm II}$. For both cases, we plot the results by the original IM-SRG(2), denoted by IM-SRG, and those based on the consistent truncation scheme, denoted by IM-SRG'. The results for both generators are found to be in good agreement with the coupled-cluster CCSD(T) energies (based on the code of Ref. [44]), with slightly more binding at larger $\hbar\omega$ values. In addition, the $e_{\max} = 8$ energies are essentially converged and within 20 keV of the exact NCSM diagonalization [40]. Likewise, the $\eta^{\rm I}$ and $\eta^{\rm II}$ results agree within 20 keV, which suggests the truncation to normal-ordered two-body interactions is a controlled approximation.

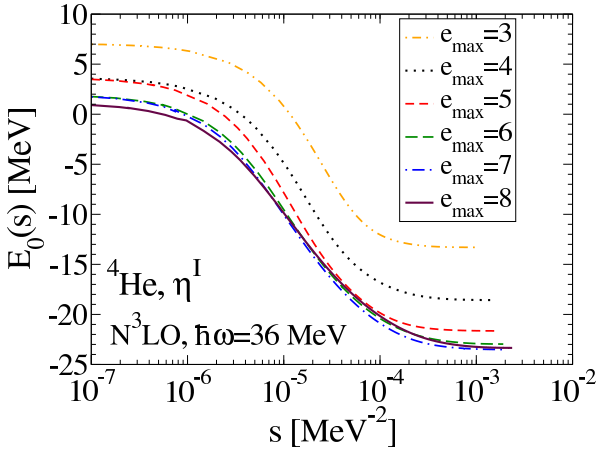

(a) Model space dependence

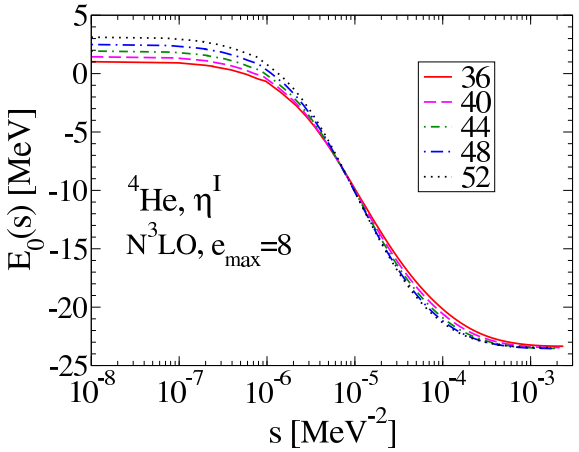

(b) $\hbar\omega$ dependence

Figure 5.1: The evolution of the ground-state energy $E_0(s)$ for ^{4}He as a function of the flow parameter s. Left panel: Different curves correspond to the $E_0(s)$ solved in different model spaces, which are truncated Hilbert space. The $E_0(\infty)$ converges as the model space increases. Right panel: Different curves correspond to the results solved with different frequencies of the underlying oscillator basis, $\hbar\omega$ ranging from 36 to 52 MeV.

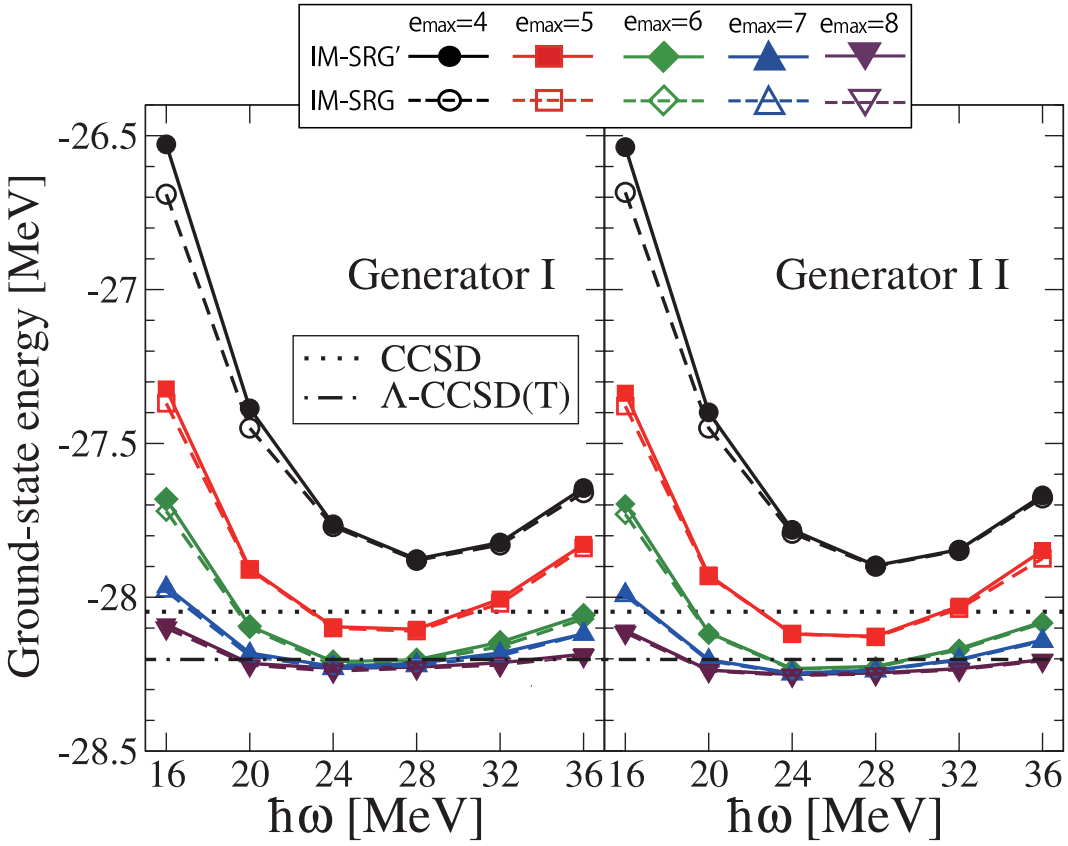

Figure 5.2: Convergence of the in-medium SRG results at the normal-ordered two-body level, IM-SRG(2), for ^{4}He using the generators η^{I} (left) and η^{II} (right panel). For both generators, the results of the IM-SRG(2), denoted by IM-SRG, and those obtained by the additional truncation, denoted by IM-SRG', are plotted. The ground-state energy is given as a function of the harmonic oscillator parameter $\hbar\omega$ with increasing single-particle space $e_{\max} \equiv \max(2n+l)$. The initial NN interaction is a free-space SRG-evolved potential with $\lambda = 2.0\,\mathrm{fm}^{-1}$ from the N^{3}LO ($\Lambda = 500\,\mathrm{MeV}$) potential of Ref. [7]. For comparison we show coupled-cluster CCSD and CCSD(T) results in the same $e_{\max}$ space (based on the code of Ref. [44]), where the IM-SRG(2) energies are found to approximately follow CCSD(T).

The figure 5.2 also shows that the difference between the IM-SRG(2) and the IM-SRG(2)' is negligible in this case. This is because we start with a soft NN potential. The discrepancy stemming from the inconsistent inclusion of the terms in the flow equation occurs at the higher order in terms of the NN interactions. This should be very small for soft NN interactions, which is by construction perturbative. On the other hand, the inconsistency makes significant difference for harder interactions, for which the higher order contribution is not negligible.

This is manifested in Fig. 5.3(a). In the figure, the difference between the IM-SRG(2) and the IM-SRG(2)' are quite small for a soft initial NN interaction, and the both truncation schemes show good agreement with CC results (right panel). On the other hand, these two truncation schemes show significant discrepancy for a hard initial NN potential (left panel). The converged ground-state energies by the original IM-SRG(2) are closer to the results of CCSD(T) than the IM-SRG(2)'. This does not mean that the IM-SRG(2) is better than the IM-SRG(2)'. We emphasize that the large generator dependence of the ground-state energy is observed for the IM-SRG(2), while the IM-SRG(2)' shows smaller dependence on the choice of the generator, as shown in Fig. 5.3(b). We also note that the generator dependence in the IM-SRG(2)' depends weakly on the basis parameter $\hbar\omega$, but the original IM-SRG(2) shows uncontrollable dependence on the $\hbar\omega$.

Figure 5.4 demonstrates the fact that the IM-SRG is intrinsically non-perturbative. In the figure, the results with several many-body methods are compared for the N^{3}LO potential. The exact solution by Faddeev-Yakubowski calculation is shown as the solid horizontal line. This is very close to the converged result by the Λ-CCSD(T), which is the most accurate treatment of the triple correction in the CC theory. The IM-SRG(2) ground-state energy $E_0(\infty)$ for ^{4}He with the N^{3}LO potential. The results in all model spaces are between CCSD and CCSD(T), converging to the values closer to CCSD as expected by the truncation level (Eq. (3.16)- (3.18)). One should note that the low-order perturbation theory denoted as "MBPT(2,3)" for the second and the third order,respectively in the figure, does not work for this hard interaction, showing the uncontrollable $\hbar\omega$ dependence.

The suppression of $H^{\rm od}(s)$ is illustrated in Fig. 5.5(a), which shows the $\eta^{\rm I}$-evolution of normal-ordered two-body matrix elements Γ_{ijkl} at three different steps in s. In order to clearly show the suppression of the terms belonging to $H^{\rm od}$, we only show the evolution of the terms, Γ_{pppp}, Γ_{hhhh}, Γ_{pphh} and Γ_{hhpp} but do not plot Γ_{ppph}, Γ_{hhhp} and their hermitian conjugate. In the initial Hamiltonian $H(0)$, there are certain couplings (Γ_{pphh}, Γ_{hhpp}). As the Hamiltonian is evolved, the off-diagonal couplings ($ijkl = pphh$ or $hhpp$) are rapidly driven to zero, as

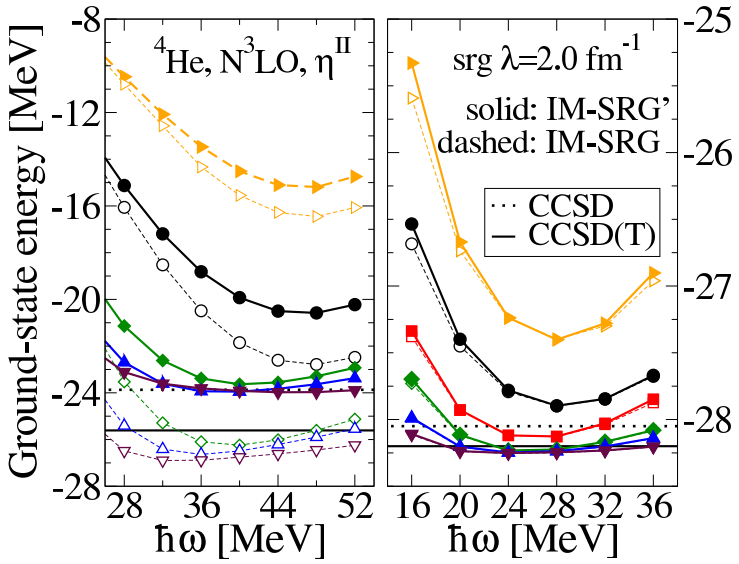

(a)

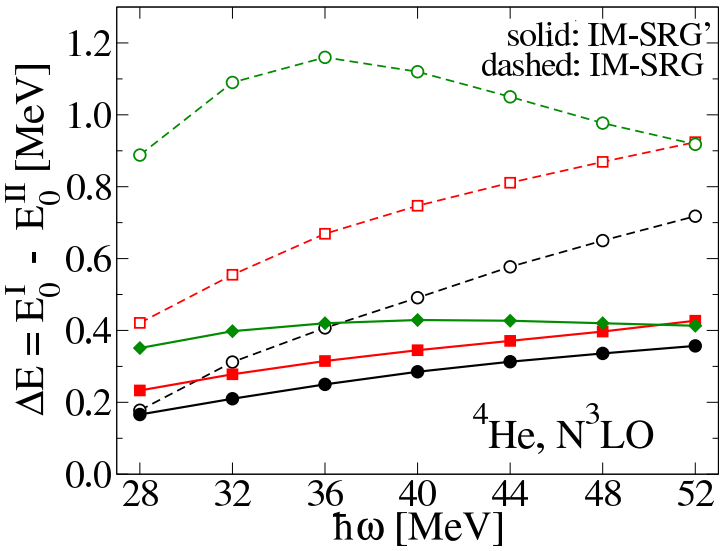

(b)

Figure 5.3: (a) Comparison between the original IM-SRG(2) and the one with consistent truncation scheme, IM-SRG', for the ground-state energy of ^{4}He. The left panel shows the results with N^{3}LO potential [7], while the right panel is for the SRG-evolved version down to $\lambda = 2.0\text{fm}^{-1}$. There are significant discrepancies between the original and consistently truncated IM-SRG(2). On the other hand, the the results with a softer interaction shows negligible discrepancies. (b) The generator dependence of the ground-state energies of ^{4}He obtained for N^{3}LO with the generator I and II. The difference $\Delta E_0 = E_0(\infty;\eta^I) - E_0(\infty;\eta^{II})$ is plotted as a function of the basis parameter $\hbar\omega$ for different sizes of the model spaces. For both choices of the generators, the flow equation is solved within the IM-SRG(2) and the IM-SRG(2)'.

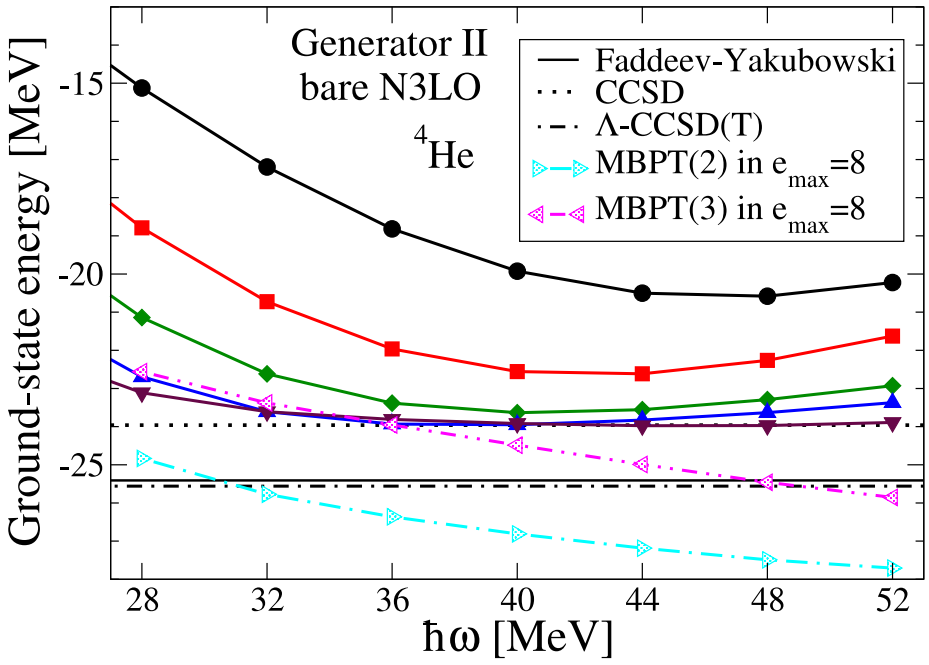

Figure 5.4: Convergence of the IM-SRG(2) for ^{4}He using the generators η^{II}. The notation is the same as Fig. 5.2. The initial NN interaction is the N^{3}LO ($\Lambda = 500\,\mathrm{MeV}$) potential of Ref. [7]. The IM-SRG(2) energies are found to approximately follow CCSD , while perturbation theory (MBPT(2,3)) breaks down.

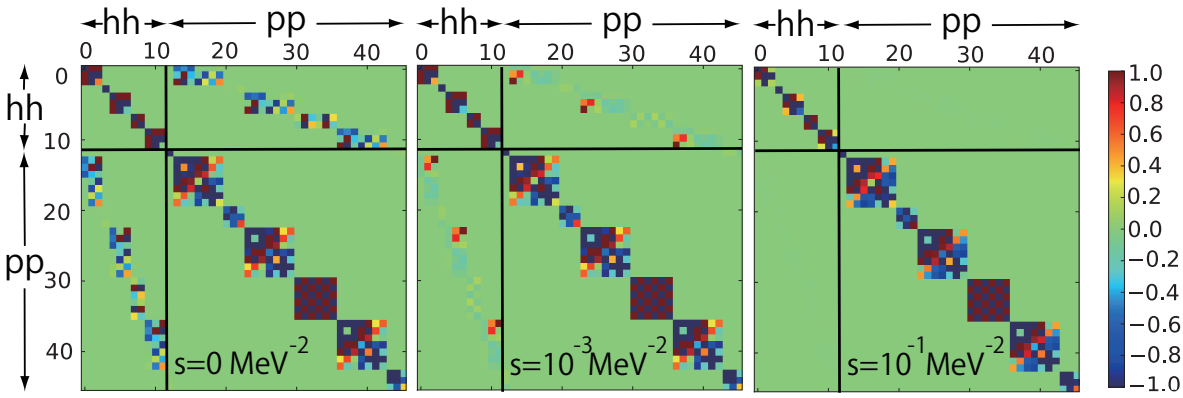

(a) Evolution of the two-body vertices.

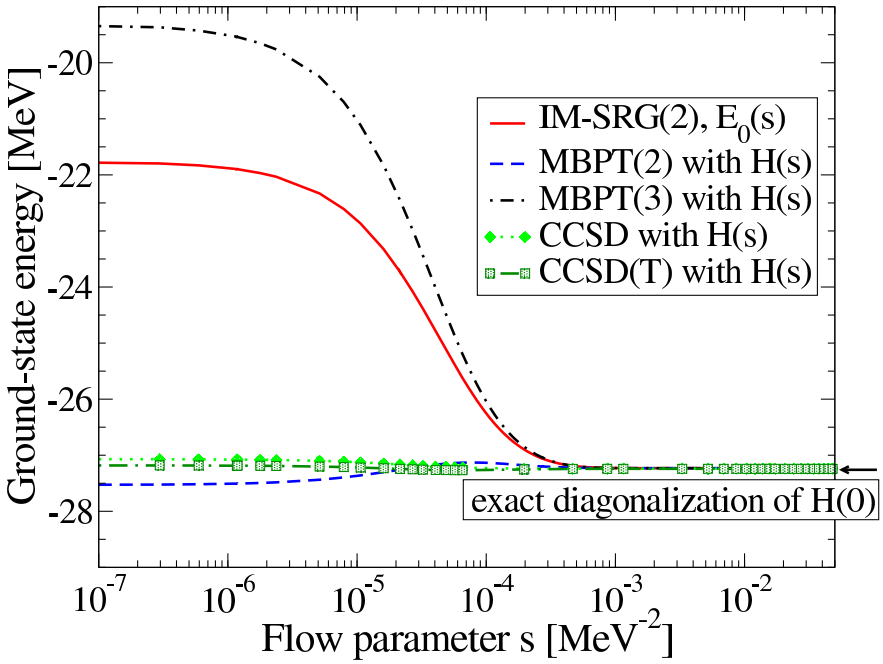

(b) Many-body theories with evolving $H(s)$.

Figure 5.5: **(a)**: In-medium SRG evolution of normal-ordered two-body matrix elements Γ_{ijkl} connecting hole-hole (hh) and particle-particle (pp) states for ^{16}O starting from a smooth-cutoff $V_{\mathrm{low}\,k}$ with $\Lambda = 1.8\,\mathrm{fm}^{-1}$. The color scale is in MeV and results for three values of the flow parameter s are shown. The axes label two-body jj-coupled states $|(n_a, l_a, j_a, t_{z_a}), (n_b, l_b, j_b, t_{z_b}); J = 0\rangle$. The Γ_{ijkl} where $ijkl = pppp$ or $hhhp$ are not shown to avoid the confusion. **(b)**: Evolution of the IM-SRG(2) ground-state energy $E_0(s)$ for ^{4}He as a function of the flow parameter s. The results are for $\hbar\omega = 24\,\mathrm{MeV}$ and $e_{\max} = 3$, starting from the same initial V_{NN} as in Fig. 5.2. The evolving IM-SRG(2) energy is compared to second- and third-order many-body perturbation theory, MBPT(2) and MBPT(3), respectively, and to CCSD and CCSD(T) results based on the evolving Hamiltonian $H(s)$. The arrow indicates the result of an exact diagonalization in $e_{\max} = 3$ of the initial $H(0)$.

expected, confirming the decoupling of the reference state $|\Phi_0\rangle$ from the Hilbert space (3.82).

One important practical consequence is that perturbative many-body approximations become more effective under the SRG evolution before complete decoupling has been reached. This is demonstrated in Fig. 5.5(b), where the ground-state energy of ^{4}He with the several many-body methods are plotted as a function of the flow parameter s. At each s, we calculate the ground-state energy by the second- and third-order MBPT(2,3), the CCSD and CCSD(T), for which we use the flowing Hamiltonian $H(s)$ as an input. For the initial Hamiltonian $H(0)$, the MBPT(2) and (3) deviate significantly, showing that the order-by-order perturbative approximation does not work even for relatively "soft" NN interaction. As s increases, the MBPT(2,3) approach the non-perturbative CC energies, reflecting the suppression of the off-diagonal part of the Hamiltonian $H^{\rm od}(s)$. One sees that the CCSD(T) is practically exact for this case since the result with the $H(0)$ is already very close the exact diagonalization. It is also important to note the approximately s-independent CCSD(T) results give further evidence that the normal-ordered two-body truncation, IM-SRG(2), is reliable.

5.2 Heavier systems: ^{16}O and ^{40}Ca

We apply the IM-SRG to calculate the ground-state energies of ^{16}O and ^{40}Ca in Fig. 5.6 using η^{II}. As for the ^{4}He results, the calculations are well converged and have accuracies between CCSD and CCSD(T).

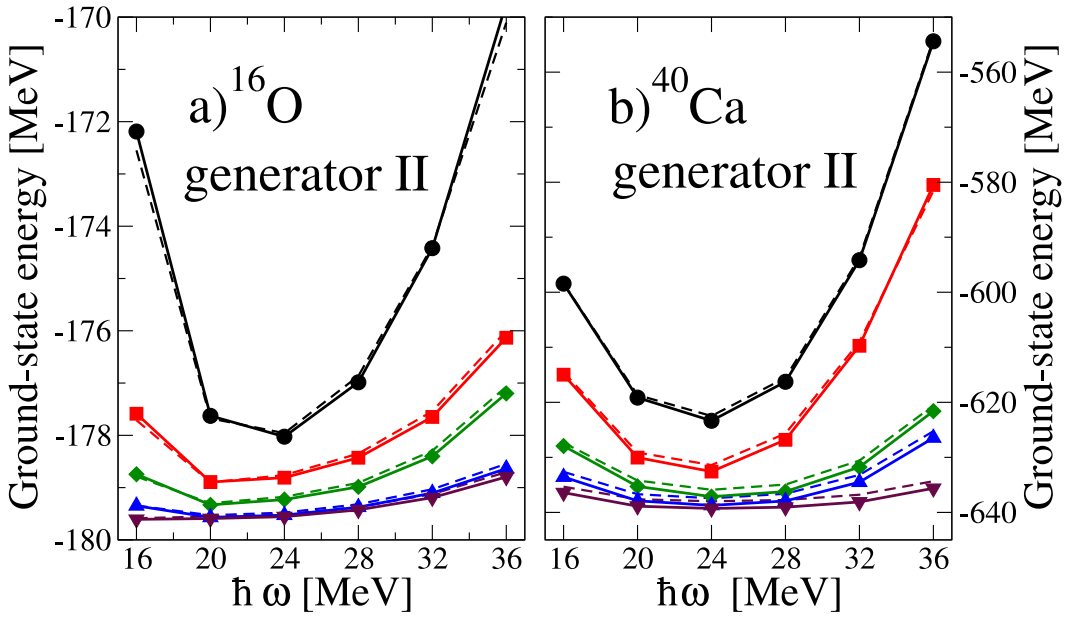

Figure 5.6: Convergence of the IM-SRG(2) ground-state energy $E_0(\infty)$ for ^{16}O (left) and ^{40}Ca (right panel) using η^{II}. For the legend see Fig. 5.2. The initial V_{NN} is a smooth-cutoff $V_{\mathrm{low}\,k}$ with $\Lambda = 1.8\,\mathrm{fm}^{-1}$ for ^{16}O and a free-space SRG potential with $\lambda = 1.8\,\mathrm{fm}^{-1}$ for ^{40}Ca, both evolved from the N^{3}LO ($\Lambda = 500\,\mathrm{MeV}$) potential of Ref. [7]. The IM-SRG(2) energies are found to lie between the CCSD and CCSD(T) results.

As discussed above, the IM-SRG(2) partially contains simultaneous $3p3h$ excitation for the $E_0(s)$ that partially cancel against contributions that would arise if three-body normal-ordered operators were kept in the flow equations. This motivates keeping only the underlined terms in Eqs. (4.149-4.151). The contribution from the excluded terms is negligible for soft interactions, while it becomes larger for the N^{3}LO and heavier systems, and thus require a consistent treatment either by omitting them in the IM-SRG(2) equations, or by including normal-ordered three-body operators in the flow equations. In the former case, one finds an accuracy that is comparable to CCSD calculations. Depending on how large the omitted $3p3h$

excitations are, the IM-SRG(2) energy gets close to CCSD or CCSD(T). For ^{4}He with "soft" interactions as seen in Fig. 5.2, IM-SRG(2) is very close to CCSD(T), where the interaction is perturbative and the simultaneous $3p3h$ excitations occurs less frequently. For heavier system, ^{16}O and ^{40}Ca, IM-SRG(2) results are CCSD level, where the simultaneous $3p3h$ excitations are more frequent than in ^{4}He.

Figure 5.7 shows the ground-state energy $E_0(\infty)$ of ^{16}O within the IM-SRG(2) with consistent truncation scheme for two different generators, $\eta^{\rm II}$ and $\eta^{\rm III}$. Although the fully converged results are not obtained in the figure, for each model spaces, the results of the IM-SRG(2)' are essentially generator-independent and lie in-between CCSD and CCSD(T).

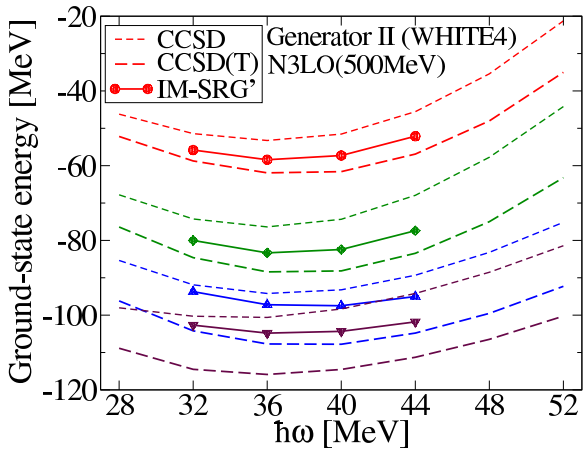

(a) generator II

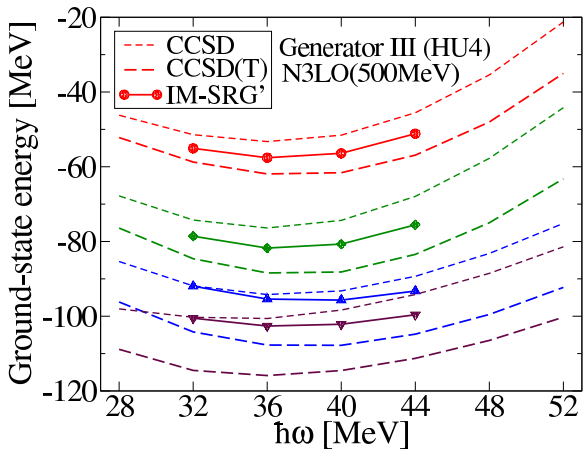

(b) generator III

Figure 5.7: Convergence of the IM-SRG(2) ground-state energy $E_0(\infty)$ for ^{16}O using η^{II} (left) and η^{III} (right). For the legend see Fig. 5.2. The initial V_{NN} is the N^{3}LO (Λ = 500 MeV) potential of Ref. [7]. The IM-SRG(2) energies are found to lie between the CCSD and CCSD(T) results.

5.3 Center of mass problem

In this section, we discuss to what extent the ground-state many-body wave function obtained by the IM-SRG(2) has the contamination by the center of mass excitation. The nuclear A-body Hamiltonian H_A is given by

$$H_A = H_{\rm in} + H_{\rm cm}. \tag{5.2}$$

The intrinsic part is

$$H_{\rm in} = \sum_{i=1}^{A} \frac{\boldsymbol{p}_i^2}{2m} - \frac{\boldsymbol{P}^2}{2mA} + \sum_{i<j} V(i,j) \tag{5.3}$$

$$= \frac{1}{A}\sum_{i<j}^{A} \left(\frac{(\boldsymbol{p}_i - \boldsymbol{p}_j^2)}{2m} + V(i,j) \right). \tag{5.4}$$

Here we define the center of mass (c.m.) coordinates as

$$\boldsymbol{P} \equiv \sum_{i=1}^{A} \boldsymbol{p}_i, \quad \boldsymbol{R} \equiv \frac{1}{A}\sum_{i=1}^{A} \boldsymbol{r}_i. \tag{5.5}$$

Since the nucleonic interactions are constructed so as to satisfy the rotation and translation invariance, the $H_{\rm in}$ is invariant under translation and rotation. The $H_{\rm in}$ does not depend on the c.m. coordinates thus one can add an arbitrary operator $H_{\rm cm}$ that depends on $\boldsymbol{P}$ and $\boldsymbol{R}$, keeping the intrinsic properties of the system unchanged. If the decoupling of the A-body wave function is achieved

$$|\psi_A\rangle = |\psi_{\rm in}\rangle \otimes |\psi_{\rm cm}\rangle\,, \tag{5.6}$$

the eigenenergy is $E_A = E_{\rm in} + E_{\rm cm}$. Usually, one is interested in the intrinsic properties of the system, $E_{\rm in}$.

If the many-body problem is solved in a full Hilbert space, $(H_{\rm in} + H_{\rm cm})\,|\psi\rangle = E\,|\psi\rangle$, then the intrinsic and c.m. Hamiltonian is separated

$$[H_{\rm in}, H_{\rm cm}] = 0, \tag{5.7}$$

therefore the A-body wave function can be factorized into its intrinsic and c.m. parts as in Eq. (5.6).

In practical cases, however, the many-body problem is solved in a truncated finite space, which is the subspace of the A-body Hilbert space, called model space. Defining a operator P as the projection operator onto a space, then the problem is written as

$$P(H_{\rm in} + H_{\rm cm})P\,|\psi_A\rangle = EP\,|\psi_A\rangle\,. \tag{5.8}$$

In this case, the P-space wave function $P|\psi\rangle$ can be factorized only when the condition

$$[PH_{\rm in}P, PH_{\rm cm}P] = 0 \quad \Longleftrightarrow \quad [P, H_{\rm cm}] = 0 \tag{5.9}$$

is satisfied.

There are several ways to remove the contamination of c.m. components in the A-body wave function $|\psi_A\rangle$. The basic point is the use of the Harmonic oscillator (HO) basis, since the HO potential is the only one that permits the partition into a c.m. and relative Hamiltonian. For few-body systems ($A \leq 6$), the Jacobi coordinate HO basis is an efficient basis, where the intrinsic and c.m. degrees of freedom are separated exactly within the construction of the basis states. For heavier systems, the process of antisymmetrization becomes complicated and the use of Slater determinant HO basis is more efficient. In this case, the basis truncation should be done by maximum of the sum of all HO excitations, $\sum_{i=1}^{A}(2n_i + l_i) \leq N_{\rm max}$. The reason for this specific choice of the truncation scheme can be explained by the property of the HO basis. The single-particle Hamiltonian for the HO potential can be divided into two commuting parts,

$$\begin{aligned} h_{\rm s.p.} &= \sum_{i=1}^{A} \frac{\boldsymbol{p}_i^2}{2m} + \frac{1}{2}\sum_{i=1}^{A} m\omega^2 \boldsymbol{r}_i^2 \\ &= \sum_{i=1}^{A} \frac{1}{2m}\left(\boldsymbol{p}_i - \frac{\boldsymbol{P}}{A}\right)^2 + \frac{1}{2}\sum_{i=1}^{A} m\omega^2 (\boldsymbol{r}_i - \boldsymbol{R})^2 + \frac{\boldsymbol{P}^2}{2Am} + \frac{1}{2}Am\omega^2\boldsymbol{R}^2 \end{aligned} \tag{5.10}$$

or equivalently written as

$$\sum_{i=1}^{A} \boldsymbol{a}^\dagger(i)\boldsymbol{a}(i) = \sum_{i=1}^{A} \boldsymbol{a}_{\rm rel}^\dagger(i)\boldsymbol{a}_{\rm rel}(i) + \boldsymbol{A}^\dagger\boldsymbol{A}, \tag{5.11}$$

where

$$\boldsymbol{a}^\dagger(i) = \sqrt{\frac{m\omega}{2\hbar}}\boldsymbol{r}_i - \frac{i}{\sqrt{2m\hbar\omega}}\boldsymbol{p}_i, \quad \boldsymbol{a}(i) = \sqrt{\frac{m\omega}{2\hbar}}\boldsymbol{r}_i + \frac{i}{\sqrt{2m\hbar\omega}}\boldsymbol{p}_i, \tag{5.12}$$

and

$$\boldsymbol{A}^\dagger = \sqrt{\frac{m\omega}{2\hbar}}\boldsymbol{R} - \frac{i}{\sqrt{2m\hbar\omega}}\boldsymbol{P} = \frac{1}{\sqrt{A}}\sum_{i=1}^{A}\boldsymbol{a}_i^\dagger, \quad \boldsymbol{A} = \sqrt{\frac{m\omega}{2\hbar}}\boldsymbol{R} + \frac{i}{\sqrt{2m\hbar\omega}}\boldsymbol{P} = \frac{1}{\sqrt{A}}\sum_{i=1}^{A}\boldsymbol{a}_i, \tag{5.13}$$

$$\boldsymbol{a}_{\rm rel}^\dagger(i) = \boldsymbol{a}^\dagger(i) - \frac{1}{\sqrt{A}}\boldsymbol{A}^\dagger, \quad \boldsymbol{a}_{\rm rel}(i) = \boldsymbol{a}(i) - \frac{1}{\sqrt{A}}\boldsymbol{A}. \tag{5.14}$$

Since $[\boldsymbol{a}_{\rm rel}^\dagger(i)\boldsymbol{a}_{\rm rel}(i), \boldsymbol{A}^\dagger\boldsymbol{A}] = 0$, the single-particle number operator of HO commutes with that of c.m. HO,

$$\left[\sum_{i=1}^{A}\boldsymbol{a}^\dagger(i)\boldsymbol{a}(i), \boldsymbol{A}^\dagger\boldsymbol{A}\right] = 0. \tag{5.15}$$

Eq. (5.15) is an important property of HO basis. If one define the truncation of the Hilbert space following the total HO excitations, the truncation can be expresses by the projection operator

$$P_{\rm NCSM} = \sum_{\alpha} |\alpha\rangle\, \theta(N_{\rm max} - q_\alpha)\, \langle\alpha| \,, \tag{5.16}$$

where the $|\alpha\rangle$ is a Slater determinant that spans the Hilbert space and q_α is the eigenvalue of the single-particle operator

$$\sum_{i=1}^{A} \boldsymbol{a}^\dagger(i)\boldsymbol{a}(i)\, |\alpha\rangle = q_\alpha\, |\alpha\rangle \,, \tag{5.17}$$

counting the total number of HO excitations of the state $|\alpha\rangle$. The $\theta(x)$ is the step function defined as

$$\theta(x) = \begin{cases} 1 & (x \geq 0) \\ 0 & (x < 0). \end{cases} \tag{5.18}$$

The relation (5.15) guarantees

$$[P_{\rm NCSM}, \boldsymbol{A}^\dagger \boldsymbol{A}] = 0. \tag{5.19}$$

Therefore, if one chooses the c.m. Hamiltonian as

$$H_{\rm cm} = \frac{\boldsymbol{P}^2}{2mA} + \frac{1}{2} mA\omega^2 \boldsymbol{R}^2 - \frac{3}{2}\hbar\omega = \hbar\omega \boldsymbol{A}^\dagger \boldsymbol{A}, \tag{5.20}$$

where the frequency ω is the same as the underlying frequency in the HO basis, and employs the operator $P_{\rm NCSM}$ for the model space, then the condition (5.9) is satisfied. In that case, the irrelevant states caused by the c.m. excitations can be exactly eliminated by diagonalizing the Hamiltonian $H(\beta) = H_{\rm in} + \beta H_{\rm cm}$ with sufficiently large value of the β. This is the prescription used in the NCSM.

In the case of general many-body methods, however, this prescription cannot be applied and thus the decoupling of the c.m. degrees of freedom (5.6) cannot be guaranteed. The IM-SRG is not the exception, and one has to examine the degree of the factorization of the A-body wave function. We employ the prescription that has recently been introduced in the CC [83] by Hagen *et. al.* We consider the c.m. Hamiltonian,

$$H_{\rm cm}(\tilde{\omega}) = \frac{\boldsymbol{P}^2}{2mA} + \frac{1}{2} mA\tilde{\omega}^2 \boldsymbol{R}^2 - \frac{3}{2}\hbar\tilde{\omega} = \hbar\tilde{\omega} \boldsymbol{A}^\dagger \boldsymbol{A}, \tag{5.21}$$

where the frequency $\tilde{\omega}$ can in general be different from that of the underlying oscillator basis, ω. Then we calculate the expectation value of this operator in the ground-state A-body wave function, evolving the c.m. Hamiltonian $H_{\rm cm}(\omega)$,

$$\frac{d}{ds}H_{\rm cm}(s) = [\eta(s), H_{\rm cm}(s)].$$

Note that the SRG evolve an arbitral operator with the same generator that is used for the evolution of a Hamiltonian. Namely, the simultaneous evolution of an arbitral operator with Hamiltonian is possible.

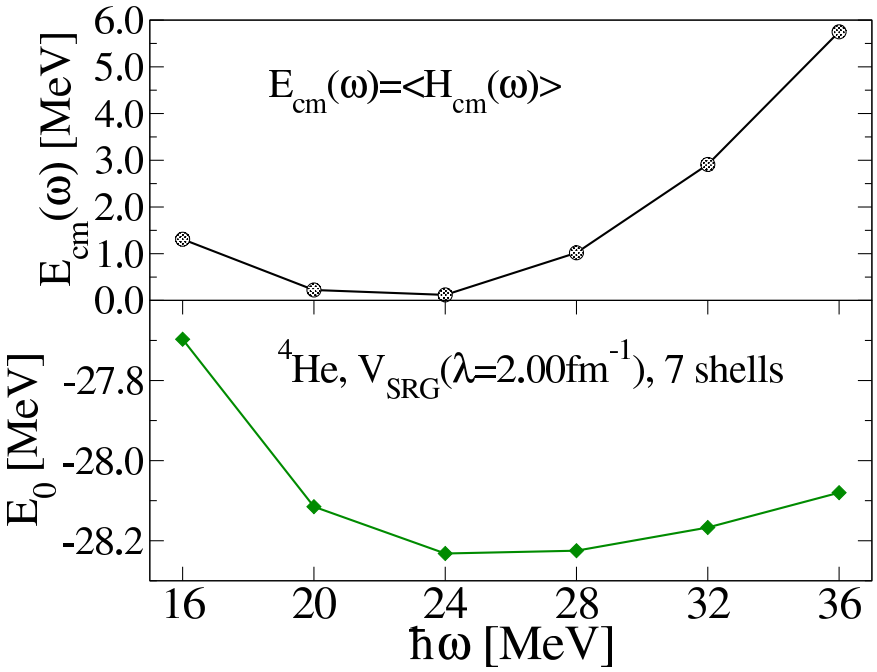

Figure 5.8: Lower panel: Ground-state energy of ^{4}He with a SRG-evolved N^{3}LO interactions as a function of the frequency of the underlying HO basis, $\hbar\omega$. The energy is obtained by the IM-SRG in 7 shells. Upper panel: Expectation value of the c.m. Hamiltonian $E_{\rm cm}(\omega) = \langle H_{\rm cm}(\omega)\rangle$.

Figure 5.8 shows the ground-state energy and the c.m. energy for ^{4}He, *i.e.*, the expectation values, $E_0 = \langle H_{\rm in}\rangle$ and $E_{\rm cm}(\omega) = \langle H_{\rm cm}(\omega)\rangle$, in the A-body wave function. These values are obtained within the IM-SRG(2) in $e_{\rm max} = 6$ space, where the NN interaction is the SRG-evolved chiral N^{3}LO potential. The expectation value, $E_{\rm cm}(\omega)$ is not always zero, indicating the A-body wave function obtained by the IM-SRG is not generally an eigenstate of the c.m.

Hamiltonian $H_{\rm cm}(\omega)$. But at the frequency $\hbar\omega = 24$ MeV which gives the minimum point for the ground-state energy, the $E_{\rm cm}$ vanishes. This means that at this frequency, the IM-SRG wave function is in good approximation factorized into its intrinsic and c.m. component, and the c.m. part is the ground state of the $H_{\rm cm}$.

We assume that there is a common c.m. Hamiltonian $H_{\rm cm}(\tilde{\omega})$ with an unknown frequency $\tilde{\omega}$ for which the factorization of the A-body wave function is achieved, and the c.m. wave function is in the ground state of $H_{\rm cm}(\tilde{\omega})$. Following the ref. [83], we determine the $\tilde{\omega}$ by using the identity

$$H_{\rm cm}(\omega) + \frac{3}{2}\hbar\omega - T_{\rm cm} \equiv \frac{\omega^2}{\tilde{\omega}^2}\left(H_{\rm cm}(\tilde{\omega}) + \frac{3}{2}\hbar\tilde{\omega} - T_{\rm cm}\right). \tag{5.22}$$

Taking the expectation value of (5.22) with the A-body wave function $|\psi_A\rangle = |\psi_{\rm in}\rangle \otimes |\psi_{\rm cm}(\tilde{\omega})\rangle$, in which the factorization is assumed, one gets the estimation

$$\hbar\tilde{\omega} = \hbar\omega + \frac{2}{3}E_{\rm cm}(\omega) \pm \sqrt{\frac{4}{9}E^2_{\rm cm}(\omega) + \frac{4}{3}\hbar\omega E_{\rm cm}(\omega)}\ (\equiv \hbar\tilde{\omega}^{\pm}), \tag{5.23}$$

where $\langle T_{\rm cm}\rangle = 3\hbar\tilde{\omega}/4$, $\langle H_{\rm cm}(\omega)\rangle = E_{\rm cm}(\omega) \neq 0$, and we assume the condition, $\langle H_{\rm cm}(\tilde{\omega})\rangle = 0$.

The obtained values of $\hbar\tilde{\omega}$ are plotted in Fig. 5.9 together with the line of $\tilde{\omega} = \omega$. The figure clearly shows that the optimal $\hbar\tilde{\omega}$ ($= 24$ MeV) is approximately independent of the $\hbar\omega$ of the basis, indicating the presence of a common c.m. Hamiltonian $H_{\rm cm}(\tilde{\omega})$ with $\hbar\tilde{\omega} = 24$ MeV. In fact, the lower panel of the Fig. 5.9 shows that the expectation values of the c.m. Hamiltonian with the optimal frequency $\tilde{\omega}$ are very small (less than 100 keV).

This holds for ^{16}O with a soft initial NN interaction, $V_{\rm low-k}$ with $\Lambda = 1.8$ fm^{-1} evolved from the N^{3}LO. Figure 5.10(a) shows the optimal $\hbar\tilde{\omega}$ (upper panel) and the expectation value of $H_{\rm cm}(\tilde{\omega})$ (lower panel) as a function of the $\hbar\omega$ of the underlying HO basis. Figure 5.10(b) shows the $E_{\rm cm}(\tilde{\omega}) = \langle H_{\rm cm}(\tilde{\omega})\rangle$ with the optimal $\hbar\tilde{\omega}$ for ^{4}He. The initial NN potential is the N^{3}LO, namely a hard interaction. In this case, even in the largest model space we have $E_{\rm cm}(\tilde{\omega}) \sim 300$keV at most, although the expectation value is sufficiently small at the $\hbar\omega$ of the energy minimum. Since the spurious component carries at least $\langle H_{\rm cm}\rangle \sim \hbar\tilde{\omega}$, the contamination by this spurious state can be estimated as $E_{cm}(\tilde{\omega})/\hbar\tilde{\omega} < 1\%$ at the worst case. The figure also shows that the admixture of the c.m. excitation becomes smaller for larger model space. The origin of the admixture of the c.m. excitation is the non-commutable feature between the model-space projection P and the c.m. Hamiltonian $H_{\rm cm}$. The inequality of Eq. (5.9) corresponds to how much the projection operator differs from the unity, $\mathbf{1} - P$. Therefore, when we go to larger model space ($P \to \mathbf{1}$), the admixture of the c.m. excitation becomes smaller.

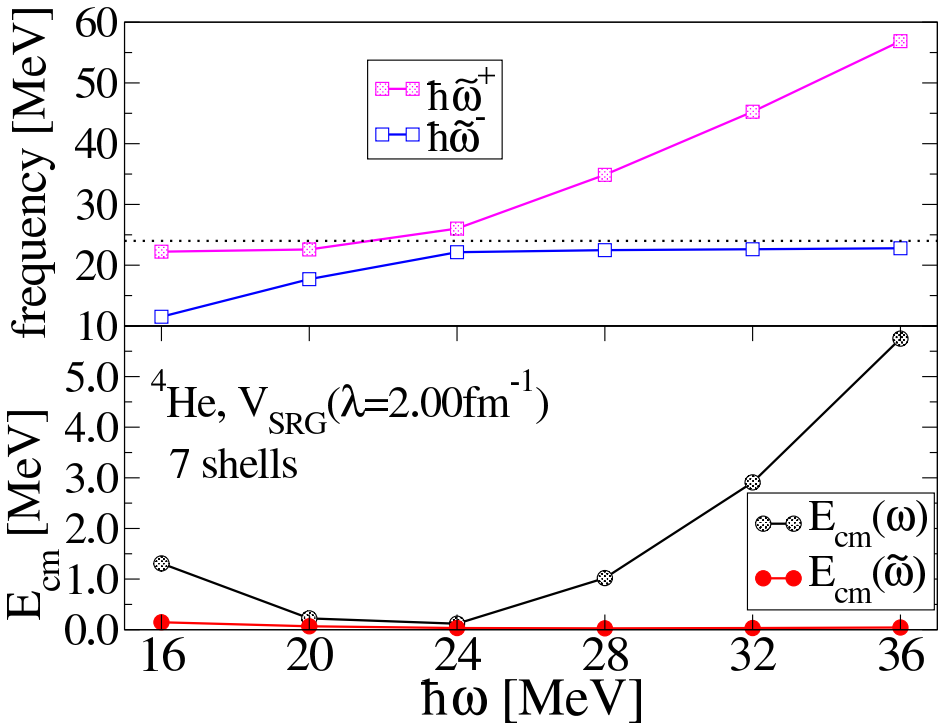

Figure 5.9: Upper panel: The optimal frequency $\hbar\tilde{\omega}$ of the c.m. Hamiltonian as a function of $\hbar\omega$. Lower panel: Expectation values of $H_{\rm cm}(\omega)$ and $H_{\rm cm}(\tilde{\omega})$.

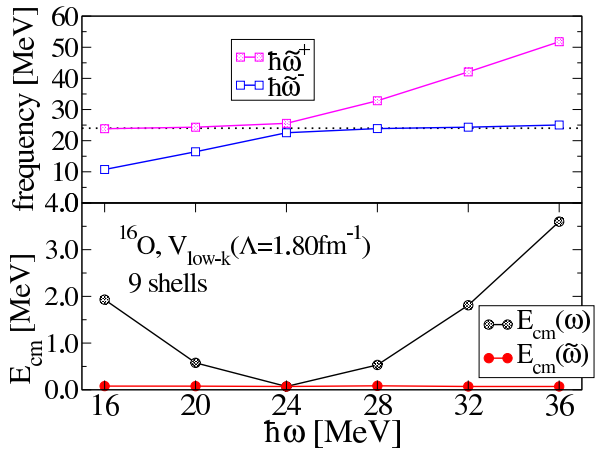

(a) ^{16}O

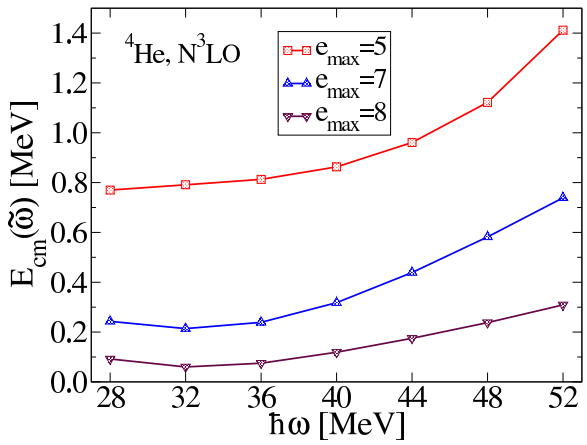

(b) ^{4}He with N^{3}LO(500)

Figure 5.10: Upper panel of (a): The optimal frequency $\hbar\tilde{\omega}$ of the c.m. Hamiltonian as a function of $\hbar\omega$. Lower panel of (a): Expectation values of $H_{\rm cm}(\omega)$ and $H_{\rm cm}(\tilde{\omega})$. (b): The expectation values of $H_{\rm cm}(\tilde{\omega})$ for ^{4}He with N^{3}LO potential.

5.4 Point-nucleon root mean square radius

The SRG can be applied to the evolution of an arbitral operator. In the case of the IM-SRG, one can obtain the evolution of the expectation value of an operator in a reference state.

Here, we show the first application of the IM-SRG to the calculation of the point-nucleon root mean square (rms) radius. We consider the evolution of the point-nucleon radius operator in the center of mass system

$$\mathcal{O}_r(s=0) = \mathcal{O}_r = \frac{1}{A}\sum_{i=1}^{A}(\boldsymbol{r}_i - \boldsymbol{R})^2\,. \tag{5.24}$$

This can be expressed in two different ways with the single-particle degrees of freedom,

$$\mathcal{O}_r = \left(\frac{1}{A} - \frac{1}{A^2}\right)\sum_{i=1}^{A}\boldsymbol{r}_i^2 - \frac{1}{A^2}\sum_{i<j}^{A}\boldsymbol{r}_i\cdot\boldsymbol{r}_j (\equiv \mathcal{O}_r^{\mathrm{I}}) \tag{5.25}$$

$$= \frac{1}{A^2}\sum_{i<j}(\boldsymbol{r}_i - \boldsymbol{r}_j)^2 (\equiv \mathcal{O}_r^{\mathrm{II}}). \tag{5.26}$$

The operator is divided into one- and two-body parts in (5.25), while it is written as only two-body operator in Eq. (5.26). The difference should not affect the observable, and we use these two different initial operator, $\mathcal{O}_r^{\mathrm{I}}$ and $\mathcal{O}_r^{\mathrm{II}}$, to assess the truncation error of the flow equation. The operator is generally given as

$$\mathcal{O}_r(s) = \mathcal{O}_r^{(0)}(s) + \sum_{ij}\mathcal{O}_{r,ij}^{(1)}(s)\{a_i^\dagger a_j\} + \frac{1}{4}\sum_{ijkl}\mathcal{O}_{r,ijkl}^{(2)}\{a_i^\dagger a_j^\dagger a_l a_k\} + \cdots, \tag{5.27}$$

where the $\sqrt{\mathcal{O}_r^{(0)}(0)}$ is the point-nucleon r.m.s. radius in an initial basis. The operator $\mathcal{O}_r(s)$ can be evolved as

$$\frac{d}{ds}\mathcal{O}_r(s) = [\eta(s), \mathcal{O}_r(s)]. \tag{5.28}$$

We obtain the point-nucleon r.m.s. radius by

$$\langle r^2\rangle = \sqrt{\langle\psi|\,\mathcal{O}_r\,|\psi\rangle} = \lim_{s\to\infty}\mathcal{O}_r^{(s)}(\infty). \tag{5.29}$$

In Figs 5.11-5.14, we plot the point-nucleon r.m.s. radius of ^{4}He and ^{16}O as a function of the basis parameter $\hbar\omega$ for different sizes of the model space. The initial NN interactions, which determine the evolution of the radius via the generator, are the N^{3}LO(500) potential and the SRG-evolved version with $\lambda = 3.0$, 2.5, 2.0 and 1.8 fm^{-1}. For all cases, we perform the IM-SRG transformations using the generator II, starting with two different representations for the radius operator $\mathcal{O}_r^{\mathrm{I}}$ and $\mathcal{O}_r^{\mathrm{II}}$. The figures show that the dependence upon the

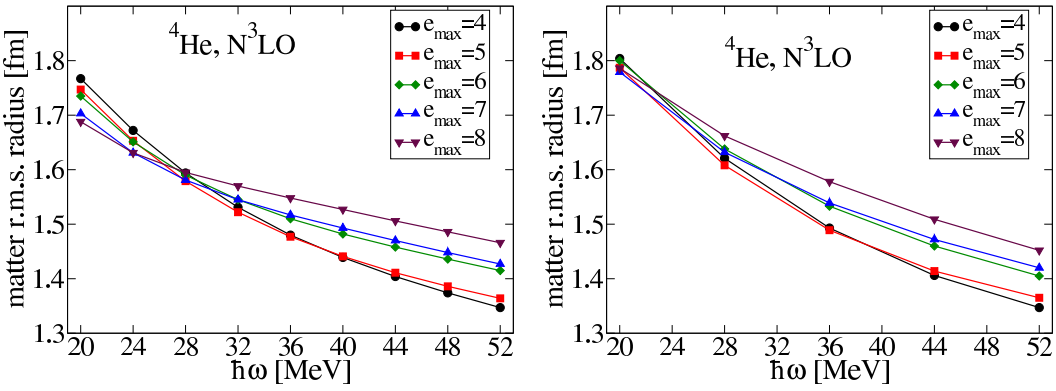

(a) $\mathcal{O}_r^{\mathrm{I}}$, N^{3}LO

(b) $\mathcal{O}_r^{\mathrm{II}}$, N^{3}LO

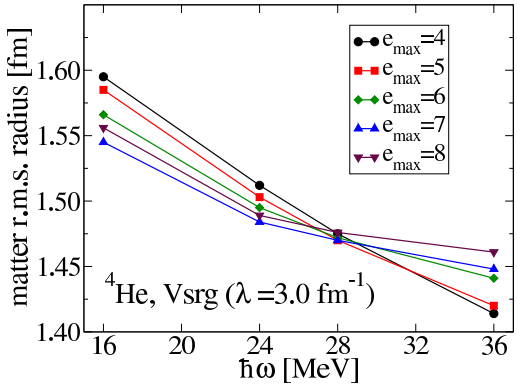

(c) $\mathcal{O}_r^{\mathrm{I}}$, $V_{\mathrm{SRG}}, \lambda = 3.0\mathrm{fm}^{-1}$

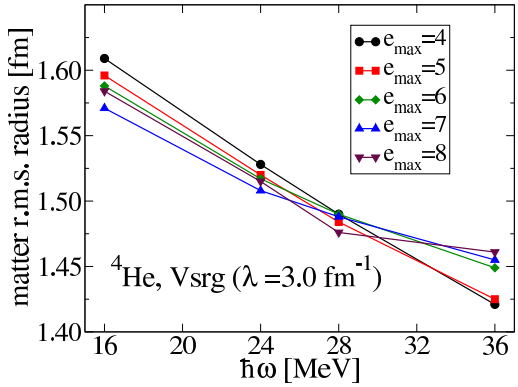

(d) $\mathcal{O}_r^{\mathrm{II}}$, $V_{\mathrm{SRG}}, \lambda = 3.0\mathrm{fm}^{-1}$

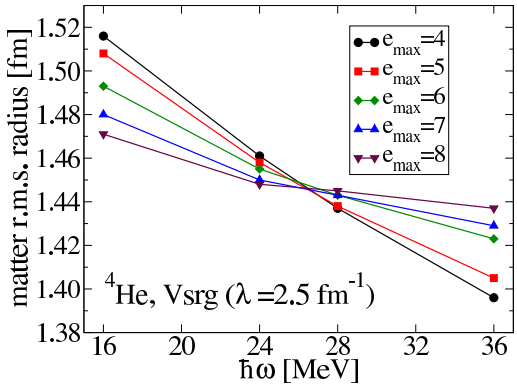

(e) $\mathcal{O}_r^{\mathrm{I}}$, $V_{\mathrm{SRG}}, \lambda = 2.5\mathrm{fm}^{-1}$

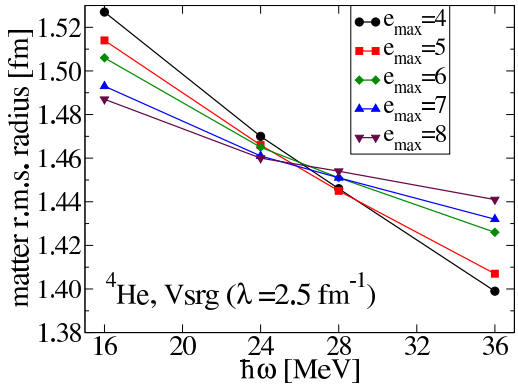

(f) $\mathcal{O}_r^{\mathrm{II}}$, $V_{\mathrm{SRG}}, \lambda = 2.5\mathrm{fm}^{-1}$

Figure 5.11: The point-nucleon r.m.s. radius of ^{4}He with the evolution of the operator $\mathcal{O}^{\mathrm{I}}$ (left) and $\mathcal{O}^{\mathrm{II}}$ (right). The initial NN interaction is the N^{3}LO (upper panels) and the SRG-evolved N^{3}LO with $\lambda = 3.0$ fm^{-1} (middle panels), $\lambda = 2.5$ fm^{-1} (bottom panels).

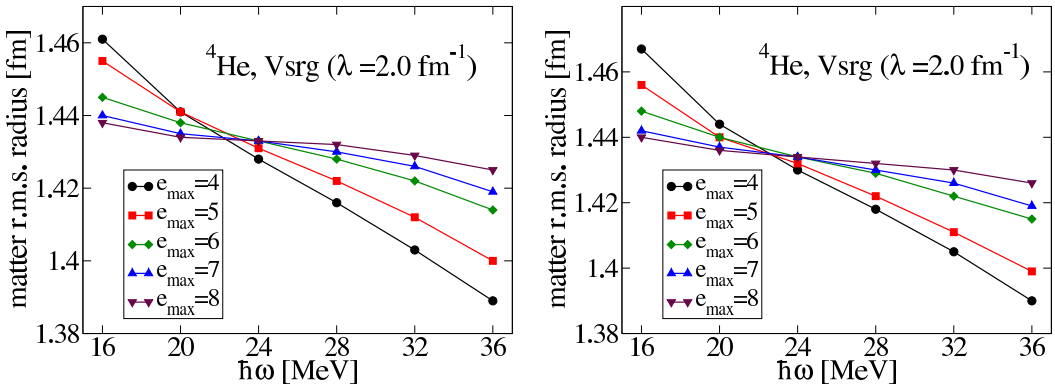

(a) $\mathcal{O}_r^{\mathrm{I}}$, $V_{\mathrm{SRG}}, \lambda = 2.0\mathrm{fm}^{-1}$

(b) $\mathcal{O}_r^{\mathrm{II}}$, $V_{\mathrm{SRG}}, \lambda = 2.0\mathrm{fm}^{-1}$

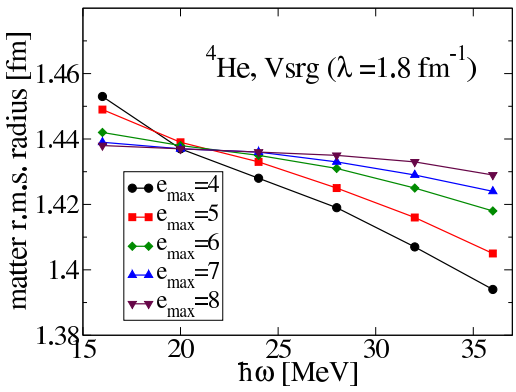

(c) $\mathcal{O}_r^{\mathrm{I}}$, $V_{\mathrm{SRG}}, \lambda = 1.8\mathrm{fm}^{-1}$

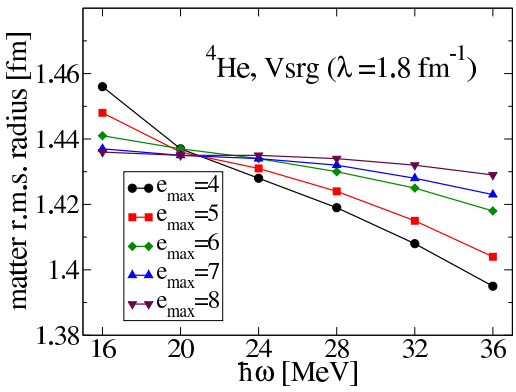

(d) $\mathcal{O}_r^{\mathrm{II}}$, $V_{\mathrm{SRG}}, \lambda = 1.8\mathrm{fm}^{-1}$

Figure 5.12: The point-nucleon r.m.s. radius of ^{4}He with the evolution of the operator $\mathcal{O}^{\mathrm{I}}$ (left) and $\mathcal{O}^{\mathrm{II}}$ (right). The initial NN interaction is the SRG-evolved N^{3}LO with $\lambda = 2.0$ fm^{-1} (upper panels), $\lambda = 1.8$ fm^{-1} (bottom panels).

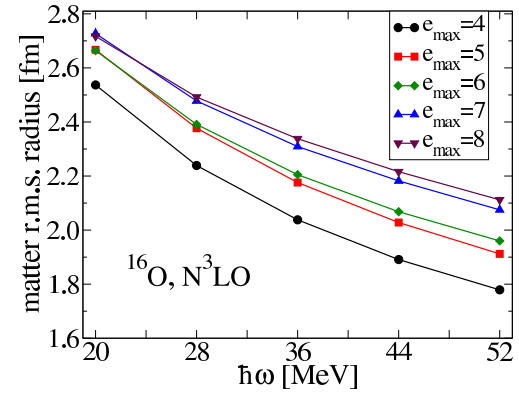

(a) $\mathcal{O}_r^{\mathrm{I}}$, N^{3}LO

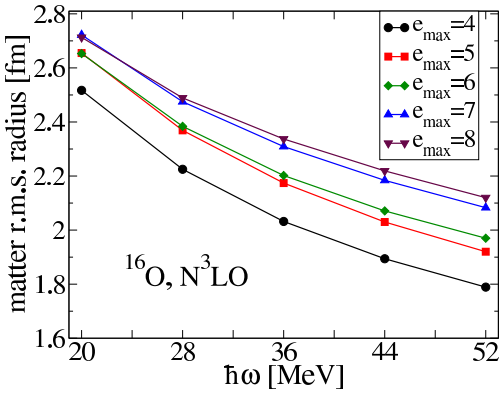

(b) $\mathcal{O}_r^{\mathrm{II}}$, N^{3}LO

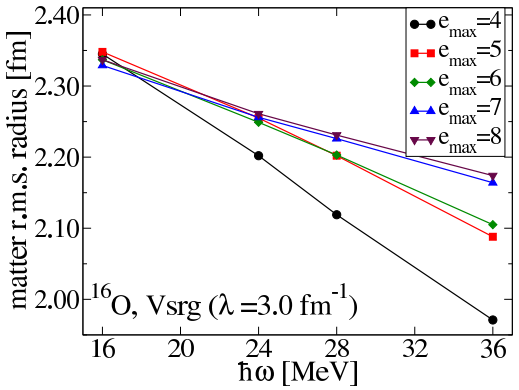

(c) $\mathcal{O}_r^{\mathrm{I}}$, $V_{\mathrm{SRG}}, \lambda = 3.0\mathrm{fm}^{-1}$

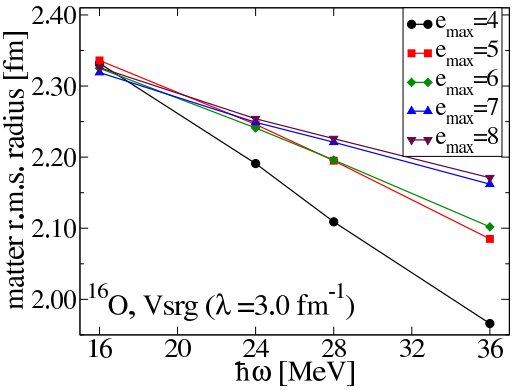

(d) $\mathcal{O}_r^{\mathrm{II}}$, $V_{\mathrm{SRG}}, \lambda = 3.0\mathrm{fm}^{-1}$

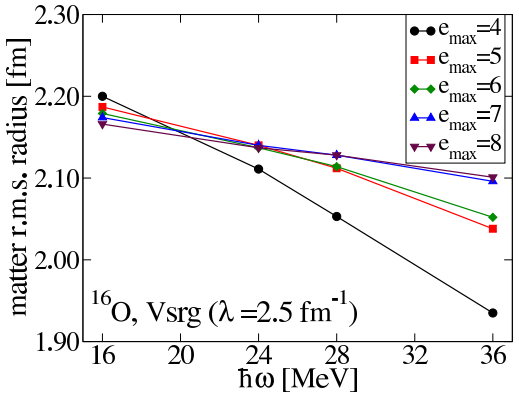

(e) $\mathcal{O}_r^{\mathrm{I}}$, $V_{\mathrm{SRG}}, \lambda = 2.5\mathrm{fm}^{-1}$

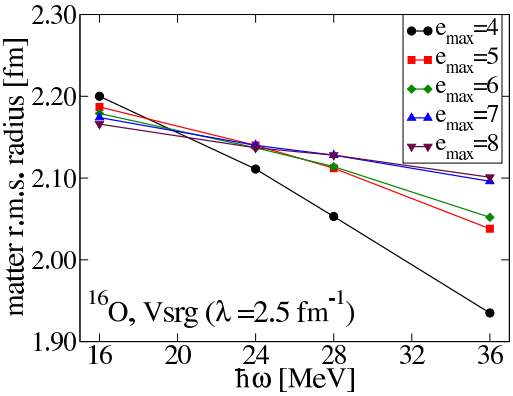

(f) $\mathcal{O}_r^{\mathrm{II}}$, $V_{\mathrm{SRG}}, \lambda = 2.5\mathrm{fm}^{-1}$

Figure 5.13: The point-nucleon r.m.s. radius of ^{16}O with the evolution of the operator $\mathcal{O}^{\mathrm{I}}$ (left) and $\mathcal{O}^{\mathrm{II}}$ (right). The initial NN interaction is the N^{3}LO (upper panels) and the SRG-evolved N^{3}LO with $\lambda = 3.0$ fm^{-1} (middle panels), $\lambda = 2.5$ fm^{-1} (bottom panels).

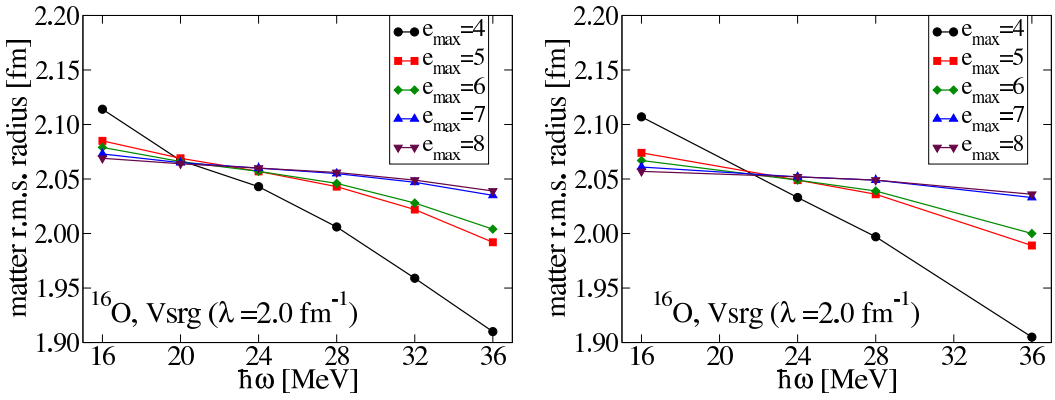

(a) $\mathcal{O}^{\mathrm{I}}_r$, $V_{\mathrm{SRG}}, \lambda = 2.0\mathrm{fm}^{-1}$

(b) $\mathcal{O}^{\mathrm{II}}_r$, $V_{\mathrm{SRG}}, \lambda = 2.0\mathrm{fm}^{-1}$

(c) $\mathcal{O}^{\mathrm{I}}_r$, $V_{\mathrm{SRG}}, \lambda = 1.8\mathrm{fm}^{-1}$

(d) $\mathcal{O}^{\mathrm{II}}_r$, $V_{\mathrm{SRG}}, \lambda = 1.8\mathrm{fm}^{-1}$

Figure 5.14: The point-nucleon r.m.s. radius of ^{16}O with the evolution of the operator $\mathcal{O}^{\mathrm{I}}$ (left) and $\mathcal{O}^{\mathrm{II}}$ (right). The initial NN interaction is the SRG-evolved N^{3}LO with $\lambda = 2.0$ fm^{-1} (upper panels), $\lambda = 1.8$ fm^{-1} (bottom panels).

initial representation of $\mathcal{O}_r$ is negligible, meaning the truncation scheme for the IM-SRG(2) is controllable approximation.

Strictly speaking, when one starts with a SRG-evolved NN potential, one has to take the corresponding evolved r^2 operator rather than the bare one. However, the r^2 operator acts on relatively long-distance scale, thus the free-space SRG very little renormalize the operator [84]. Going to many-body systems, this feature holds. Especially for lower λ of the initial NN interactions, the radius weakly depends on the cutoff. Regarding the larger λ, one sees relatively large change of the radius, which is partly because the error from the normal-ordered two-body truncation in the flow equation becomes larger for harder interactions. In fact, the radius of ^{4}He obtained by NCSM is 1.510(50) [85], indicating that IM-SRG(2) seems to overestimate the radius for the initial N^{3}LO.

One can also observe the correlation between the binding energy and the radius. As we decrease the cutoff λ, the binding energies become larger, meaning that nuclei are bound more strongly. Therefore, the size of nuclei becomes smaller, showing the decreasing radius.

Chapter 6

Connection to the shell model

In this Chapter, we discuss the connection between the IM-SRG and the shell model. The latter is called configuration interaction method in more general word. The nuclear shell model has been one of the most successful theories in nuclear structure physics. The starting point of the shell model is the spherical mean field with the spin-orbit splitting, which describes the magic numbers of nuclei very well. Based on the mean field picture, the correlations among nucleons are taken into account by the mixing of the all possible configurations via residual 2N or 3N forces in a given model space. The shell model in which all constituent nucleons of a nucleus are taken into account is called no-core shell model (NCSM) or no-core full configuration (NCFC) method. The main difference between the two methods is how to truncate the model space. The former employs the model space defined by the total HO excitation, while the latter takes the single-particle (s.p.) energy cutoff defined by the $e_{\max}$ as the IM-SRG does. Today, both the NCSM and the NCFC start with realistic 2N or 3N interactions and provide us with the fully *ab-initio* description of bound nuclear systems. The wall for these method is that the reachable region is limited to light nuclei.

On the other hand, the standard shell model, which we call merely shell model hereafter, assumes the presence of an inert core composed by a doubly-magic nucleus and solves an effective problem for valence-shell nucleons governed by an effective Hamiltonian H_{eff}, which typically consists of one- and two-body interactions. To date, the H_{eff} is constructed by fitting to the experimental data fully or partially. The assumption of the inert core obviously reduces the degrees of freedom therefore makes the mass region which is accessible wider. The shell model has succeeded to explain details of nuclear structure, including the evolution of the shell structure with the varying neutron/proton numbers, spectroscopies, deformations, electromagnetic responses. These successes suggest that the valence nucleons on top of an

inert core are relevant degrees of freedom to describe the low-energy nuclear structure, and the corresponding effective Hamiltonian can be constructed within one- and two-body interaction in most cases.

Here, the obvious interest is how to construct the effective Hamiltonian $H_{\rm eff}$ for a given model space. This has actually been the longstanding problem. The method which is most widely used is the Q-box expansion discussed in Section 4.2.2. To date, the Q-box expansion is not a perfect tool for the shell model in wide range of mass region. The Q-box expansion neglects the induced many-body interactions and assumes the degenerate model space. The latter would be a serious problem when one constructs effective Hamiltonians defined in multi shells, like *psd*- or *sdpf*-shells, which are of great importance for the microscopic description of the nuclei in the island of inversion.

In the next Section, we discuss the strategy to derive effective Hamiltonian for valence-shell nucleons with the flexible choice of model spaces. In the last Section of this Chapter, we also consider the description of exotic nuclei, where *ab-initio* method is very hard to reach.

6.1 Effective interactions by IM-SRG

It has already seen that the perturbative solution of the IM-SRG has the clear correspondence to the effective interactions which are derived in the Q-box expansion introduced in Section 4.2.2.

In order to construct a generator which decouples the reference state and suppresses the couping between nucleons in a valence model space and those outside the model space, we define $H^{\rm od}(s) = f^{\rm od}(s) + \Gamma^{\rm od}(s)$, as

$$f^{\rm od}(s) = \sum_{ph} f_{ph}(s)\,\{a_p^\dagger a_h\} + \sum_{vq} f_{vq}(s)\,\{a_v^\dagger a_q\} + \sum_{vh} f_{vq}(s)\,\{a_v^\dagger a_h\} + \text{h.c.}, \tag{6.1}$$

$$\Gamma^{\rm od}(s) = \sum_{pp'hh'} \Gamma_{pp'hh'}(s)\,\{a_p^\dagger a_{p'}^\dagger a_{h'} a_h\} + \sum_{vv'qq'} \Gamma_{vv'qq'}(s)\,\{a_v^\dagger a_{v'}^\dagger a_{q'} a_q\} \tag{6.2}$$

$$+ \sum_{pp'vh} \Gamma_{pp'vh}\,\{a_p^\dagger a_{p'}^\dagger a_h a_v\} + \sum_{vv'v''h} \Gamma_{vv'v''h}\,\{a_v^\dagger a_{v'}^\dagger a_h a_{v''}\} + \text{h.c.} \tag{6.3}$$

where v, v', v'' and q, q' denote particle orbitals inside and outside of a given model space, respectively. The first terms in one- and two-body generators are responsible for the decoupling of the ground state as defined in Section 3.2, while the rest corresponds to the elimination of the couping between model space and the outside of it. We take the Wegner's choice $\eta^{\rm I}$ and White's choice $\eta^{\rm II}$ so as to eliminate the $H^{\rm od}(s)$ during the flow.

One can understand our choice of $H^{\rm od}$ as follows. Assume one tries to derive an effective interaction for valence-shell nucleons by MBPT, starting with the evolved Hamiltonian $H(\infty)$. Then the perturbation diagrams contain at least one vertex of $\Gamma_{pp'hh'}(\infty)$, $\Gamma_{vv'qq'}(\infty)$ or $\Gamma_{pp'vh}(\infty)$. These vertices are required to vanish during the flow, therefore the valence-shell interactions in $H(\infty)$ do not need perturbative corrections. Having obtained the evolved Hamiltonian,

$$H(\infty) = E_0(\infty) + f^{\rm v}(\infty) + \Gamma^{\rm v}(\infty) + f^{\rm q}(\infty) + \Gamma^{\rm q}(\infty), \tag{6.4}$$

we take the $H_{\rm eff} = f^{\rm v}(\infty) + \Gamma^{\rm v}(\infty)$ as an effective Hamiltonian for valence-shell nucleons and diagonalize it in a given model space.

We show the first application to p-shell, taking an example of ^{6}Li. Instead of solving the six-body problem, we solve the effective Hamiltonian for two valence nucleons on top of alpha particle. Figure 6.1 shows the convergence of the ground-state energy of ^{4}He by the

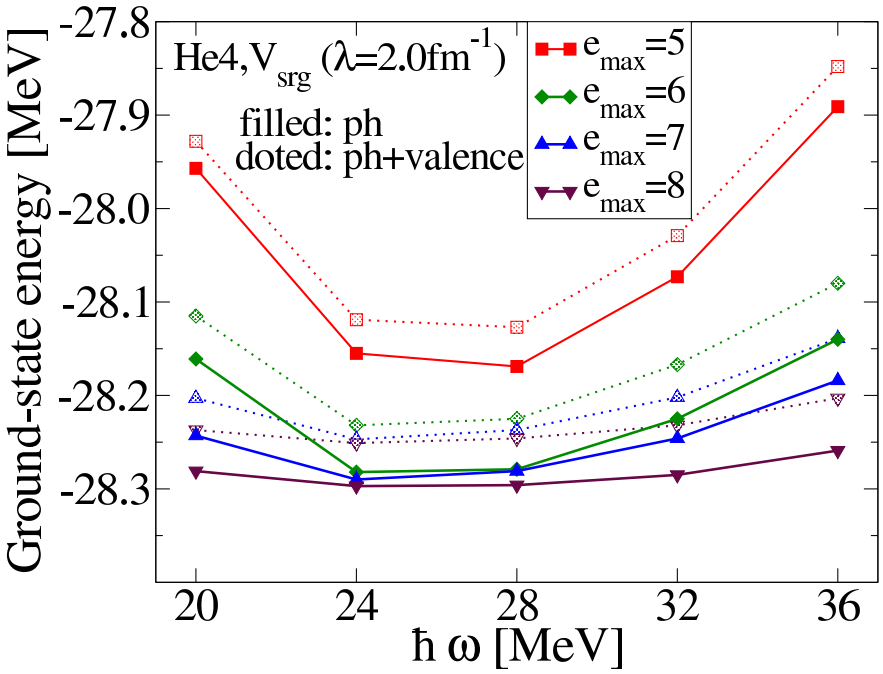

Figure 6.1: The ground-state energy of ^{4}He by the IM-SRG(2) with two different choices of $H^{\rm od}$. Dotted symbols correspond to the choice that decouples the ground state, and the filled symbols stand for the choice that decouples valence space.

IM-SRG(2) with the two different choices of $H^{\rm od}$. The dotted symbols correspond to the

definition of H^{od} of Eq (3.30) that decouples only the reference state, while the filled symbols stand for the H^{od} of Eq. (6.3). One sees that both definitions of H^{od} give good agreement as anticipated within 50keV for all the model spaces in which the flow equation is solved. Since both of the choices guarantee the decoupling of the reference state, the obtained ground-state energy should be the same within a truncation error. The figure manifests that this condition is satisfied to large extent.

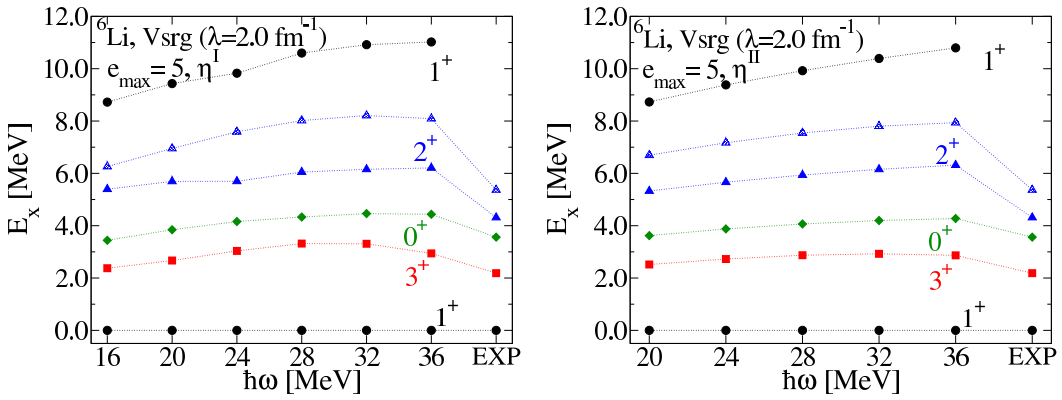

(a) η^{I} (b) η^{II}

Figure 6.2: Spectra of ^{6}Li with the effective p-shell interactions obtained by IM-SRG(2). As a reference, the experimental data are also shown.

Figure 6.2 shows the spectra of ^{6}Li with the $H_{\mathrm{eff}} = f^v(\infty) + \Gamma^v(\infty)$ obtained by IM-SRG(2) with two different generators η^{I} and η^{II}, where the $H^{\mathrm{od}}(s)$ is chosen to decouple the reference state and the valence space as defined in Eq. (6.3). The initial Hamiltonian is the SRG-evolved N^{3}LO(500) at $\lambda = 2.0$ fm^{-1}, defined in the model space $e_{\max} = 5$. We checked that in $e_{\max} = 5$ the ground-state energy of ^{4}He almost converges, as observed in Fig. 5.2, meaning that the ground state is decoupled. Figure 6.2 shows the weak dependence of spectra on the underlying basis parameter $\hbar\omega$ and the choice of the generator, which also indicates that the H is converged to large extent.

Having obtained the generator independence at smaller space, $e_{\max} = 5$, we investigate the convergence properties for larger spaces in Fig. 6.3. As already seen in $e_{\max} = 5$, the low-lying 3^+ and 0^+ states converge rather well, while the high-lying states, 2^+ and 1^+, are not fully converged even at the largest space. These high-lying states are still going down in energy. The slow convergence of the 2^+ and 1^+ states means that it is important to take into account the coupling to the high-energy s.p. states in order to reproduce these high-lying

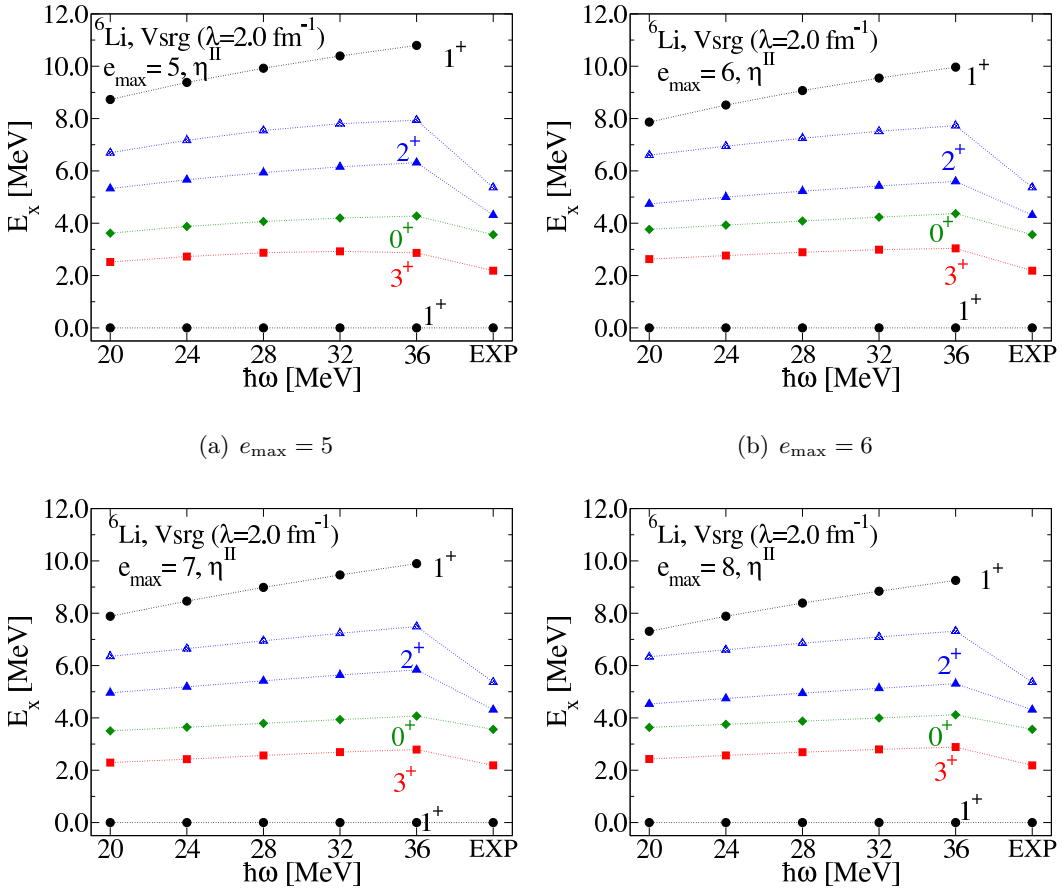

(a) $e_{\max} = 5$ (b) $e_{\max} = 6$

(c) $e_{\max} = 7$ (d) $e_{\max} = 8$

Figure 6.3: Convergence of low-lying spectra in ^{6}Li with the p-shell effective interactions derived by the IM-SRG(2). The flow equation is solved in subspaces of the Hilbert space, defined by $e_{\max} = \max(2n + l)$.

states.

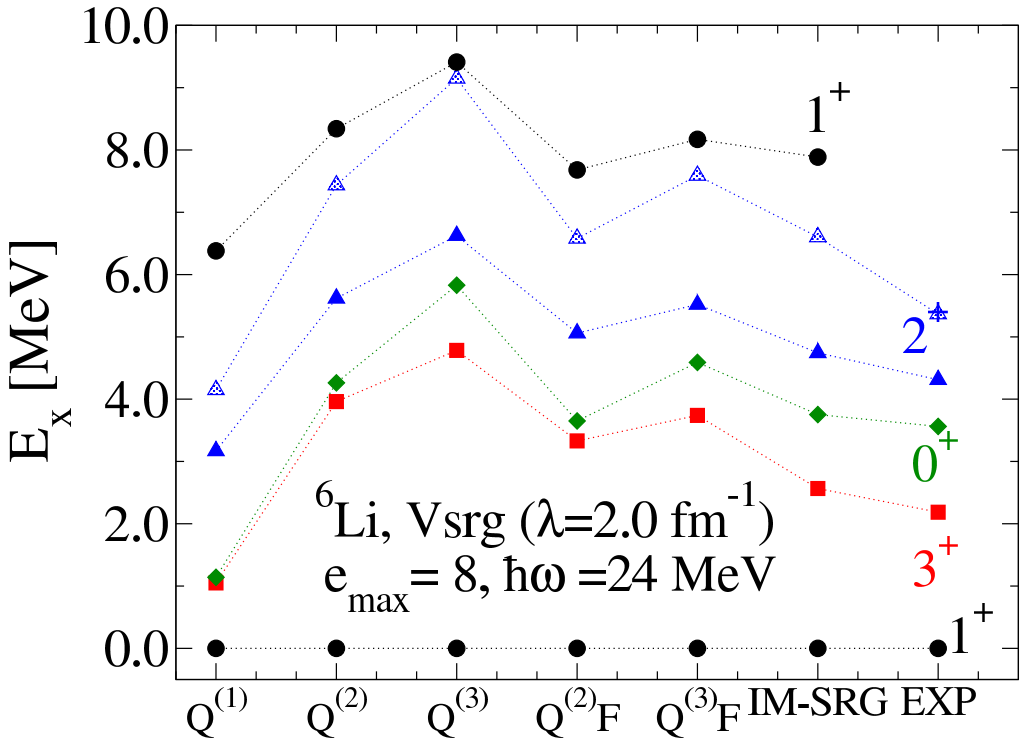

Figure 6.4: Spectra of ^{6}Li with the effective p-shell interactions obtained by i) the MBPT(1,2,3), namely, non-folded Q-box $Q^{(1,2,3)}$, ii) non-perturbative resummation by the folded diagram expansion, denoted by $Q^{2,3}$F and iii) the IM-SRG(2). All calculations are performed with SRG-evolved N^{3}LO(500) potential in $e_{\max} = 8$. As a reference, the experimental data are shown.

Figure 6.4 shows the comparison between the IM-SRG(2) and Q-box expansion with $V_{\rm SRG}(\lambda = 2.0{\rm fm}^{-1})$. The $\hbar\omega = 24$ MeV is the basis parameter at which the ground-state energy of alpha particle is minimized ($E_0(\infty) = -28.30$ MeV). As a reference, we also plot the experimental data [86]. Although the results by IM-SRG(2) are close to experimental data for $V_{\rm SRG}(\lambda = 2.0{\rm fm}^{-1})$, the agreement with data is not what is required since the 3N forces are not included in the initial Hamiltonian $H(0)$.

We rather emphasize the agreement with the Q-box expansion. As we discussed in Chapter 4.2, there is a close connection between the IM-SRG and the MBPT. From the perturbative analysis, the IM-SRG(2) includes the ladder, ring diagrams and their iterations to

infinite order, while certain diagrams at the third-order Q-box are missing. The spectra by the IM-SRG(2) are closer to non-perturbative Q-box expansion in terms of the second- and third-order non-folded Q-box $Q^{(2,3)}$. The expansion by construction includes the higher-order correlations via folded diagrams, while there is a structural difference between the low-order non-folded Q-box itself $Q^{(1,2,3)}$, which only includes the low-order perturbation in the initial NN interactions. One can observe that the low-lying 0^+ and 3^+ states can be described by many-body correlations composed by nucleons with relatively low-energy states, while the high-lying two 2^+ states and 1^+ states require the correlations of high-energy states.

We here mention about the absolute value of the ground state energy of ^{6}Li. The experimental data is $-31.9945(5)$ MeV, while the NCSM with the $V_{\rm srg}(\lambda = 2.0{\rm fm}^{-1})$ is $-33.1(1)$ MeV [87][*1]. The converged ground-state energy by the IM-SRG(2) is about -13 MeV relative to the alpha particle, which means the overbinding by 8 MeV compared to the experiment and by 6MeV to practically exact calculation. This is mainly due to the normal-ordered two-body truncation in the flow equation. Based on the perturbative analysis in section 4.2, the truncation error is $\mathcal{O}(g^4)$ for the $E_0(s)$ flow and $\mathcal{O}(g^3)$ for the evolution of $\Gamma(s)$ and $f(s)$. Note that the similar overbinding is obtained by the Q-box expansion. Regarding the bare N^{3}LO potential, we obtained the similar tendency of convergence, but we do not show the results since the enough convergence is not acquired.

We repeat that the IM-SRG has no conceptional problem to derive effective interactions defined in multi shells, while the conventional Q-box formalism encounters the divergence due to the zero denominator. In fact, we checked the IM-SRG flow equation for the effective *psd*-shell interactions gives stable convergence with respect to the flow parameter s for at least $e_{\rm max} = 5, 6$.

6.2 Beyond the standard shell model

In the previous section, the strong potential of the IM-SRG for the systematic construction of effective interactions of valence-shell nucleons.

[*1] In this calculation, they made a different treatment for the electromagnetic interaction in the N^{3}LO. Only proton-neutron sector in the initial potential is evolved by the free-space SRG, and the Coulomb interaction is added by perturbation after the RG evolution. The binding energy of ^{6}Li can be different if they initially include electromagnetic interaction at the beginning and evolve all the NN interactions by RG. But the difference should be less that 1 MeV, therefore the fact that the IM-SRG overestimates the binding energy of ^{6}Li is unchanged.

However, the description of loosely-bound system is still not reachable from *ab-initio*, except a few example including coupled cluster in Gamow basis [88]. The coupling to continuum has to be taken into account when one treats the weakly bound systems around the drip line. The interplay between the many-body correlations and the effects of the continuum coupling determines the limit of existence of nuclei. The oxygen isotope is a very interesting target along this context both experimentally and theoretically. The oxygen isotopes are the heaviest isotopes for which the drip line is well established. Many experiments [89, 90, 91] reveal that the drip line of Oxygen is anomalously close to the valley of stability, compared to neighboring nuclei. This cannot be explained by microscopic many-body theories within 2N forces without a phenomenological modification of the theory. Only recently, the drip line of Oxygen isotope has been explained by the inclusion of the missing effects of 3N forces as a reduced effective 2N forces [92]. We will show a feasible method to attack the many-body correlations at weakly-bound systems, Gamow Shell Model (GSM) [93], which in principle has a possibility to be combined with the IM-SRG. In the first stage, we focus on the investigation of the continuum effects on drip-line nuclei within the GSM.

6.3 Gamow shell model for drip-line Oxygen isotopes

Nuclei near the drip line are open-quantum many-body systems for which the coupling with the scattering continuum plays an important role, and should therefore be explicitly taken into account. Configuration interaction (shell-model) methods, such as the Gamow shell model (GSM) (see Ref. [49] for a recent review of the GSM), the continuum shell model (CSM) [94] or a time-dependent CSM approach [95], have been developed in order to properly include the coupling with the scattering continuum. The inclusion of continuum states complicates the solution of the many-body problem considerably, as the number of many-body basis states will explode. This has therefore motivated different approaches to the description of loosely bound and unbound nuclear states, such as the Density-Matrix-Renormalization-Group (DMRG) [96] and Coupled-Cluster approaches [42]. Furthermore, to complicate the solution strategies of the nuclear many-body problem is the need to include three-nucleon forces (3NFs). Recent results for light nuclei using *ab-initio* methods such as the Green's function Monte-Carlo (GFMC) [97] and the no-core shell model (NCSM) [98], demonstrate that 3NFs are needed in order to give the correct binding energies and spectroscopy when comparing to experiment. It is still an open research problem what the role of 3NFs is in medium mass and neutron-rich nuclei close to the drip line. This applies also to our

understanding of how different parts of the underlying nucleon-nucleon (NN) interaction, such as the spin-orbit force [45, 46] and the tensor force [47, 48], affect the structure of nuclei close to the drip line. In this section we study the ground- and low-lying states of ^{24}O and ^{25}O within the GSM framework. We derive a realistic effective shell-model interaction that includes the effect of the scattering continuum. The effective interaction is derived using many-body perturbation theory (MBPT) starting with a Hamiltonian which reproduces NN scattering data. The choice of the oxygen isotopes is motivated by several reasons. First, the oxygen isotopes are the heaviest isotopes for which the drip line is well established. There are large experimental campaigns worldwide [89, 90, 91] which aim at uncovering the properties of the oxygen isotopes, both at or close to the drip line and beyond. Two out of four stable even-even isotopes exhibit a doubly magic nature, namely ^{22}O (Z=8,N=14) [99] and ^{24}O (Z=8, N=16) [100, 101]. The isotopes $^{25-28}$O are all believed to be unstable towards neutron emission, even though ^{28}O is a doubly magic nucleus within the standard shell-model picture. Secondly, many-body descriptions starting with effective two-body Hamiltonians defined for a model space comprising the $1s_{1/2}$, $0d_{5/2}$, and $0d_{3/2}$ s.p. orbitals, have always defied a proper reproduction of experimental data [102, 103, 24]. To remedy this, the two-body shell-model interaction is usually fitted (fully or partially) [102, 103, 104, 94] to reproduce experimental data for nuclei in the range $16 < A < 40$. Without fitting the two-body Hamiltonians, which are typically derived using MBPT, shell-model calculations of the oxygen isotopes fare reasonably up to ^{20}O, but yield too compressed spectra in ^{22}O and lead to neutron separation energies that are always positive up to ^{28}O. All isotopes $^{17-28}$O that can be reached via this model space result as well bound, in clear contradiction with experiment. Within the above model space, these results pertain to all effective interactions defined via existing two-body NN interactions [102, 24]. The ground states and excited states of the odd-even isotopes are also poorly reproduced (see for example Refs. [102, 103]).

Recent coupled-cluster calculations of the oxygen isotopes [105] showed that chiral NN interactions can produce a rather flat binding energy curve of the oxygen isotopes ranging from ^{24}O to ^{28}O. It was illustrated that the existence of ^{28}O cannot be ruled out from *ab-initio* theory starting from modern chiral interactions. It was concluded that 3NFs will eventually decide the matter. Recent shell-model calculations of the oxygen isotopes within the *sd* shell showed that inclusion of effective 3NFs give added repulsion in the heavier oxygen isotopes and resulted in an unstable ^{28}O [92].

Obviously, the understanding of the evolution of binding energies and the location of

the drip line in the oxygen isotopes are still unsolved theoretical problems. As shown in Refs. [105, 92], proper treatment of many-body effects are crucial in the oxygen isotopes. However, it is still an open issue which role the continuum plays in the evolution of shell structure and in a correct description of binding energy systematics in neutron-rich oxygen isotopes. As discussed in Ref. [106], a proper treatment of the continuum was necessary in order to explain the parity inversion of the ^{11}Be ground state. It is therefore important to investigate what the role of continuum is on ground and excited states in neutron-rich oxygen isotopes. It is the aim of this section to throw light on, and disentangle the effects coming from many-body correlations and the proximity of the continuum on the evolution of binding energies and shell structure in neutron-rich oxygen isotopes. Further, we will investigate how different components of the NN interaction influence the low-lying resonance states in drip-line oxygen isotopes.

Construction of Gamow basis

We use the GSM to describe the low-lying states in ^{24}O and the ground state of ^{25}O. We construct the effective shell-model interaction starting from ^{22}O as a closed-shell core and use MBPT through second order [24]. The isotope ^{22}O has been found to be a closed-shell nucleus with a considerable shell gap, making it suitable as a starting point for shell-model calculations. With ^{22}O as a closed-shell core we have at most three valence particles, making effects coming from a proper treatment of the continuum more transparent. So far, the effective interaction has typically been constructed using oscillator states as intermediate particle states. In this work, we investigate for the first time what the role of the continuum is in constructing a realistic effective shell-model interaction and in describing spectra of neutron-rich oxygen isotopes.

The major advantage of the GSM is that it unifies structure and reaction properties of nuclei, that is, bound and scattering degrees of freedom are treated equally. Nuclei close to the scattering threshold have low-lying states that are in the continuum, and the GSM provides a simple framework for calculating the energy and lifetimes of these states. The starting point of the GSM is the Berggren completeness relation [107, 108, 109, 110, 111]. This s.p. basis treats bound, resonant, and scattering states on an equal footing, and it is the basic idea of the GSM to expand the many-body wave function in Slater determinants built from this basis. The representation of the Hamiltonian will no longer be Hermitian but rather complex symmetric, and a diagonalization will yield bound state spectra in addition to resonant state

spectra. Hence, the energy and lifetime of the many-body resonant state comes out directly from the approach.

In constructing the s.p. Berggren basis, we start from the one-body Hamiltonian for a spherical Woods-Saxon (WS) potential (see for example Ref. [112]). The Berggren basis is obtained by diagonalizing the one-body Hamiltonian in a plane wave basis defined on a deformed contour L^+ in the complex momentum plane (see Ref. [113] for details).

$$\frac{\hbar^2 k^2}{2\mu}\psi_{nl}(k) + \int_{L^+} dq q^2 V_l(k,q)\psi_{nl}(q) = E_{nl}\psi_{nl}(k), \tag{6.5}$$

This method is also known as the Contour-Deformation-Method. There is freedom in choosing the contour L^+ provided the Schrödinger equation can be analytically continued in the complex momentum plane. Fully converged results should be independent of the choice of the contour, and in the following we used two different contours, L_1^+ and L_2^+, as given in Ref. [113] and shown in Fig. 6.5, to check that our results are converged. These contours are specified by the points $A(2 - i\ \mathrm{fm}^{-1})$, $B(5\ \mathrm{fm}^{-1})$ and $C(0.3 - 0.2i)\ \mathrm{fm}^{-1}$. Here μ is the reduced mass between a neutron and a ^{22}O core. We will treat ^{22}O as a closed shell core throughout in our studies. The term $V_l(k,k')$ is the Fourier-Bessel transform of the spherical Woods-Saxon (W.S.) potential

$$V(r) = -V_0 f(r) - V_{so}\vec{l}\cdot\vec{s}\frac{1}{r}\frac{df(r)}{dr}, \quad f(r) = \left[1 + \exp\left(\frac{r-R}{d}\right)\right]^{-1}, \tag{6.6}$$

with $V_0 = 55$ MeV, $V_{so} = 29$ MeV, $R = 3.1$ fm, and $d = 0.45$ fm, where the shorthand $V_{so} = 29$ stands for the spin-orbit term. These parameters are chosen such that the energies of the s.p. orbitals $\nu 0d_{5/2}$, $\nu 1s_{1/2}$, and $\nu 0d_{3/2}$ are close to the experimental values obtained by taking the binding energy differences of ^{21}O-^{22}O and ^{23}O-^{22}O. We obtain, in units of MeV, $\varepsilon_{\nu 0d5/2}$=$-6.53(-6.85)$, $\varepsilon_{\nu 1s1/2}$ =$-2.73(-2.74)$ and $\varepsilon_{\nu d3/2}$=$1.43 - 0.01i$ $(1.26 - 0.2i)$, where numbers in parenthesis are experimental values. We refer hereafter to this basis as a WS Gamow basis. In our shell-model study of the oxygen isotopes ^{24}O and ^{25}O we will use the WS Gamow basis for the neutron partial waves $s_{1/2}$, $d_{3/2}$, and $d_{5/2}$, while for protons and all other partial waves, we use the oscillator representation.

Effective interaction for GSM

In constructing the effective shell-model interaction for neutron-rich oxygen isotopes, we start from the intrinsic nuclear Hamiltonian $H = t - t_{\mathrm{c.m.}} + V$, where t denotes the kinetic energy, and $t_{\mathrm{c.m.}}$ is the kinetic energy of the center of mass. For the interaction V, we employ the NN

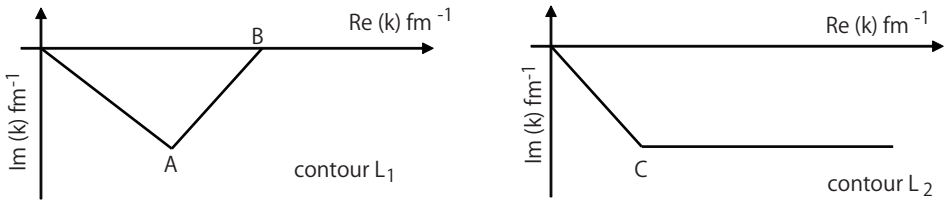

Figure 6.5: The contours L_1 and L_2 used in the construction of the Gamow basis.

interaction by Entem and Machleidt [114, 7] derived from chiral effective field theory (EFT) at next-to-next-to-next-to-leading order (N^3LO) and with a 500 MeV cutoff. This interaction still has considerable high-momentum components, making MBPT non-convergent. In order to construct the effective shell-model interaction V_{eff} using MBPT, we use a low-momentum interaction V=$V_{\text{low}-k}$, obtained by integrating out those momentum components above a certain cutoff Λ [63]. It is well known that this renormalization induces forces of higher rank. In a completely renormalized theory, all observables are independent on the cutoff Λ, and therefore the dependence of our results on the cutoff Λ tells us about the missing many-body physics. In this work we start from a ^{22}O core and limit ourselves to two-body effective shell-model interactions only. Since we have at most three neutrons outside the closed-shell core, it is reasonable to expect that the effect coming from effective three-body forces is small.

Thereafter we represent the matrix elements of the two-body interaction in the WS Gamow basis using the procedure outlined in Ref. [113]. We repeat briefly our calculational scheme here. The renormalized nucleon-nucleon interaction in an arbitrary two-particle basis (in our case either a Woods-Saxon Gamow basis) in the laboratory frame is given by

$$\langle ab; JT_z | \, V_{\text{low}-\text{k}} \, | cd; JT_z \rangle \tag{6.7}$$

The two-body state $|ab\rangle$ is implicitly coupled to good angular momentum J. The labels $a = (n_a, l_a, j_a, t_{za})$ number all bound, resonant and discretized scattering states. The the matrix elements of Eq. (6.7) are calculated by using the completeness relation composed by a two-particle harmonic oscillator basis

$$\sum_{\alpha \leq \beta} |\alpha\beta\rangle\langle\alpha\beta| = \mathbf{1}, \tag{6.8}$$

where the sum is not restricted in the proton-neutron ($T_z = 0$) case. We use the Greek single particle labels α, β for the single-particle harmonic oscillator states and the Latin single-particle labels a, b for Gamow states. The interaction can then be expressed in the oscillator

basis of Eq. (6.8)

$$V_{\rm low-k} = \sum_{\alpha\leq\beta}\sum_{\gamma\leq\delta} |\alpha\beta\rangle\langle\alpha\beta|V_{\rm low-k}|\gamma\delta\rangle\langle\gamma\delta|, \tag{6.9}$$

where the sums over two-particle harmonic oscillator states are infinite. Matrix elements of Eq. (6.7) are calculated numerically in an arbitrary two-particle Gamow basis by truncating the completeness expansion of Eq. (6.9) up to $n_{\rm max}$ harmonic oscillator two-body states

$$\langle ab|V_{\rm low-k}|cd\rangle \approx \sum_{\alpha\leq\beta}^{n_{\rm max}}\sum_{\gamma\leq\delta}^{n_{\rm max}} \langle ab|\alpha\beta\rangle\langle\alpha\beta|V_{\rm low-k}|\gamma\delta\rangle\langle\gamma\delta|cd\rangle. \tag{6.10}$$

The overlap between two-particle states $\langle ab|\alpha\beta\rangle$ is given by

$$\langle ab|\alpha\beta\rangle = \frac{\langle a|\alpha\rangle\langle b|\beta\rangle - (-1)^{J-j_\alpha-j_\beta}\langle a|\beta\rangle\langle b|\alpha\rangle}{\sqrt{(1+\delta_{ab})(1+\delta_{\alpha\beta})}} \tag{6.11}$$

for $|T_z| = 1$ (proton-proton or neutron-neutron states) and

$$\langle ab|\alpha\beta\rangle = \langle a|\alpha\rangle\langle b|\beta\rangle \tag{6.12}$$

for the proton-neutron case, $T_z = 0$. The one-body overlaps $\langle a|\alpha\rangle$ are given by,

$$\langle a|\alpha\rangle = \int d\tau\, \tau^2 \varphi_a(\tau) R_\alpha(\tau)\, \delta_{l_a l_\alpha}\delta_{j_a j_\alpha}\delta_{t_a t_\alpha}, \tag{6.13}$$

where φ_a is a Gamow single-particle state and R_α is a harmonic oscillator wave function. The radial integral is either evaluated in momentum or coordinate space, denoted by the integration variable τ. The overlap of Eq. (6.13) is in our case computed using either the Gamow Hartree-Fock basis or the Woods-Saxon Gamow basis.

Model space

In order to proceed with the construction of the effective shell-model interaction, we need to define a model space for the valence neutrons. Since we will perform our GSM calculations starting with ^{22}O as a closed shell core, i.e., the $0d_{5/2}$ shell is filled, our many-body states are constructed by letting all valence neutrons act in the model space defined by the the s.p. orbitals $1s_{1/2}$ and $id_{3/2}$, where $i = 0, 1, \ldots$ denote the i-th discretized continuum state for the $d_{3/2}$ partial wave. The effect of the continuum from the $s_{1/2}$ and $d_{5/2}$ partial waves are taken into account through the construction of the effective interaction. The effective shell-model interaction $V_{\rm eff}$ is then constructed for this model space using MBPT [24],

$$V_{eff} = \hat{Q} - \hat{Q}' \int \hat{Q} + \hat{Q}' \int \hat{Q} \int \hat{Q} - \cdots .$$

Here $\hat{Q}(\omega)$ is given by diagrams which are valence-linked and irreducible. The argument ω is the starting energy, which is the sum of the unperturbed s.p. energies. The object $\hat{Q}(\omega)$ is defined as in Eq. (4.27). Here we repeat the expression

$$\hat{Q}(\omega) = PH_1P + PH_1Q\frac{1}{\omega - QHQ}QH_1P.$$

In this work we take into account diagrams up through second order in perturbation theory in order to construct $\hat{Q}(\omega)$. We list in Fig. 6.6 the diagrams that contribute up to second order in the effective interaction. We do not include the folded diagrams, therefore the higher-order effects are not included in our effective interactions for the Gamow shell model. The intermediate s.p. states in each diagram in can be either resonant states, non-resonant

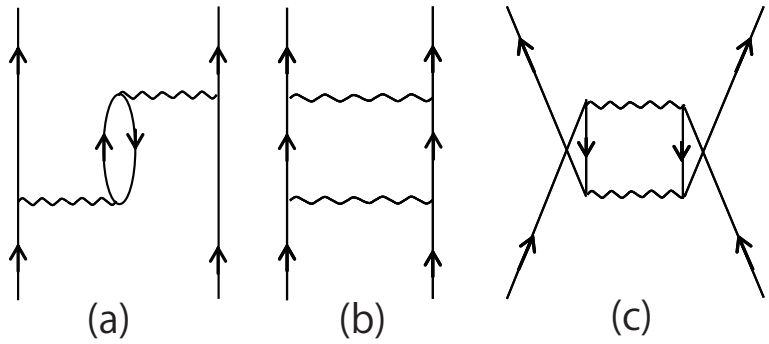

Figure 6.6: The second-order contributions to $V_{\rm eff}$.

continuum states, or bound states.

Results

We now turn to the GSM calculations of low-lying states in ^{24}O and ^{25}O. For the case of ^{24}O we have two neutrons outside the ^{22}O core, and we express the ground state of ^{24}O by filling the $1s_{1/2}$ orbital. This orbital is well bound, and with a neutron separation energy of S_n=2.7 MeV for ^{23}O [115]. We therefore expect mixing of higher-lying states to be small in the ground state of ^{24}O, as convinced by the recent experiment [116], and we take this effect into account through the construction of the effective interaction using many-body perturbation theory. For the excited states $J = 1$ and $J = 2$ of ^{24}O, we expand the wave function in a set of basis states $|iJ^+\rangle = |1s_{1/2} \otimes id_{3/2}; J^+\rangle$. The orbital $id_{3/2}$ denotes the i-th discretized s.p. state of the WS Gamow basis, and i=1, $\cdots n_{\rm Gamow}$, where $n_{\rm Gamow}$ is typically between 20 and 35. In our calculations we used $n_{\rm Gamow}$=30, and we checked that this was sufficient

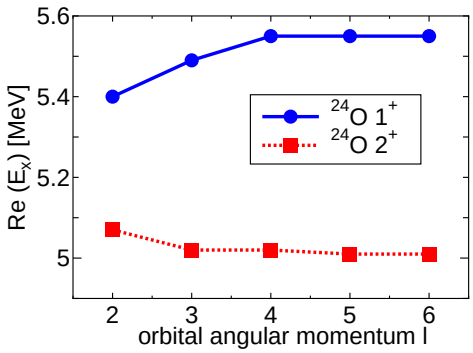

Figure 6.7: Excitation energies for ^{24}O as a function of the maximum orbital angular momentum l which is included in the diagrams.

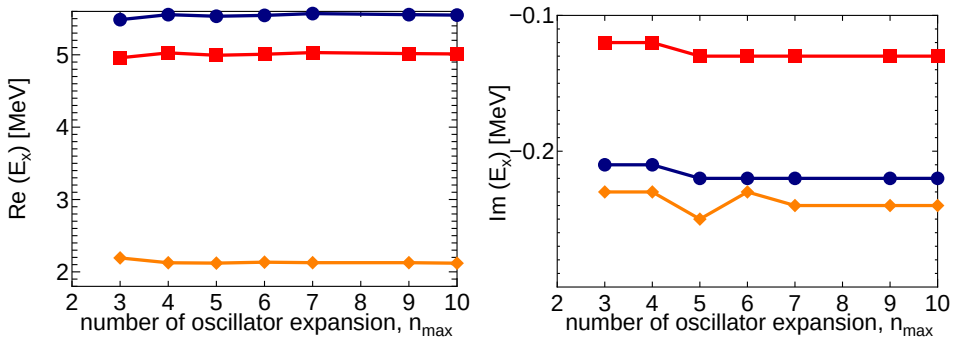

(a) Re E_x (b) Im E_x

Figure 6.8: The low-lying states in ^{24,25}O as a function of the number of oscillator states which are used to expand the Gamow states.

to reach convergence. Fig. 6.7 shows the convergence of the excitation energies in ^{24}O as a function of the maximum orbital angular momentum l of single-particle states. These states are included in the diagrams in Fig. 6.6 as intermediate states. One sees that the perturbation converges at $l = 6$. Figs. 6.8 show again the excitation energies in ^{24}O and the decay energy of the ground state of ^{25}O as a function of the maximum oscillator state $n_{\max}$ in Eq. (6.10). One sees that the results converge with respect to the number of oscillator states that are used to expand the Gamow states.

We show in Fig. 6.9 the excitation energies of the low-lying states in ^{24}O and the ground state in ^{25}O with respect to the ground state of ^{24}O. We used a cutoff $\Lambda = 2.1\text{fm}^{-1}$ for the $V_{\text{low}-k}$ interaction. We varied the cutoff Λ around 2.1 fm^{-1} and found that our results are

nearly independent of the cutoff Λ, meaning that the effect of neglected three- and many-body forces are small and will not change our conclusions. Our GSM calculations give energies for the low-lying states that compare well with the experimental values. The splitting between the 1^+ and the 2^+ states of ^{24}O is close to experiment. The theoretical spacing obtained with our GSM approach is 540 keV, while the corresponding experimental value is 600 keV. Our calculated widths for the 1^+ and 2^+ resonant states are 0.44 and 0.26 MeV, respectively. In Ref. [91], Hoffman reported that the widths are $0.03^{+0.12}_{-0.03}$ MeV for the 1^+ state and $0.05^{+0.21}_{-0.05}$MeV for the 2^+ state. Our calculations overestimate the width of the 1^+ state compared to experiment. On the other hand, our calculated width of the 2^+ state is within the experimental uncertainties. For the sake of comparison, we show results obtained with other effective interactions. The new universal *sd* Hamiltonians (USDA and USDB), obtained by revising the USD interaction in order to be more suitable for exotic nuclei [103], results in a good agreement with experimental data. However, one should note that some effects coming from the continuum and 3NFs are implicitly included in the new USD two-body matrix elements due to the fit made to experimental data. Although the USD interaction reproduces nicely two of the three experimental data points, the 2^+ state in ^{24}O comes out as a bound excited state, a fact which disagrees with recent experiments. We also show results obtained with a pure harmonic oscillator basis. In this case, the discretized continuum is not included in the model space, and we construct the effective interaction using perturbation theory through second order (see Fig. 6.6), and a model space consisting of neutrons in the orbitals $(1s_{1/2}, 0d_{3/2})$. Using a model space consisting of only bound oscillator orbitals puts the 1^+ and 2^+ states in ^{24}O too high in energy when comparing with experiment. With the inclusion of the continuum in the model space, the 1^+ and 2^+ states get lower in energy and also closer to experiment. This clearly shows an effect coming from a proper treatment of the continuum, and should therefore be included in a realistic description of low-lying states in ^{24}O. In a recent work by Volya [95], it was also found that the inclusion of the continuum significantly improves the description of these states using the standard USD interaction. Further, the 2^+ state in ^{24}O is a resonant state and cannot be properly described in an oscillator basis.

Turning to the case of the ground state of ^{25}O, our GSM calculations correctly predict that it is particle unstable, but puts it at a higher energy (E=2.1, Γ=0.5 MeV) compared with recent experimental data (E=0.77, Γ=0.17 MeV). To get a better description of this state, configurations like $\nu(1s_{1/2})(id_{3/2})^2$ should be included since the GSM is currently solved in a

filling configuration. We compare again our GSM result for ^{25}O with a shell-model calculation

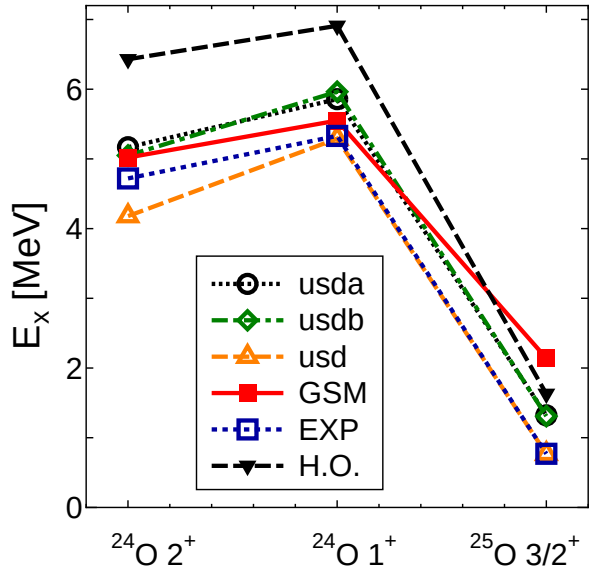

Figure 6.9: The excitation energies of the $J^\pi = 1^+$ and $J^\pi = 2^+$ states in ^{24}O and the ground-state energy of ^{25}O measured from the ground states in ^{24}O.

where only the bound oscillator orbitals $(1s_{1/2}, 0d_{3/2})$ define the model space. An important point to note is that ^{25}O comes out higher in energy compared to ^{24}O, reflecting that it is unstable towards neutron emission. Even though the oscillator basis cannot provide us with a width or a lifetime for the ground state of ^{25}O, it predicts ^{25}O as particle unstable and illustrates that the continuum coupling is not a dominant mechanism in explaining the position of the drip line of the oxygen isotopes. Thus, irrespective of whether we use a complex Gamow s.p. basis that defines a model space consisting of the $(1s_{1/2}, id_{3/2})$ states (with $i = 0, \ldots, n_{\text{Gamow}}$), or a harmonic oscillator basis with the $(1s_{1/2}, 0d_{3/2})$ states only, ^{25}O is unstable against particle emission as long as we use ^{22}O as a closed-shell core. This has important consequences for our theoretical understanding of the stability of matter. As pointed out in a recent calculation by Otsuka *et al* [92] or Hagen *et al* [105], many-body forces such as three-body interactions are crucial in explaining the correct position of the drip lines. The fact that a calculation of ^{25}O with ^{22}O as a closed-shell core gives the correct qualitative description of the ground state of ^{25}O, hints at the fact that with three valence neutrons only, missing many-body physics does not play a central role. This should be contrasted to realistic calculations that utilize ^{16}O as a closed core. With nine valence neutrons, ^{25}O is strongly over bound using the standard model space comprising the oscillator orbitals $(1s_{1/2}, 0d_{5/2}, 0d_{3/2})$

and a two-body effective interaction derived using MBPT. However, the location of the excited states in ^{24}O and the width of the ground state of ^{25}O depend crucially on the choice of basis, and we have shown that a GSM basis is needed in order to explain these states.

We conclude this work with an investigation of which parts of the NN interaction may play an important role in our understanding of the above excited states in ^{24}O. To achieve this, we single out the $^1S_0$ partial wave component of the NN interaction and vary its strength. This partial wave is particularly important to our understanding of pairing correlations in nuclei. In order to investigate the importance of this partial wave on the low-lying resonance states in ^{24}O, we vary the strength as $\tilde{V}(\alpha)=\alpha\times\langle S=0, L=0; J=0|V|S=0, L=0; J=0\rangle, \alpha\in[0,1]$ in an initial NN potential. Clearly, α=0 corresponds to an NN interaction with no contribution from this partial wave while α=1 corresponds to the original interaction. The low-lying resonance states are calculated for each $\tilde{V}(\alpha)$, and the results are shown in Fig. 6.10. One can clearly see how the $^1S_0$ partial wave in the NN interaction influences the many-body resonances in ^{24}O. The ground state gains additional binding when α increases since the ground state can be well described by the $\nu(1s_{1/2})^2$ configuration. At α=0 the position of 1^+ and 2^+ are interchanged with respect to experiment, and they are degenerate if one analyzes the real part of the resonance energies. When α increases to the full interaction strength, the 1^+-2^+ splitting increases to 530 keV, a result close to experiment. The $^1S_0$ partial wave, a central contribution to pairing in nuclei, is thus crucial in order to explain correctly the low-lying resonant states in ^{24}O.

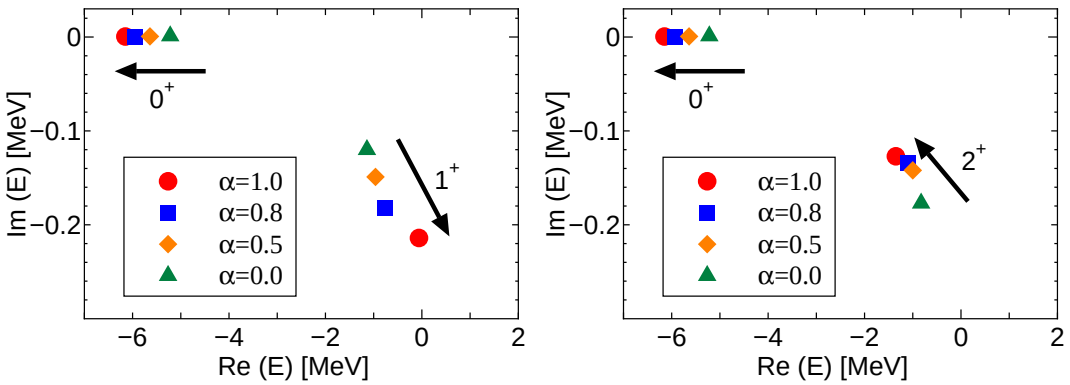

(a) The ground state and the 1^+ in ^{24}O

(b) The ground state and the 2^+ in ^{24}O

Figure 6.10: The energies of low-lying resonance states in ^{24}O, as a function of the strength α of the $^1S_0$ partial wave component of the nucleon-nucleon interaction. See text for further details.

Summary of the GSM

We have described the low-lying states in the oxygen isotopes ^{24}O and ^{25}O within the framework of the GSM and effective interactions derived through many-body perturbation theory. We have shown that there is a fine interplay between many-body effects and the proximity of the continuum, and we demonstrated that the inclusion of the continuum has significant effect on the excited states of ^{24}O. In order to predict the location of the drip line, we found that a proper inclusion of many-body forces and correlation effects are the deciding factors, which is consistent with the recent research [92] that includes the effects of 3N forces within a two-body machinery. Furthermore, the $^1S_0$ partial wave component of the NN interaction, an important contribution to strong pairing correlations in nuclei, plays an important role in explaining the correct value of these states. We conclude that the location of the drip line and excited states in the oxygen isotopes can only be determined by proper inclusion of both many-body correlations and the coupling with continuum degrees of freedom.

Chapter 7

Summary and future directions

We have shown that the in-medium SRG is a promising method for *ab-initio* calculations of light and medium-mass nuclei. The use of normal-ordering allowed us to evolve the dominant induced $3, ..., A$-body interactions using only two-body machinery. In Chapter 3, we have formulated the SRG flow equation in a nuclear many-body system up to the normal-ordered three-body operators. Utilizing the rotational invariance of the nuclear Hamiltonians, we derived the J-coupled expression of the flow equation of the IM-SRG at the normal-ordered two-body truncation. The representation of the flow equation in a spherical basis together with additional efforts in computer coding has made it possible to converge the calculations for real nuclei. The choice of the generator of the IM-SRG transformation was discussed in detail in section 3.2. In addition to the Wegner's original choice, other two generators have been imported to nuclear case, and the condition to decouple a reference state from the rest of Hilbert space was introduced.

In Chapter 4, we have clearly shown the perturbative contents of the IM-SRG. By making the perturbative expansion of the Hamiltonian and analytically solving the flow equation order by order, the connection to the perturbation theory and other many-body methods was demonstrated. It was shown that the IM-SRG(2) is the third-order exact for the ground-state energy and the second-order exact for the effective interactions, while the IM-SRG(3) is the third-order exact for the effective interactions, indicating the fourth-order exactness for the ground-state energy. The perturbative analysis has provided the systematic way of improving the flow equation. By considering the order $\mathcal{O}(g^k)$ $(k, 0, 1, \cdots)$, we have reached the systematic organization of the flow equation, which gives the machinery to control the accuracy of the IM-SRG transformation. Based on the consistent truncation scheme, we have presented first IM-SRG(2) results for the ground-state energies of closed-shell nuclei, which were in very

good agreement with CC calculations for both soft and hard interactions. We numerically demonstrated the important features of the IM-SRG: i) The decoupling of the reference state, ii) size-extensive and iii) non-perturbative structure. We also investigated the extent to which the center of mass motion is decoupled in section 5.3. Following the prescription that has been introduced in the CC theory, we reached the conclusion that for the IM-SRG results with sufficient convergence the A-body wave function can be well factorized into its intrinsic and c.m. part, therefore the contamination of the spurious c.m. excitation is sufficiently small.

In Chapter 6, we have shown for the first time the derivation of effective valence shell-model Hamiltonians for p-shell, taking an example of ^{6}Li. We introduced a naive but efficient prescription to decouple the nucleons in a valence shell(s) and the reference state $|\Phi\rangle$ from the rest of the Hilbert space simultaneously. We observed the clear agreement of the spectra including the ground-state energy with the Q-box expansion, which is a non-perturbative method. We emphasize that the IM-SRG has an advantage that it can be applied to the derivation of effective interactions defined in multi shells, for which the Q-box expansion has a serious problem of divergence due to the zero denominator. This is very important point because the derivation of the effective interactions in multi shells is crucially inevitable task to describe the nuclei belonging the island of inversion. From the RG perspective, the derivation of effective interaction is the decoupling or extraction of the relevant degrees of freedom, from which the observables of interest can be described. The IM-SRG has a flexibility to choose different model space without any conceptional problem. Together with the systematic organization of the flow equation suggested in Section 4.4, the IM-SRG has a strong potential to be used as a controllable theory of effective interactions for valence shell(s).

In section 6.3, we employed the Gamow shell model and described the low-lying states in drip-line oxygen isotopes based on realistic NN interactions. We concentrated upon the continuum effects for the drip-line nuclei, while the effects of three- or higher-body correlations were renormalized into the phenomenological single-particle energies in the model space. We found that the continuum coupling is important for the excited states but not crucial for the ground state. This means that the drip line of Oxygen isotopes is mainly explained by the effect of 3N forces not by continuum effects, which is consistent with the recent microscopic explanations.

As a whole, we introduced and developed a new many-body method, the in-medium SRG, which can be used for the *ab-initio* calculations of the ground state of the doubly magic nuclei and for the non-perturbative derivation of the valence shell-model effective interactions.

The IM-SRG at the same time can evolve an arbitral operator solving a single set of flow equation. It is important to note that the IM-SRG does have a machinery to make a systematic improvement of the accuracy of the flow equation based on the perturbative analysis as discussion in section 4.4. With this systematic framework, the IM-SRG has a strong potential for various applications for nuclear structure and other fields.

Work is in progress to include 3N forces and to study effective valence shell-model Hamiltonians and operators for open-shell systems. The IM-SRG also has a flexibility to choose the generator so as to construct effective valence shell-model interactions. The derivation of the effective interactions with the full inclusion of 3N forces will enable us to make a direct comparison between shell model and experimental data, which must be a great impact for nuclear structure physics. Especially, the impact of the 3N forces on the determination of the drip line would be an exciting subject.

Acknowledgments

I am greatly indebted to my supervisor, Prof. Takaharu Otsuka for his efforts in guiding me along my research projects. I would also like to thank Dr. Noritaka Shimizu for his kind help and valuable comments and discussion on my research and computational techniques. I am equally grateful to all the other members of the Nuclear Theory Group who have contributed to a spirited atmosphere of curiosity and helpfulness in research efforts.

I would like to mention that without my collaborators I could not have developed my research. I want to thank especially Prof. Morten Hjorth-Jensen for his helpful discussions, guidance and the hospitality during my stay in Oslo. I am equally grateful to Prof. Achim Schwenk for his constructive discussions, encouraging me and the hospitality for my stay in Vancouver and Darmstadt. I am also very grateful towards Dr. Scott. K. Bogner for his kind guiding on my research and encouraging me during the Ph.D. I would like to thank Dr. Gaute Hagen for his collaboration and kind help for my research.

Finally, spacial thanks to my family for their quiet understanding and encouragement for my challenge.

This work was supported in part by the a Research Fellowship of the Japan Society of the Promotions of Science, International Network for Exotic Femto Systems.

Appendix A

A.1 Fundamental commutators

In the derivation of the flow equations, it is convenient to first calculate all the basic commutators. We write one-, two and three-body operators as

$$A^{(1)} = \sum_{12} A_{ij}\{a_i^\dagger a_j\}, \quad A^{(2)} = \frac{1}{(2!)^2}\sum_{ijkl} A_{ijkl}\{a_i^\dagger a_j^\dagger a_l a_k\}, \tag{A.1}$$

$$A^{(3)} = \frac{1}{(3!)^2}\sum_{ijklmn} A_{ijklmn}\{a_i^\dagger a_j^\dagger a_k^\dagger a_n a_m a_l\}, \tag{A.2}$$

assuming that the two-body matrix elements are antisymmetrized,

$$A_{ijkl} = -P_{ij}A_{ijkl} = -P_{kl}A_{ijkl} = P_{ij}P_{kl}A_{jilk}, \tag{A.3}$$

$$\begin{aligned} A_{ijkllmn} &= -P_{ij}A_{ijklmn} = -P_{ik}A_{ijklmn} = -P_{jk}A_{ijklmn} \\ &= -P_{lm}A_{ijklmn} = -P_{ln}A_{ijklmn} = -P_{mn}A_{ijklmn} \\ &= P_{ij}P_{lm}A_{ijklmn} = P_{ik}P_{lm}A_{ijklmn} = P_{jk}P_{lm}A_{ijklmn} \\ &= P_{ij}P_{ln}A_{ijklmn} = P_{ik}P_{ln}A_{ijklmn} = P_{jk}P_{ln}A_{ijklmn} \\ &= P_{ij}P_{mn}A_{ijklmn} = P_{ik}P_{mn}A_{ijklmn} = P_{jk}P_{mn}A_{ijklmn}. \end{aligned} \tag{A.4}$$

The important commutators are obtained as follows.

$$[A^{(1)}, B^{(1)}]^{(1)} = \sum_{ij}\{a_i^\dagger a_j\}\left\{\sum_a (A_{ia}B_{aj} - B_{ia}A_{aj})\right\} \tag{A.5a}$$

$$[A^{(1)}, B^{(1)}]^{(0)} = \sum_{ij} A_{ij}B_{ji}(n_i - n_j) \tag{A.5b}$$

$$[A^{(1)}, B^{(2)}]^{(2)} = \frac{1}{4}\sum_{ijkl}\sum_a \{a_i^\dagger a_j^\dagger a_l a_k\}\left\{(1-P_{ij})A_{ia}B_{ajkl} - (1-P_{kl})A_{ak}B_{ijal}\right\} \tag{A.5c}$$

$$[A^{(1)},B^{(2)}]^{(1)} = \sum_{ij}\{a_i^\dagger a_j\}\left\{\sum_{ab}(n_a-n_b)A_{ab}B_{biaj}\right\} \tag{A.5d}$$

$$[A^{(1)},B^{(3)}]^{(3)} = \frac{1}{36}\sum_{ijklmn}\{a_i^\dagger a_j^\dagger a_k^\dagger a_n a_m a_l\}$$
$$\sum_a\{(1-P_{ij}-P_{ik})A_{ia}B_{ajklmn}-(1-P_{lm}-P_{ln})A_{al}B_{ijkamn}\} \tag{A.5e}$$

$$[A^{(1)},B^{(3)}]^{(2)} = \sum_{ijkl}\{a_i^\dagger a_j^\dagger a_l a_k\}\sum_{ab}(n_a-n_b)A_{ab}B_{b12a34} \tag{A.5f}$$

$$[A^{(2)},B^{(2)}]^{(3)} = \frac{1}{36}\sum_{ijklmn}\{a_i^\dagger a_j^\dagger a_k^\dagger a_n a_m a_l\}$$
$$P(ij/k)P(l/mn)\sum_x(A_{ijlx}B_{xkmn}-B_{ijlx}A_{xkmn}) \tag{A.5g}$$

$$[A^{(2)},B^{(2)}]^{(2)} = \frac{1}{4}\sum_{ijkl}\{a_i^\dagger a_j^\dagger a_l a_k\}\left\{\frac{1}{2}\sum_{ab}(A_{ijab}B_{abkl}-B_{ijab}A_{abkl})(1-n_a-n_b)\right.$$
$$\left.+\sum_{ab}(n_a-n_b)(1-P_{ij}-P_{kl}+P_{ij}P_{kl})A_{aibk}B_{bjal}\right\} \tag{A.5h}$$

$$[A^{(2)},B^{(2)}]^{(1)} = \sum_{ij}\{a_i^\dagger a_j\}\left\{\frac{1}{2}\sum_{abc}(A_{ciab}B_{abcj}-B_{ciab}A_{abcj})(\bar{n}_a\bar{n}_b n_c+n_a n_b\bar{n}_c)\right\} \tag{A.5i}$$

$$[A^{(2)},B^{(2)}]^{(0)} = \frac{1}{4}\sum_{ijkl}n_i n_j\bar{n}_k\bar{n}_l(A_{ijkl}B_{klij}-B_{ijkl}A_{klij}) \tag{A.5j}$$

$$[A^{(2)},B^{(3)}]^{(3)} = \frac{1}{36}\sum_{ijklmn}\{a_i^\dagger a_j^\dagger a_k^\dagger a_n a_m a_l\}$$
$$\cdot\frac{1}{2}\sum_{ab}(1-n_a-n_b)\left\{P(ij/k)A_{ijab}B_{abklmn}-P(l/mn)A_{abmn}B_{ijklab}\right\} \tag{A.5k}$$

$$[A^{(2)},B^{(3)}]^{(2)} = -\frac{1}{4}\sum_{ijkl}\{a_i^\dagger a_j^\dagger a_l a_k\}$$
$$\cdot\frac{1}{2}(n_a\bar{n}_b\bar{n}_c+\bar{n}_a n_b n_c)(1-P_{ij}P_{ik}P_{jl}-P_{kl}+P_{ik}P_{jl})A_{bcak}B_{aijbcl} \tag{A.5l}$$

$$[A^{(2)},B^{(3)}]^{(1)} = -\sum_{ij}\{a_i^\dagger a_j\}\frac{1}{4}\sum_{abcd}(n_a n_b\bar{n}_c\bar{n}_d-\bar{n}_a\bar{n}_b n_c n_d)A_{cdab}B_{abijcd} \tag{A.5m}$$

$$[A^{(3)},B^{(3)}]^{(3)} = \frac{1}{36}\sum_{ijklmn}\{a_i^\dagger a_j^\dagger a_k^\dagger a_n a_m a_l\}$$
$$\cdot\left[\frac{1}{6}\sum_{abc}(n_a n_b n_c+\bar{n}_a\bar{n}_b\bar{n}_c)(A_{ijkabc}B_{abclmn}-B_{ijkabc}A_{abclmn})\right.$$

$$+\frac{1}{2}\sum_{abc}(n_a n_b \bar{n}_c + \bar{n}_a \bar{n}_b n_c)P(ij/k)P(l/mn)(A_{abkcmn}B_{cijabl} - A_{cjkabn}B_{iablmc})\Bigg] \tag{A.5n}$$

$$[A^{(3)}, B^{(3)}]^{(2)} = \frac{1}{4}\sum_{ijkl}\{a_i^\dagger a_j^\dagger a_l a_k\}\Bigg[\frac{1}{6}\sum_{abcd}(n_a\bar{n}_b\bar{n}_c\bar{n}_d - \bar{n}_a n_b n_c n_d)(A_{aijbcd}B_{bcdakl} - A_{bcdakl}B_{aijbcd})$$
$$+\frac{1}{4}\sum_{abcd}(\bar{n}_a\bar{n}_b n_c n_d - n_a n_b \bar{n}_c\bar{n}_d)(1-P_{ij})(1-P_{kl})A_{abicdl}B_{cdjabk}\Bigg] \tag{A.5o}$$

$$[A^{(3)}, B^{(3)}]^{(1)} = \sum_{ij}\{a_i^\dagger a_j\}\frac{1}{12}\sum_{acde}(n_a n_b\bar{n}_c\bar{n}_d\bar{n}_e + \bar{n}_a\bar{n}_b n_c n_d n_e)(A_{abicde}B_{cdeabj} - B_{abicde}A_{cdeabj}) \tag{A.5p}$$

$$[A^{(3)}, B^{(3)}]^{(0)} = \frac{1}{36}\sum_{ijklmn}(n_i n_j n_k \bar{n}_l\bar{n}_m\bar{n}_n - \bar{n}_i\bar{n}_j\bar{n}_k n_l n_m n_n)A_{ijklmn}B_{lmnijk} \tag{A.5q}$$

A.2 Derivation of the J-coupled flow equations

In this Section, we give the derivation of the IM-SRG(2) flow equations in the J-coupled basis. First, we introduce the quantum numbers $k_a = (n_a, l_a, j_a, t_{za})$ and $\omega_a = (l_a, j_a, t_{za}, m_a)$. Note that M-scheme indices label $a = (n_a, l_a, j_a, t_{za}, m_a)$. M-scheme matrix elements and J-scheme matrix elements are related as bellow

$$f_{ij} = \delta_{\omega_i\omega_j}f_{k_ik_j}, \tag{A.6}$$

$$\Gamma_{ijkl} = \sqrt{(1+\delta_{k_ik_j})(1+\delta_{k_kk_l})}\sum_{JM}(j_i m_i j_j m_j|JM)(j_k m_k j_l m_l|JM)\Gamma^J_{k_ik_jk_kk_l}$$
$$\equiv \sum_{JM}(j_i m_i j_j m_j|JM)(j_k m_k j_l m_l|JM)\tilde{\Gamma}^J_{k_ik_jk_kk_l} \tag{A.7}$$

In the same way,

$$\eta^{(1)}_{ij} = \delta_{\omega_i\omega_j}\eta^{(1)}_{k_ik_j} \tag{A.8}$$

$$\eta^{(2)}_{ijkl} = \sum_{JM}(j_i m_i j_j m_j|JM)(j_k m_k j_l m_l|JM)\tilde{\eta}^{2b,J}_{k_ik_jk_kk_l} \tag{A.9}$$

For the derivation of the J-coupled equations, the following relations can be useful.

$$\sum_{m_k}\begin{pmatrix} j_i & j_j & j_k \\ m_i & m_j & m_k\end{pmatrix}\begin{pmatrix} j_l & j_5 & j_k \\ m_l & m_5 & -m_k\end{pmatrix} = \sum_{j_6m_6}(-1)^{j_k+j_6+m_i+m_l}(2j_6+1)$$

$$\cdot \left\{ \begin{array}{ccc} j_i & j_j & j_k \\ j_l & j_5 & j_6 \end{array} \right\} \left(\begin{array}{ccc} j_l & j_j & j_6 \\ m_l & m_j & m_6 \end{array} \right) \left(\begin{array}{ccc} j_i & j_5 & j_6 \\ m_i & m_5 & -m_6 \end{array} \right), \tag{A.10}$$

or equivalently,

$$\sum_{m_k} (j_i m_i j_j m_j | j_k - m_k) (j_l m_l j_5 m_5 | j_k m_k) = (2j_k + 1) \sum_{j_6 m_6} (-1)^{j_k + j_6 + m_i + m_l} \cdot \left\{ \begin{array}{ccc} j_i & j_j & j_k \\ j_l & j_5 & j_6 \end{array} \right\} (j_l m_l j_j m_j | j_6 - m_6) (j_i m_i j_5 m_5 | j_6 m_6) . \tag{A.11}$$

For the expansion of 9j symbol,

$$\left\{ \begin{array}{ccc} j_i & j_j & J_{12} \\ j_k & j_l & J_{34} \\ J_{13} & J_{24} & J \end{array} \right\} = \sum_{J'} (-1)^{2J'} (2J' + 1) \left\{ \begin{array}{ccc} j_i & j_k & J_{13} \\ J_{24} & J & J' \end{array} \right\} \left\{ \begin{array}{ccc} j_j & j_l & J_{24} \\ j_k & J' & J_{34} \end{array} \right\} \left\{ \begin{array}{ccc} J_{12} & J_{34} & J \\ J' & j_i & j_j \end{array} \right\}, \tag{A.12}$$

is often used. We start from the M-scheme flow equations.

A.2.1 derivation of zero-body sector

The M-scheme equation is

$$\frac{d}{ds} E_0(s) = \sum_{ij} \eta^{(1)}_{ij} f^{od}_{ji} (n_i - n_j) + \frac{1}{2} \sum_{ijkl} \eta^{(2)}_{ijkl} \Gamma_{ijkl} n_i n_j \bar{n}_k \bar{n}_l . \tag{A.13}$$

The first term in Eq. (A.13) is

$$\begin{aligned} & \sum_{k_i k_j m_i m_j} \eta^{(1)}_{k_i m_i, k_j m_j} f^{od}_{k_i m_i, k_j m_j} (n_i - n_j) \delta_{m_i m_j} \delta_{j_i j_j} \delta_{l_i l_j} \\ &= \sum_{k_i k_j} \sum_{m} \eta^{(1)}_{k_i k_j} f^{od}_{k_i k_j} (n_i - n_j) \delta_{j_i j_j} \delta_{l_i l_j} \\ &= \sum_{k_i k_j} (2j_i + 1) \eta^{(1)}_{k_i k_j} f^{od}_{k_i k_j} (n_i - n_j) \delta_{j_i j_j} \delta_{l_i l_j} . \end{aligned} \tag{A.14}$$

The second term in Eq. (A.13) is

$$\frac{1}{2} \sum_{k_i k_j k_k k_l} \sum_{m_i m_j m_k m_l} \sum_{J M J' M'} (j_i m_i j_j m_j | J M) (j_k m_k j_l m_l | J' M') \tilde{\eta}^{(2),J}_{k_i k_j k_k k_l} \tilde{\Gamma}^{J}_{k_i k_j k_k k_l} n_i n_j \bar{n}_k \bar{n}_l \tag{A.15}$$

$$= \frac{1}{2} \sum_{k_i k_j k_k k_l} \sum_{JM} \tilde{\eta}^{(2),J}_{k_i k_j k_k k_l} \tilde{\Gamma}^{J}_{k_i k_j k_k k_l} n_i n_j \bar{n}_k \bar{n}_l \tag{A.16}$$

$$= \frac{1}{2} \sum_{k_i k_j k_k k_l} \sum_{J} (2J+1) \tilde{\eta}^{(2),J}_{k_i k_j k_k k_l} \tilde{\Gamma}^{J}_{k_i k_j k_k k_l} n_i n_j \bar{n}_k \bar{n}_l. \tag{A.17}$$

The normalization of the Clebsch-Gordan coefficients

$$\sum_{mm'} (jmj'm|JM)(jmj'm'|J'M') = \delta_{JJ'}\delta_{MM'} \tag{A.18}$$

is used. Therefore

$$\frac{d}{ds}E_0 = \frac{1}{2} \sum_{k_i k_j k_k k_l} \sum_{J} (2J+1) \tilde{\eta}^{(2),J}_{k_i k_j k_k k_l} \tilde{\Gamma}^{(2),J}_{k_i k_j k_k k_l} n_i n_j \bar{n}_k \bar{n}_l + \sum_{k_i k_j} (2j_i+1) \eta^{(1)}_{k_i k_j} f^{od}_{k_i k_j} (n_i - n_j). \tag{A.19}$$

A.2.2 derivation of one-body sector

The M-scheme equation is

$$\begin{aligned} \frac{df_{12}}{ds} &= \sum_a (\eta^{(1)}_{1a} f_{a2} - \eta^{(1)}_{a2} f_{1a}) + \sum_{ab} \eta^{(1)}_{ab} \Gamma_{b1a2} (n_a - n_b) - \sum_{ab} f^{od}_{ab} \eta^{(2)}_{b1a2} (n_a - n_b) \\ &\quad + \frac{1}{2} \sum_{abc} (\eta^{(2)}_{c1ab} \Gamma_{abc2} - \eta^{(2)}_{abc2} \Gamma_{c1ab}) (n_a n_b \bar{n}_c + \bar{n}_a \bar{n}_b n_c). \end{aligned} \tag{A.20}$$

The first term in Eq. (A.20) is

$$\begin{aligned} (1\text{st}) &= \sum_{k_a m_a} \left(\eta^{(1)}_{k_i m_i, k_j m_j} f_{k_a m_a, k_j m_j} - f_{k_i m_i, k_j m_j} \eta^{(1)}_{k_a m_a, k_j m_j} \right) \delta_{m_i m_a} \delta_{m_a m_j} \delta_{l_i l_a} \delta_{l_a l_j} \delta_{j_i j_a} \delta_{j_a j_j} \\ &= \sum_{k_a} \left(\eta^{(1)}_{k_i k_a} f_{k_a k_j} - f_{k_i k_a} \eta^{(1)}_{k_a k_j} \right) \delta_{l_i l_j} \delta_{j_i j_j}. \end{aligned} \tag{A.21}$$

The second term in Eq. (A.20) is

$$\begin{aligned} (2\text{nd}) &= \sum_{k_a k_b m_a m_b} (n_a - n_b) \tilde{\eta}^{(1)}_{k_a k_b} \delta_{m_a m_b} \sum_{JM} (j_b m_b j_i m_i | JM)(j_a m_a j_j m_j | JM) \tilde{\Gamma}^{J}_{k_a k_i k_b k_j} \\ &= \sum_{k_a k_b} (n_a - n_b) \eta^{(1)}_{k_a k_b} \\ &\quad \times \sum_{J} \sum_{mM} \tilde{\Gamma}^{J}_{k_a k_i k_b k_j} (-1)^{j_b - m} \sqrt{\frac{2J+1}{2j_i+1}} (j_b m J - M | j_i - m_i) \\ &\qquad\qquad (-1)^{j_a - m} \sqrt{\frac{2J+1}{2j_j+1}} (j_a m J - M | j_j - m_j) \end{aligned} \tag{A.22}$$

$$= \frac{1}{2j_i+1} \sum_{k_a k_b} (n_{k_a} - n_{k_b}) \eta^{(1)}_{k_a k_b} \sum_{J} (2J+1) \tilde{\Gamma}^{J}_{k_b k_i k_a k_j}. \tag{A.23}$$

Here, the relation

$$(j_i m_i j_j m_j | JM) = (-1)^{j_i - m_i} \sqrt{\frac{2J+1}{2j_i+1}} (j_i m_i J - M | j_j - m_j) \tag{A.24}$$

is used. The third term is in the same way,

$$(\text{3rd}) = -\frac{1}{2j_i+1} \sum_{k_a k_b} (n_{k_a} - n_{k_b}) f^{od}_{k_a k_b} \sum_J (2J+1) \tilde{\eta}^{(2),J}_{k_b k_i k_a k_j}. \tag{A.25}$$

The last term is

$$\begin{aligned}
(\text{last}) &= \frac{1}{2} \sum_{k_a k_b k_c} \sum_{m_a m_b m_c} \sum_{JMJ'M'} (\bar{n}_a \bar{n}_b n_c + n_a n_b \bar{n}_c)(\tilde{\eta}^{(2),J}_{k_c k_i k_a k_b} \tilde{\Gamma}^{J'}_{k_a k_b k_c k_j} - \tilde{\Gamma}^{J}_{k_c k_i k_a k_b} \tilde{\eta}^{(2),J'}_{k_a k_b k_c k_j}) \\
&\times (j_a m_a j_b m_b | JM)(j_a m_a j_b m_b | J'M')(j_c m_c j_i m_i | JM)(j_c m_c j_j m_j | J'M') \qquad \text{(A.26)} \\
&= \frac{1}{2} \sum_{k_a k_b k_c} \sum_{JMm_c} (\bar{n}_a \bar{n}_b n_c + n_a n_b \bar{n}_c)(\tilde{\eta}^{(2),J}_{k_c k_i k_a k_b} \tilde{\Gamma}^{J}_{k_a k_b k_c k_j} - \tilde{\Gamma}^{J}_{k_c k_i k_a k_b} \tilde{\eta}^{(2),J}_{k_a k_b k_c k_j}) \\
&\times (j_c m_c j_i m_i | JM)(j_c m_c j_j m_j | JM) \qquad \text{(A.27)} \\
&= \frac{1}{2} \sum_{k_a k_b k_c} \sum_{JMm_c} (\bar{n}_a \bar{n}_b n_c + n_a n_b \bar{n}_c)(\tilde{\eta}^{(2),J}_{k_c k_i k_a k_b} \tilde{\Gamma}^{J}_{k_a k_b k_c k_j} - \tilde{\Gamma}^{J}_{k_c k_i k_a k_b} \tilde{\eta}^{(2),J}_{k_a k_b k_c k_j}) \delta_{j_i j_j} \\
&\times (-1)^{j_c - m_c} \sqrt{\frac{2J+1}{2j_i+1}} (j_c m_c J - M | j_i - m_i) \\
&\times (-1)^{j_c - m_c} \sqrt{\frac{2J+1}{2j_j+1}} (j_c m_c J - M | j_j - m_j) \qquad \text{(by } Eq.\ (A.24)\text{)} \qquad \text{(A.28)} \\
&= \frac{1}{2(2j_i+1)} \sum_{k_a k_b k_c} \sum_J (2J+1)(\bar{n}_a \bar{n}_b n_c + n_a n_b \bar{n}_c)(\tilde{\eta}^{(2),J}_{k_c k_i k_a k_b} \tilde{\Gamma}^{J}_{k_a k_b k_c k_j} - \tilde{\Gamma}^{J}_{k_c k_i k_a k_b} \tilde{\eta}^{(2),J}_{k_a k_b k_c k_j}). \qquad \text{(A.29)}
\end{aligned}$$

Summing up all the terms, one obtains the jj-coupled equation for one-body sector

$$\begin{aligned}
\frac{d}{ds} f_{k_i k_j} &= \sum_{k_a} \left(\eta^{(1)}_{k_i k_a} f_{k_a k_j} - f_{k_i k_a} \eta^{(1)}_{k_a k_j} \right) \\
&+ \frac{1}{(2j_i+1)} \sum_J (2J+1) \left[\sum_{k_a k_b} (n_a - n_b) \left\{ \eta^{(1)}_{k_a k_b} \tilde{\Gamma}^{J}_{k_b k_i k_a k_j} - f^{od}_{k_a k_b} \tilde{\eta}^{(2),J}_{k_b k_i k_a k_j} \right\} \right. \\
&\left. \frac{1}{2} \sum_{k_a k_b k_c} \left(\tilde{\eta}^{(2),J}_{k_c k_i k_a k_b} \tilde{\Gamma}^{J}_{k_a k_b k_c k_j} - \tilde{\Gamma}^{J}_{k_c k_i k_a k_b} \tilde{\eta}^{(2),J}_{k_a k_b k_c k_j} \right) (\bar{n}_a \bar{n}_b n_c + n_a n_b \bar{n}_c) \right]
\end{aligned} \tag{A.30}$$

In the four terms in Eq. (A.30), $\delta_{l_i l_j} \delta_{j_i j_j}$ is obviously required and just abbreviated.

A.2.3 derivation of two-body sector

The M-scheme equation is

$$\begin{aligned}\frac{d\Gamma_{ijkl}}{ds} &= \sum_a \left(\eta^{(1)}_{ia}\Gamma_{ajkl} + \eta^{(1)}_{ja}\Gamma_{iakl} - \eta^{(1)}_{ak}\Gamma^{(2)}_{ijal} - \eta^{(1)}_{al}\Gamma^{(2)}_{ijka}\right) \\ &- \sum_a \left(f_{ia}\eta^{(2)}_{ajkl} + f_{ja}\eta^{(2)}_{iakl} - f_{ak}\eta^{(2)}_{ijal} - f_{al}\eta^{(2)}_{ijka}\right) \\ &+ \frac{1}{2}\sum_{ab}(\eta^{(2)}_{ijab}\Gamma_{abkl} - \eta^{(2)}_{abkl}\Gamma_{ijab})(1-n_a-n_b) \\ &- \sum_{ab}(n_a-n_b)\left\{\eta^{(2)}_{bjal}\Gamma_{aibk} - \eta^{(2)}_{aibk}\Gamma_{bjal} + \eta^{(2)}_{ajbk}\Gamma_{bial} - \eta^{(2)}_{bial}\Gamma_{ajbk}\right\} \end{aligned} \tag{A.31}$$

The l.h.s. of Eq. (A.31) is expanded as

$$\frac{d}{ds}\Gamma_{ijkl} = \sum_{JM}(j_i m_i j_j m_j|JM)(j_k m_k j_l m_l|JM)\frac{d}{ds}\tilde{\Gamma}^J_{k_i k_j k_k k_l}. \tag{A.32}$$

The first term in the r.h.s. of Eq. (A.32) is

$$\begin{aligned}(\text{r.h.s. } 1) &= \sum_{k_a m_a}\sum_{JM}(j_a m_a j_j m_j|JM)(j_k m_k j_l m_l|JM)\eta^{(1)}_{k_i k_a}\tilde{\Gamma}^J_{k_a k_j k_k k_l}\delta_{m_a m_i}\delta_{j_a j_i} \\ &+ \sum_{k_a m_a}\sum_{JM}(j_i m_i j_a m_a|JM)(j_k m_k j_l m_l|JM)\eta^{(1)}_{k_j k_a}\tilde{\Gamma}^J_{k_i k_a k_k k_l}\delta_{m_a m_j}\delta_{j_a j_j} \\ &- \sum_{k_a m_a}\sum_{JM}(j_i m_i j_j m_j|JM)(j_a m_a j_l m_l|JM)\eta^{(1)}_{k_a k_k}\tilde{\Gamma}^J_{k_i k_j k_a k_l}\delta_{m_a m_k}\delta_{j_a j_k} \\ &- \sum_{k_a m_a}\sum_{JM}(j_i m_i j_j m_j|JM)(j_k m_k j_a m_a|JM)\eta^{(1)}_{k_a k_l}\tilde{\Gamma}^J_{k_i k_j k_k k_a}\delta_{m_a m_l}\delta_{j_a j_l} \end{aligned} \tag{A.33}$$

$$\begin{aligned}&= \sum_{JM}(j_i m_i j_j m_j|JM)(j_k m_k j_l m_l|JM) \\ &\times \sum_{k_a}\left(\eta^{(1)}_{k_i k_a}\tilde{\Gamma}^J_{k_a k_j k_k k_l} + \eta^{(1)}_{k_j k_a}\tilde{\Gamma}^J_{k_i k_a k_k k_l} - \eta^{(1)}_{k_a k_k}\tilde{\Gamma}^J_{k_i k_j k_a k_l} - \eta^{(1)}_{k_a k_l}\tilde{\Gamma}^J_{k_i k_j k_k k_a}\right). \end{aligned} \tag{A.34}$$

In the same way, the second term in the r.h.s. of Eq. (A.31) is

$$\begin{aligned}(\text{r.h.s. } 2) &= -\sum_{JM}(j_i m_i j_j m_j|JM)(j_k m_k j_l m_l|JM) \\ &\times \left(f^{(1)}_{k_i k_a}\tilde{\eta}^{(2),J}_{k_a k_j k_k k_l} + f^{(1)}_{k_j k_a}\tilde{\eta}^{(2),J}_{k_i k_a k_k k_l} - f^{(1)}_{k_a k_k}\tilde{\eta}^{(2),J}_{k_i k_j k_a k_l} - f^{(1)}_{k_a k_l}\tilde{\eta}^{(2),J}_{k_i k_j k_k k_a}\right). \end{aligned} \tag{A.35}$$

The third term in the r.h.s. of Eq. (A.31) is

$$\begin{aligned}(\text{r.h.s. } 3) &= \frac{1}{2}\sum_{k_a k_b m_a m_b}\sum_{JMJ'M'}(1-n_a-n_b) \\ &\times \Big[(j_i m_i j_j m_j|JM)(j_a m_a j_b m_a|JM)(j_a m_a j_b m_b|J'M')(j_k m_k j_l m_l|J'M')\tilde{\eta}^{(2),J}_{k_i k_j k_a k_b}\tilde{\Gamma}^{J'}_{k_a k_b k_k k_l}\end{aligned}$$

$$
\begin{aligned}
&- (j_i m_i j_j m_j|JM)(j_a m_a j_b m_a|JM)(j_a m_a j_b m_b|J'M')(j_k m_k j_l m_l|J'M')\tilde{\eta}^{(2),J}_{k_a k_b k_k k_l}\tilde{\Gamma}^{J'}_{k_i k_j k_a k_b}\Big] \\
&= \frac{1}{2}\sum_{k_a k_b}\sum_{JM}(j_i m_i j_j m_j|JM)(j_k m_k j_l m_l|JM)(1-n_a-n_b) \\
&\times \left(\tilde{\eta}^{(2),J}_{k_i k_j k_a k_b}\tilde{\Gamma}^{J'}_{k_a k_b k_k k_l} - \tilde{\eta}^{(2),J}_{k_a k_b k_k k_l}\tilde{\Gamma}^{J'}_{k_i k_j k_a k_b}\right) \qquad \text{(A.36)}
\end{aligned}
$$

As for the fourth term in Eq. (A.31), we consider the general form in M-scheme basis.

$$
\Gamma_l = \sum_{ab}(n_a - n_b)A_{bpaq}B_{arbs}. \qquad \text{(A.37)}
$$

This can be transformed as

$$
\begin{aligned}
\Gamma_l &= \sum_{k_a k_b m_a m_b}(n_a - n_b)\sum_{JMJ'M'}\tilde{A}^J_{k_b k_p k_a k_q}\tilde{B}^J_{k_a k_r k_b k_s} \\
&\times (j_b m_b j_p mp|JM)(j_a m_a j_q m_q|JM)(j_a m_a j_r mr|J'M')(j_b m_b j_s m_s|J'M') \qquad \text{(A.38)} \\
&= \sum_{k_a k_b m_a m_b}(n_a - n_b)\sum_{JMJ'M'}\tilde{A}^J_{k_b k_p k_a k_q}\tilde{B}^J_{k_a k_r k_b k_s} \\
&\times (j_p - m_p j_b - m_b|J - M)(j_a m_a j_q m_q|JM)(j_a m_a j_r mr|J'M')(j_s - m_s j_b - m_b|J' - M'). \qquad \text{(A.39)}
\end{aligned}
$$

Using the relation Eq. (A.10) or Eq. (A.11), the CG coefficients are re-coupled as

$$
\begin{aligned}
\Gamma_l &= \sum_{k_a k_b m_a m_b}(n_a - n_b)\sum_{JJ'}\sum_{J_6 M_6 J'_6 M'_6}\hat{J}^2\hat{J}'^2\tilde{A}^J_{k_b k_p k_a k_q}\tilde{B}^J_{k_a k_r k_b k_s} \\
&\times (-1)^{J+J_6-m_p+m_a}(-1)^{J'+J'_6+m_a-m_s}\left\{\begin{array}{ccc} j_p & j_b & J \\ j_a & j_q & J_6\end{array}\right\}\left\{\begin{array}{ccc} j_a & j_r & J' \\ j_s & j_b & J'_6\end{array}\right\} \\
&\times (j_a m_a j_b - m_b|J_6 M_6)(j_p - m_p j_q m_q|J_6 M_6)(j_s - m_s j_r m_r|J'_6 M'_6)(j_a m_a j_b - m_b|J'_6 M'_6) \qquad \text{(A.40)} \\
&= \sum_{k_a k_b}(n_a - n_b)\sum_{JJ'}\sum_{J_6 M_6}\hat{J}^2\hat{J}'^2\tilde{A}^J_{k_b k_p k_a k_q}\tilde{B}^J_{k_a k_r k_b k_s} \\
&\times (-1)^{J+J_6-J'-J_6+m_s-m_p}\left\{\begin{array}{ccc} j_p & j_b & J \\ j_a & j_q & J_6\end{array}\right\}\left\{\begin{array}{ccc} j_a & j_r & J' \\ j_s & j_b & J'_6\end{array}\right\}(j_p - m_p j_q m_q|J_6 M_6)(j_s - m_s j_r m_r|J_6 M_6). \qquad \text{(A.41)}
\end{aligned}
$$

We again use the relation Eq. (A.10) or Eq. (A.11) to obtain

$$
\begin{aligned}
\Gamma_l &= \sum_{k_a k_b m_a m_b}(n_a - n_b)\sum_{JJ'}\sum_{J_6}(-1)^{J-J'-J_6+j_p+j_q+m_s-m_p}\hat{J}^2\hat{J}'^2\tilde{A}^J_{k_b k_p k_a k_q}\tilde{B}^J_{k_a k_r k_b k_s} \\
&\times \sum_{J_7 M_7}\hat{J}_6^2(-1)^{J_6+J_7+m_p-m_s}\left\{\begin{array}{ccc} j_p & j_q & J_6 \\ j_s & j_r & J_7\end{array}\right\}\left\{\begin{array}{ccc} j_p & j_b & J \\ j_a & j_q & J_6\end{array}\right\}\left\{\begin{array}{ccc} j_a & j_r & J' \\ j_s & j_b & J_6\end{array}\right\}
\end{aligned}
$$

$$\times (j_s - m_s j_q - m_q | J_7 - M_7)(j_p m_p j_r m_r | J_7 M_7) \tag{A.42}$$

$$= \sum_{J_7 M_7} (j_p m_p j_r m_r | J_7 M_7)(j_q m_q j_s m_s | J_7 M_7)$$
$$\times \sum_{k_a k_b} (n_a - n_b) \sum_{J J' J_6} (-1)^{j_p + j_q + J - J' + J_7} \hat{J}^2 \hat{J}'^2 \hat{J}_6^2$$
$$\times \begin{Bmatrix} j_p & j_q & J_6 \\ j_s & j_r & J_7 \end{Bmatrix} \begin{Bmatrix} j_p & j_b & J \\ j_a & j_q & J_6 \end{Bmatrix} \begin{Bmatrix} j_a & j_r & J' \\ j_s & j_b & J_6 \end{Bmatrix} \tilde{A}^{J}_{k_b k_p k_a k_q} \tilde{B}^{J'}_{k_a k r k_b k_s}. \tag{A.43}$$

Replacing the indices as $(J_7, M_7) \to (J, M)$, $J \to J_1$, $J' \to J_j$ and $J_6 \to J_k$, one obtains the final expression

$$\Gamma_l = \sum_{JM} (j_p m_p j_r m_r | JM)(j_q m_q j_s m_s | JM)$$
$$\times \sum_{k_a k_b} (n_a - n_b) \sum_{J_1 J_j J_k} (-1)^{j_p + j_q + J_1 - J_j + J} \hat{J}_i^2 \hat{J}_j^2 \hat{J}_k^2$$
$$\times \begin{Bmatrix} j_p & j_b & J_1 \\ j_a & j_q & J_k \end{Bmatrix} \begin{Bmatrix} j_a & j_r & J_j \\ j_s & j_b & J_k \end{Bmatrix} \begin{Bmatrix} j_p & j_q & J_k \\ j_s & j_r & J \end{Bmatrix} \tilde{A}^{J_1}_{k_b k_p k_a k_q} \tilde{B}^{J_j}_{k_a k r k_b k_s}. \tag{A.44}$$

Now this expression can be further simplified with 9j-symbols. Since 6j-symbol are invariant under permutation of their columns

$$\begin{Bmatrix} j_i & j_j & j_k \\ J_1 & J_j & J_k \end{Bmatrix} = \begin{Bmatrix} j_j & j_i & j_k \\ J_j & J_1 & J_k \end{Bmatrix}, \tag{A.45}$$

and under exchange of two corresponding elements between rows,

$$\begin{Bmatrix} j_i & j_j & j_k \\ J_1 & J_j & J_k \end{Bmatrix} = \begin{Bmatrix} J_1 & J_j & j_k \\ j_i & j_j & J_k \end{Bmatrix}, \tag{A.46}$$

The three 6j-symbols in the r,h,s, of Eq. (A.42) can be written as

$$\begin{Bmatrix} j_p & j_b & J_1 \\ j_a & j_q & J_k \end{Bmatrix} \begin{Bmatrix} j_a & j_r & J_j \\ j_s & j_b & J_k \end{Bmatrix} \begin{Bmatrix} j_p & j_q & J_k \\ j_s & j_r & J \end{Bmatrix} = \begin{Bmatrix} J_1 & j_p & j_b \\ J_k & j_a & j_q \end{Bmatrix} \begin{Bmatrix} j_a & J_j & j_r \\ j_s & J_k & j_b \end{Bmatrix} \begin{Bmatrix} j_p & j_r & J \\ j_s & j_q & J_k \end{Bmatrix} \tag{A.47}$$

$$= \begin{Bmatrix} j_a & j_r & J_j \\ j_s & j_b & J_k \end{Bmatrix} \begin{Bmatrix} j_q & J & j_s \\ j_r & J_k & j_p \end{Bmatrix} \begin{Bmatrix} J_1 & j_p & j_b \\ J_k & j_a & j_q \end{Bmatrix} \tag{A.48}$$

Then Eq. (A.44) becomes

$$\begin{aligned}\Gamma_l = &\sum_{JM}(j_p m_p j_r m_r|JM)(j_q m_q j_s m_s|JM)\\ &\times\sum_{k_a k_b}(n_a-n_b)\sum_{J_1 J_j J_k}(-1)^{j_p+j_q+J_1-J_j+J}\hat{J}_1^2\hat{J}_j^2\hat{J}_k^2\\ &\times\left\{\begin{array}{ccc} j_a & j_r & J_j\\ j_s & j_b & J_k\end{array}\right\}\left\{\begin{array}{ccc} j_q & J & j_s\\ j_r & J_k & j_p\end{array}\right\}\left\{\begin{array}{ccc} J_1 & j_p & j_b\\ J_k & j_a & j_q\end{array}\right\}\tilde{A}^{J_1}_{k_b k_p k_a k_q}\tilde{B}^{J_j}_{k_a k r k_b k_s}.\end{aligned}\tag{A.49}$$

Now one can use the relation between 9j- and 6j-symbols,

$$\left\{\begin{array}{ccc} j_i & j_j & J_{12}\\ j_k & j_l & J_{34}\\ J_{13} & J_{24} & J\end{array}\right\}=\sum_{J'}(-1)^{2J'}\hat{J}'\left\{\begin{array}{ccc} j_i & j_k & J_{13}\\ J_{24} & J & J'\end{array}\right\}\left\{\begin{array}{ccc} j_j & j_l & J_{24}\\ j_k & J' & J_{34}\end{array}\right\}\left\{\begin{array}{ccc} J_{12} & J_{34} & J\\ J' & j_i & j_j\end{array}\right\},\tag{A.50}$$

and gets the expression,

$$\begin{aligned}\Gamma_l = &\sum_{JM}(j_p m_p j_r m_r|JM)(j_q m_q j_s m_s|JM)\\ &\times\sum_{k_a k_b}(n_a-n_b)\sum_{J_1 J_j}(-1)^{j_p+j_q+J_1-J_j+J}\hat{J}_1^2\hat{J}_j^2\tilde{A}^{J_1}_{k_b k_p k_a k_q}\tilde{B}^{J_j}_{k_a k r k_b k_s}\left\{\begin{array}{ccc} j_a & j_q & J_1\\ j_r & J & j_p\\ J_j & j_s & j_b\end{array}\right\}.\end{aligned}\tag{A.51}$$

Now the fourth term in the r.h.s. of Eq. (A.31) can be written with 6j-symbols

$$\begin{aligned}(\text{r.h.s. } 4) = &\sum_{JM}(j_i m_j j_j m_j|JM)(j_k m_k j_l m_l|JM)\sum_{k_a k_b}(n_a-n_b)\\ &\times\sum_{J_1 J_j J_k}\Big[(-1)^{j_i+j_j+j_k+j_l}(-1)^{j_j+j_l+J_1-J_j+J}\hat{J}_1^2\hat{J}_j^2\hat{J}_k^2\\ &\times\left\{\begin{array}{ccc} j_j & j_b & J_1\\ j_a & j_l & J_k\end{array}\right\}\left\{\begin{array}{ccc} j_a & j_i & J_j\\ j_k & j_b & J_k\end{array}\right\}\left\{\begin{array}{ccc} j_j & j_l & J_k\\ j3 & j_i & J\end{array}\right\}\left(\tilde{\eta}^{J_1}_{k_b k_j k_a k_l}\tilde{\Gamma}^{J_j}_{k_a k_i k_b k_k}-\tilde{\Gamma}^{J_1}_{k_b k_j k_a l_l}\tilde{\eta}^{J_j}_{k_a k_i k_b k_k}\right)\\ &+(-1)^{j_k+j_l-J}(-1)^{j_i+j_l+J_1-J_j+J}\hat{J}_1^2\hat{J}_j^2\hat{J}_k^2\\ &\times\left\{\begin{array}{ccc} j_i & j_b & J_1\\ j_a & j_l & J_k\end{array}\right\}\left\{\begin{array}{ccc} j_a & j_j & J_j\\ j_k & j_b & J_k\end{array}\right\}\left\{\begin{array}{ccc} j_i & j_l & J_k\\ j3 & j_j & J\end{array}\right\}\left(\tilde{\Gamma}^{J_1}_{k_b k_i k_a k_l}\tilde{\eta}^{J_j}_{k_a k_j k_b k_k}-\tilde{\eta}^{J_1}_{k_b k_i k_a l_l}\tilde{\Gamma}^{J_j}_{k_a k_j k_b k_k}\right)\Big]\\ = &\sum_{JM}(j_i m_j j_j m_j|JM)(j_k m_k j_l m_l|JM)\sum_{k_a k_b}(n_a-n_b)\\ &\times\sum_{J_1 J_j J_k}(-1)^{j_i+j_k+J_1-J_j}\hat{J}_1^2\hat{J}_j^2\hat{J}_k^2\end{aligned}$$

$$\times \left[(-1)^J \begin{Bmatrix} j_j & j_b & J_1 \\ j_a & j_l & J_k \end{Bmatrix} \begin{Bmatrix} j_a & j_i & J_j \\ j_k & j_b & J_k \end{Bmatrix} \begin{Bmatrix} j_j & j_l & J_k \\ j_k & j_i & J \end{Bmatrix} \right.$$
$$\cdot \left(\tilde{\eta}^{J_1}_{k_b k_j k_a k_l} \tilde{\Gamma}^{J_j}_{k_a k_i k_b k_k} - \tilde{\Gamma}^{J_1}_{k_b k_j k_a l_l} \tilde{\eta}^{J_j}_{k_a k_i k_b k_k} \right)$$
$$\left. - \begin{Bmatrix} j_i & j_b & J_1 \\ j_a & j_l & J_k \end{Bmatrix} \begin{Bmatrix} j_a & j_j & J_j \\ j_k & j_b & J_k \end{Bmatrix} \begin{Bmatrix} j_i & j_l & J_k \\ j_k & j_j & J \end{Bmatrix} \left(\tilde{\Gamma}^{J_1}_{k_b k_i k_a k_l} \tilde{\eta}^{J_j}_{k_a k_j k_b k_k} - \tilde{\eta}^{J_1}_{k_b k_i k_a l_l} \tilde{\Gamma}^{J_j}_{k_a k_j k_b k_k} \right) \right] . \tag{A.52}$$

One can use the relation Eq. (A.50) to obtain another expression,

$$\text{(r.h.s. 4)} = \sum_{JM} (j_i m_j j_j m_j | JM)(j_k m_k j_l m_l | JM) \sum_{k_a k_b} (n_a - n_b) \sum_{J_1 J_j} (-1)^{j_i + j_k + J_1 - J_j} \hat{J}_1^2 \hat{J}_j^2$$
$$\times \left[(-1)^J \begin{Bmatrix} j_a & j_l & J_1 \\ j_i & J & j_j \\ J_j & j_k & j_b \end{Bmatrix} \left(\tilde{\eta}^{J_1}_{k_b k_j k_a k_l} \tilde{\Gamma}^{J_j}_{k_a k_i k_b k_k} - \tilde{\Gamma}^{J_1}_{k_b k_j k_a l_l} \tilde{\eta}^{J_j}_{k_a k_i k_b k_k} \right) \right.$$
$$\left. - \begin{Bmatrix} j_a & j_l & J_1 \\ j_j & J & j_i \\ J_j & j_k & j_b \end{Bmatrix} \left(\tilde{\Gamma}^{J_1}_{k_b k_i k_a k_l} \tilde{\eta}^{J_j}_{k_a k_j k_b k_k} - \tilde{\eta}^{J_1}_{k_b k_i k_a l_l} \tilde{\Gamma}^{J_j}_{k_a k_j k_b k_k} \right) \right] \tag{A.53}$$

A.3 Matrix elements of the center of mass Hamiltonian in the spherical harmonic oscillator functions

We show the explicit expression of the matrix element of the center of mass (c.m.) Hamiltonian used in this thesis in the harmonic oscillator functions. For general many-body methods where the Hilbert space is truncated in a finite size with respect to a certain basis loose the guarantee that the c.m. motion decouples from the intrinsic degrees of freedom. Therefore, it is important to examine to what extent the c.m. motion is contaminated into the A-body wave functions. One thus needs to calculate the expectation value of the c.m. Hamiltonian in arbitral basis.

$$H_{\rm cm} = \frac{\boldsymbol{P}^2}{2M} + \frac{1}{2} M \omega^2 \boldsymbol{R}^2 - \frac{3}{2} \hbar \tilde{\omega}. \tag{A.54}$$

In doing so, it is very convenient to first express the Hamiltonian in harmonic oscillator basis. We show the expression of the matrix elements for the spherical harmonic oscillator functions with frequency ω.

$$H_{\rm cm} - \frac{3}{2}\hbar\tilde{\omega} = \frac{1}{A}\sum_i \left\{ \frac{\boldsymbol{p}_i^2}{2m} + \frac{1}{2}m\tilde{\omega}^2\boldsymbol{r}_i^2 \right\} + \sum_{i<j}\left\{ \frac{\boldsymbol{p}_i\cdot\boldsymbol{p}_j}{mA} + \frac{m\tilde{\omega}^2\boldsymbol{r}_i\cdot\boldsymbol{r}_j}{A} \right\}$$

$$= \frac{1}{A}\sum_{\alpha\beta}\tilde{h}^{\rm HO}_{\alpha\beta}a^\dagger_\alpha a_\beta + \frac{1}{4}\sum_{\alpha\beta\gamma\delta}\left\{ \frac{\langle\alpha\beta|\,\boldsymbol{p}_1\cdot\boldsymbol{p}_2\,|\gamma\delta\rangle}{mA} + \frac{m\tilde{\omega}^2\,\langle\alpha\beta|\,\boldsymbol{r}_1\cdot\boldsymbol{r}_2\,|\gamma\delta\rangle}{A} \right\} \quad \text{(A.55)}$$

$$= \frac{1}{A}\sum_{\alpha\beta}(\langle\alpha|\,t\,|\beta\rangle + \langle\alpha|\,\tilde{u}\,|\beta\rangle)a^\dagger_\alpha a_\beta$$

$$+ \frac{\hbar\tilde{\omega}}{4A}\sum_{\alpha\beta\gamma\delta}\left\{ -\langle\alpha\beta|\,(\tilde{b}\nabla_1)\cdot(\tilde{b}\nabla_2)\,|\gamma\delta\rangle + \langle\alpha\beta|\,\frac{\boldsymbol{r}_1}{\tilde{b}}\cdot\frac{\boldsymbol{r}_2}{\tilde{b}}\,|\gamma\delta\rangle \right\}, \quad \text{(A.56)}$$

where

$$t = \frac{\boldsymbol{p}^2}{2m}, \qquad \tilde{u} = \frac{1}{2}m\tilde{\omega}^2\boldsymbol{r}^2, \qquad \tilde{b} \equiv \sqrt{\frac{\hbar}{m\tilde{\omega}}}. \quad \text{(A.57)}$$

A.3.1 One-body terms

We show the matrix elements of $\tilde{h}^{\rm HO} = t + \tilde{u}$ in HO basis.

Kinetic term

$$\langle\alpha|\,t\,|\beta\rangle = \langle\alpha|\frac{p^2}{2m}|\beta\rangle = -\frac{\hbar^2}{2m}\langle\alpha|\nabla^2|\beta\rangle \quad \text{(A.58)}$$

$$= -\frac{\hbar\tilde{\omega}\tilde{b}^2}{2}\frac{\delta_{l_\alpha l_\beta}\delta_{j_\alpha j_\beta}\delta_{m_\alpha m_\beta}}{\sqrt{(2l_\alpha+1)(2l_\beta+1)}}\sum_{nl}(-1)^{l-l_\beta}\langle n_\alpha l_\alpha||\nabla||nl\rangle\langle nl||\nabla||n_\beta l_\beta\rangle \quad \text{(A.59)}$$

$$\langle n'l'||\nabla||nl\rangle = \begin{cases} -\frac{1}{b}\sqrt{(l+1)(n+l+\frac{3}{2})} & (n'=n, l'=l+1) \\ -\frac{1}{b}\sqrt{(l+1)n} & (n'=n-1, l'=l+1) \\ -\frac{1}{b}\sqrt{l(n+l+\frac{1}{2})} & (n'=n, l'=l-1) \\ -\frac{1}{b}\sqrt{l(n+1)} & (n'=n+1, l'=l-1) \end{cases} \quad \text{(A.60)}$$

Here, the b is the oscillator length, defined as

$$b = \sqrt{\frac{\hbar}{m\omega}}. \quad \text{(A.61)}$$

Then one gets

$$\langle\alpha|t|\beta\rangle = \delta_{l_\alpha l_\beta}\delta_{j_\alpha j_\beta}\delta_{tz_\alpha tz_\beta}\frac{\hbar\omega}{2}\times\begin{cases} \sqrt{(n_\beta+1)(n_\beta+l_\beta+\frac{3}{2})} & (n_\alpha = n_\beta+1) \\ 2n_\beta+l_\beta+\frac{3}{2} & (n_\alpha = n_\beta) \\ \sqrt{n_\beta(n_\beta+l_\beta+\frac{1}{2})} & (n_\alpha = n_\beta-1) \end{cases} \quad \text{(A.62)}$$

H.O. potential term

$$\begin{aligned}\langle\alpha|\, u\,|\beta\rangle &= \langle\alpha|\,\frac{1}{2}m\tilde{\omega}^2 r^2\,|\beta\rangle \\ &= \frac{1}{2}\frac{\hbar\tilde{\omega}}{\tilde{b}^2}\frac{\delta_{j_\alpha j_\beta}\delta_{l_\alpha l_\beta}\delta_{tz_\alpha t_\beta}}{2l_\alpha+1}\sum_{nl}(-1)^{l-l_\beta}\langle n_\alpha l_\alpha\|\boldsymbol{r}\|nl\rangle\langle nl\|\boldsymbol{r}\|n_\beta l_\beta\rangle. \end{aligned} \tag{A.63}$$

We define

$$x_\pm \equiv \mp\frac{1}{\sqrt{2}}(x\pm iy) = rC^{(1)}_{\pm1}, \quad x_0 \equiv z = rC^{(0)}_0, \tag{A.64}$$

where

$$C^{(k)}_q(\Omega) \equiv \sqrt{\frac{4\pi}{2k+1}}Y^{(k)}_q(\Omega). \tag{A.65}$$

Then the reduced matrix element can be written as

$$\langle n'l'\|\boldsymbol{r}\|nl\rangle = \langle n'l'\|rC^{(1)}\|nl\rangle = \langle n'l'\|C^{(1)}\|nl\rangle\left\langle n'l'\right|r\left|nl\right\rangle. \tag{A.66}$$

From

$$\langle n'l'\|C^{(1)}\|nl\rangle = \begin{cases} \sqrt{l+1} & (l'=l+1) \\ -\sqrt{l} & (l'=l-1) \end{cases} \tag{A.67}$$

and from

$$\langle n'l'|r|nl\rangle = \begin{cases} b\sqrt{n+l+\frac{1}{2}} & (n'=n, l'=l-1) \\ -b\sqrt{n} & (n'=n-1, l'=l+1) \\ -b\sqrt{n+1} & (n'=n+1, l'=l-1) \\ b\sqrt{n+l+\frac{3}{2}} & (n'=n, l'=l+1) \end{cases} \tag{A.68}$$

one gets

$$\langle n'l'||\vec{r}||nl\rangle = \begin{cases} -b\sqrt{l(n+l+\frac{1}{2})} & (n'=n, l'=l-1) \\ -b\sqrt{(l+1)n} & (n'=n-1, l'=l+1) \\ b\sqrt{l(n+1)} & (n'=n+1, l'=l-1) \\ b\sqrt{(l+1)(n+l+\frac{3}{2})} & (n'=n, l'=l+1) \end{cases} \tag{A.69}$$

Then the matrix element Eq. (A.63) becomes

$$\langle\alpha|\,\tilde{u}\,|\beta\rangle = \delta_{j_\alpha j_\beta}\delta_{l_\alpha l_\beta}\delta_{tz_\alpha tz_\beta}\frac{\hbar\tilde{\omega}}{2}\frac{\omega}{\tilde{\omega}}\times\begin{cases} -\sqrt{(n_\beta+1)(n_\beta+l_\beta+\frac{3}{2})} & (n_\alpha=n_\beta+1) \\ 2n_\beta+l_\beta+\frac{3}{2} & (n_\alpha=n_\beta) \\ -\sqrt{n_\beta(n_\beta+l_\beta+\frac{1}{2})} & (n_\alpha=n_\beta-1) \end{cases} \tag{A.70}$$

From Eqs. (A.62) and (A.70), one gets

$$\langle\alpha|\,\tilde{h}^{\rm HO}\,|\beta\rangle = \delta_{j_\alpha j_\beta}\delta_{l_\alpha l_\beta}\delta_{tz_\alpha tz_\beta}\frac{\hbar\tilde{\omega}}{2}\begin{cases}\left(\frac{\omega}{\tilde{\omega}}-\frac{\tilde{\omega}}{\omega}\right)\sqrt{(n_\beta+1)(n_\beta+l_\beta+\frac{3}{2})} & (n_\alpha=n_\beta+1)\\ \left(\frac{\omega}{\tilde{\omega}}+\frac{\tilde{\omega}}{\omega}\right)(2n_\beta+l_\beta+\frac{3}{2}) & (n_\alpha=n_\beta)\\ \left(\frac{\omega}{\tilde{\omega}}-\frac{\tilde{\omega}}{\omega}\right)\sqrt{n_\beta(n_\beta+l_\beta+\frac{1}{2})} & (n_\alpha=n_\beta-1)\end{cases}. \tag{A.71}$$

This becomes the usual relation, when $\omega=\tilde{\omega}$,

$$\langle\alpha|\,h^{\rm HO}\,|\beta\rangle = \delta_{\alpha\beta}\hbar\omega\left(2n_\beta+l_\beta+\frac{3}{2}\right) \tag{A.72}$$

A.3.2 Two-body term

The direct term of two-body operator $\frac{1}{Am}\sum_{i<j}(p_ip_j)$ in Eq. (A.56) is

$$\begin{aligned}\langle ab|\frac{1}{Am}(p_1p_2)|cd\rangle_J &= -\frac{\hbar\tilde{\omega}}{A}\tilde{b}^2\langle ab|(\nabla_1\nabla_2)|cd\rangle_J^{\rm NAS}\\ &= -\frac{\hbar\tilde{\omega}}{A}\tilde{b}^2(-1)^{j_b+j_c-J}\begin{Bmatrix} j_a & j_b & J\\ j_d & j_c & 1\end{Bmatrix}\\ &\times\langle n_a(l_a\frac{1}{2})j_a||\nabla||n_c(l_c\frac{1}{2})j_c\rangle\langle n_b(l_b\frac{1}{2})j_b||\nabla||n_d(l_d\frac{1}{2})j_d\rangle\end{aligned} \tag{A.73}$$

where the relation

$$\langle j_1j_2|\hat{T}^{(k)}(1)\cdot\hat{U}^{(k)}(2)|j_1'j_2'\rangle_J^{\rm NAS} = (-1)^{j_2+J+j_1'}\begin{Bmatrix} j_1 & j_2 & J\\ j_2' & j_1' & k\end{Bmatrix}(j_1||\hat{T}^{(k)}|j_1')(j_2||\hat{U}^{(k)}|j_2') \tag{A.74}$$

is used, and the superscript "NAS" means that the matrix element is not antisymmetrized. The reduced matrix elements in the above equation can be calculated as

$$\begin{aligned}\langle n_a(l_a\frac{1}{2})j_a||\nabla||n_b(l_b\frac{1}{2})j_b\rangle &= \sqrt{(2j_a+1)(2j_b+1)}(-1)^{\frac{3}{2}+l_a+j_b}\\ &\cdot\begin{Bmatrix} j_a & 1 & j_b\\ l_b & \frac{1}{2} & l_a\end{Bmatrix}\langle n_al_a||\nabla||n_bl_b\rangle.\end{aligned} \tag{A.75}$$

The Eq. (A.60) can be used to obtain the final expression. The similar process applies to the calculations of $\boldsymbol{r}_1\cdot\boldsymbol{r}_2$ term in Eq. (A.56). by just replacing the $\nabla\to\boldsymbol{r}$ and the prefactor of the $\boldsymbol{p}_1\cdot\boldsymbol{p}_2$ term in Eq. (A.56).

The prescription of the normalization and anti-symmetrization is the following

$$\langle j_aj_b|X|j_cj_d\rangle_J = \frac{1}{\sqrt{(1+\delta_{ab})(1+\delta_{cd})}}\left(\langle j_aj_b|X|j_cj_d\rangle_J^{\rm NAS}-(-1)^{j_c+j_d-J}\langle j_aj_b|X|j_dj_c\rangle_J^{\rm NAS}\right),$$

where the X can be either $\boldsymbol{p}_1 \cdot \boldsymbol{p}_2/(mA)$ or $m\tilde{\omega}^2 \boldsymbol{r}_1 \cdot \boldsymbol{r}_2/A$.

References

[1] N. Ishii, S. Aoki, and T. Hatsuda. Nuclear Force from Lattice QCD. *Physical review letters*, 99(2):22001, 2007.

[2] S. Aoki, T. Hatsuda, and N. Ishii. The nuclear force from Monte Carlo simulations of lattice quantum chromodynamics. *Computational Science & Discovery*, 1:015009, 2008.

[3] Sinya Aoki, Tetsuo Hatsuda, and Noriyoshi Ishii. Theoretical Foundation of the Nuclear Force in QCD and Its Applications to Central and Tensor Forces in Quenched Lattice QCD Simulations. *Progress of Theoretical Physics*, 123(1):89–128, 2010.

[4] A. Sinya. Lattice QCD and Nuclear Physics. *Les Houches Lecture on "Modern perspectives in lattice QCD", arXiv:1008.4427 [hep-lat]*, 2009.

[5] Steven Weinberg. Nuclear forces from chiral lagrangians. *Physics Letters B*, 251(2):288 – 292, 1990.

[6] U. Van Kolck. Few-nucleon forces from chiral Lagrangians. *Physical Review C*, 49(6):2932–2941, 1994.

[7] D. R. Entem and R. Machleidt. Accurate charge-dependent nucleon-nucleon potential at fourth order of chiral perturbation theory. *Phys. Rev. C*, 68(4):041001, Oct 2003.

[8] E. Epelbaum, W. Glöckle, and U.G. Meißner. The two-nucleon system at next-to-next-to-next-to-leading order. *Nuclear Physics A*, 747(2-4):362–424, 2005.

[9] F. Coester. Bound states of a many-particle system. *Nuclear Physics*, 7:421 – 424, 1958.

[10] F. Coester and H. Kmel. Short-range correlations in nuclear wave functions. *Nuclear Physics*, 17:477 – 485, 1960.

[11] J. Čížek. On the Correlation Problem in Atomic and Molecular Systems. Calculation of Wavefunction Components in Ursell-Type Expansion Using Quantum-Field Theoretical Methods. *The Journal of Chemical Physics*, 45:4256, 1966.

[12] H. Kümel, K. H. Lürmann, and J. G. Zabolitzky. Many-fermion theory in exps- (or coupled cluster) form. *Physics Reports*, 36(1):1 – 63, 1978.

[13] Rodney J. Bartlett and Monika Musiał. Coupled-cluster theory in quantum chemistry. *Rev. Mod. Phys.*, 79(1):291–352, Feb 2007.

[14] R. F. Bishop, M. F. Flynn, M. C. Boscá, E. Buenda, and R. Guardiola. Translationally invariant coupled cluster theory for simple finite systems. *Phys. Rev. C*, 42(4):1341–1360, Oct 1990.

[15] Jochen H. Heisenberg and Bogdan Mihaila. Ground state correlations and mean field in ^{16}O. *Phys. Rev. C*, 59(3):1440–1448, Mar 1999.

[16] Bogdan Mihaila and Jochen H. Heisenberg. Ground state correlations and mean field in ^{16}O. II. Effects of a three-nucleon interaction. *Phys. Rev. C*, 61(5):054309, Apr 2000.

[17] Bogdan Mihaila and Jochen H. Heisenberg. Microscopic Calculation of the Inclusive Electron Scattering Structure Function in ^{16}O. *Phys. Rev. Lett.*, 84(7):1403–1406, Feb 2000.

[18] D. J. Dean and M. Hjorth-Jensen. Coupled-cluster approach to nuclear physics. *Phys. Rev. C*, 69(5):054320, May 2004.

[19] K. Kowalski, D. J. Dean, M. Hjorth-Jensen, T. Papenbrock, and P. Piecuch. Coupled cluster calculations of ground and excited states of nuclei. *Phys. Rev. Lett.*, 92(13):132501, Apr 2004.

[20] M. Włoch, D. J. Dean, J. R. Gour, M. Hjorth-Jensen, K. Kowalski, T. Papenbrock, and P. Piecuch. *Ab-Initio* Coupled-Cluster Study of ^{16}O. *Phys. Rev. Lett.*, 94(21):212501, Jun 2005.

[21] Frank T. Avignone, Steven R. Elliott, and Jonathan Engel. Double beta decay, majorana neutrinos, and neutrino mass. *Rev. Mod. Phys.*, 80(2):481–516, Apr 2008.

[22] T.T.S. Kuo. in topics in nuclear physics. *Lecture notes in physics*, 144:248, 1981.

[23] T.T.S.Kuo Evind Osnes. Folded-diagram theory of the effective interaction in nuclei, atoms and molecules. *Lecture notes in physics*, 364:1, 1990.

[24] M. Hjorth-Jensen, T.T.S. Kuo, and E. Osnes. Realistic effective interactions for nuclear systems. *Physics Reports*, 261(3):125–270, 1995.

[25] R. B. Wiringa. Variational calculations of few-body nuclei. *Phys. Rev. C*, 43(4):1585–1598, Apr 1991.

[26] R. B. Wiringa, Steven C. Pieper, J. Carlson, and V. R. Pandharipande. Quantum Monte Carlo calculations of $A = 8$ nuclei. *Phys. Rev. C*, 62(1):014001, Jun 2000.

[27] Steven C. Pieper, K. Varga, and R. B. Wiringa. Quantum Monte Carlo calculations of $A = 9, 10$ nuclei. *Phys. Rev. C*, 66(4):044310, Oct 2002.

[28] Steven C. Pieper, R. B. Wiringa, and J. Carlson. Quantum Monte Carlo calculations of excited states in $A = 6 - 8$ nuclei. *Phys. Rev. C*, 70(5):054325, Nov 2004.

[29] P. Navrátil, J. P. Vary, and B. R. Barrett. Properties of ^{12}C in the Ab Initio Nuclear Shell Model. *Phys. Rev. Lett.*, 84(25):5728–5731, Jun 2000.

[30] P. Navrátil, V. G. Gueorguiev, J. P. Vary, W. E. Ormand, and A. Nogga. Structure of $A = 10 - 13$ Nuclei with Two- Plus Three-Nucleon Interactions from Chiral Effective Field Theory. *Phys. Rev. Lett.*, 99(4):042501, Jul 2007.

[31] P. Navratil, S. Quaglioni, I. Stetcu, and B.R. Barrett. Recent developments in no-core shell-model calculations. *Journal of Physics G: Nuclear and Particle Physics*, 36:083101, 2009.

[32] G. Hagen, T. Papenbrock, D. J. Dean, and M. Hjorth-Jensen. Medium-mass nuclei from chiral nucleon-nucleon interactions. *Phys. Rev. Lett.*, 101(9):092502, Aug 2008.

[33] G. Hagen, T. Papenbrock, D. J. Dean, A. Schwenk, A. Nogga, M. Włoch, and P. Piecuch. Coupled-cluster theory for three-body hamiltonians. *Physical Review C (Nuclear Physics)*, 76(3):034302, 2007.

[34] S. Fujii, R. Okamoto, and K. Suzuki. Ground-State and Single-Particle Energies of Nuclei around ^{16}O, ^{40}Ca, and ^{56}Ni from Realistic Nucleon-Nucleon Forces. *Phys. Rev. Lett.*, 103(18):182501, Oct 2009.

[35] K. Suzuki and S.Y. Lee. Convergent Theory for Effective Interaction in Nuclei. *Progress of Theoretical Physics*, 64(6):2091–2106, 1980.

[36] H. Feldmeier, T. Neff, R. Roth, and J. Schnack. A unitary correlation operator method. *Nuclear Physics A*, 632(1):61 – 95, 1998.

[37] T. Neff and H. Feldmeier. Tensor correlations in the unitary correlation operator method. *Nuclear Physics A*, 713(3-4):311 – 371, 2003.

[38] S.K. Bogner, R.J. Furnstahl, and A. Schwenk. From low-momentum interactions to nuclear structure. *Progress in Particle and Nuclear Physics*, 65(1):94 – 147, 2010.

[39] S. K. Bogner, R. J. Furnstahl, and R. J. Perry. Similarity renormalization group for nucleon-nucleon interactions. *Phys. Rev. C*, 75(6):061001, Jun 2007.

[40] ED Jurgenson, P. Navrátil, and RJ Furnstahl. Evolution of Nuclear Many-Body Forces with the Similarity Renormalization Group. *Physical review letters*, 103(8):82501, 2009.

[41] SK Bogner, RJ Furnstahl, A. Nogga, and A. Schwenk. Nuclear matter from chiral low-momentum interactions. *arXiv:0903.3366*, 2009.

[42] G. Hagen, D.J. Dean, M. Hjorth-Jensen, and T. Papenbrock. Complex coupled-cluster approach to an ab-initio description of open quantum systems. *Physics Letters B*, 656(4-5):169 – 173, 2007.

[43] S. Bacca, A. Schwenk, G. Hagen, and T. Papenbrock. Helium halo nuclei from low-momentum interactions. *The European Physical Journal A*, 42(3):553–558, 2009.

[44] G. Hagen, T. Papenbrock, DJ Dean, and M. Hjorth-Jensen. Ab initio coupled-cluster approach to nuclear structure with modern nucleon-nucleon interactions. *Arxiv preprint arXiv:1005.2627*, 2010.

[45] J. P. Schiffer, S. J. Freeman, J. A. Caggiano, C. Deibel, A. Heinz, C.-L. Jiang, R. Lewis, A. Parikh, P. D. Parker, K. E. Rehm, S. Sinha, and J. S. Thomas. Is the nuclear spin-orbit interaction changing with neutron excess? *Phys. Rev. Lett.*, 92(16):162501, Apr 2004.

[46] D. Warner. Nuclear physics: Not-so-magic numbers. *Nature a-z index*, 430(6999):517–519, 2004.

[47] T. Otsuka et al. Evolution of nuclear shells due to the tensor force. *Phys Rev. Lett.*, 95:232502, 2005.

[48] T. Otsuka et al. Magic numbers in exotic nuclei and spin-isospin properties of the *nn* interaction. *Phys. Rev. Lett*, 87:082502, 2001.

[49] N. Michel, W. Nazarewicz, M. Płoszajczak, and T. Vertse. Shell model in the complex energy plane. *Journal of Physics G: Nuclear and Particle Physics*, 36:013101, 2009.

[50] T. Hatsuda, S. Aoki, N. Ishii, and H. Nemura. From Lattice QCD to Nuclear Force. *Modern Physics Letters A*, 23(27-30):2265–2272, 2008.

[51] N. Ishii et al. Lattice study of nuclear forces. In *Symposium on Lattice Field Theory*, volume 1, page 19, 2009.

[52] Mituo Taketani, Seitaro Nakamura, and Muneo Sasaki. On the method of the theory of nuclear forces. *Progress of Theoretical Physics*, 6(4):581–586, 1951.

[53] Robert Jastrow. On the nucleon-nucleon interaction. *Phys. Rev.*, 81(2):165–170, Jan 1951.

[54] R. B. Wiringa, V. G. J. Stoks, and R. Schiavilla. Accurate nucleon-nucleon potential with charge-independence breaking. *Phys. Rev. C*, 51(1):38–51, Jan 1995.

[55] R. Machleidt. High-precision, charge-dependent bonn nucleon-nucleon potential. *Phys. Rev. C*, 63(2):024001, Jan 2001.

[56] V. G. J. Stoks, R. A. M. Klomp, C. P. F. Terheggen, and J. J. de Swart. Construction of high-quality nn potential models. *Phys. Rev. C*, 49(6):2950–2962, Jun 1994.

[57] Steven Weinberg. Phenomenological lagrangians. *Physica A: Statistical and Theoretical Physics*, 96(1-2):327 – 340, 1979.

[58] H. Kamada, A. Nogga, W. Glöckle, E. Hiyama, M. Kamimura, K. Varga, Y. Suzuki, M. Viviani, A. Kievsky, S. Rosati, J. Carlson, Steven C. Pieper, R. B. Wiringa, P. Navrátil, B. R. Barrett, N. Barnea, W. Leidemann, and G. Orlandini. Benchmark test calculation of a four-nucleon bound state. *Phys. Rev. C*, 64(4):044001, Aug 2001.

[59] Claude Bloch. Sur la théorie des perturbations des états liés. *Nuclear Physics*, 6:329 – 347, 1958.

[60] Claude Bloch and Jules Horowitz. Sur la détermination des premiers tats d'un systéme de fermions dans le cas dégénéré. *Nuclear Physics*, 8:91 – 97, 1958.

[61] BAIRD H. BRANDOW. Linked-cluster expansions for the nuclear many-body problem. *Rev. Mod. Phys.*, 39(4):771–828, Oct 1967.

[62] S. Y. Lee and K. Suzuki. The effective interaction of two nucleons in the s-d shell. *Physics Letters B*, 91(2):173 – 176, 1980.

[63] S. K. Bogner, T. T. S. Kuo, and A. Schwenk. Model-independent low momentum nucleon interaction from phase shift equivalence. *Physics Reports*, 386(1):1 – 27, 2003.

[64] S. Fujii, E. Epelbaum, H. Kamada, R. Okamoto, K. Suzuki, and W. Glöckle. Low-momentum nucleon-nucleon interaction and its application to few-nucleon systems. *Physical Review C*, 70(2):24003, 2004.

[65] P. Navrátil and B. R. Barrett. No-core shell-model calculations with starting-energy-independent multivalued effective interactions. *Phys. Rev. C*, 54(6):2986–2995, Dec 1996.

[66] P. Navrátil and B. R. Barrett. Large-basis shell-model calculations for ¥it p-shell nuclei. *Phys. Rev. C*, 57(6):3119–3128, Jun 1998.

[67] S. Ôkubo. Diagonalization of Hamiltonian and Tamm-Dancoff Equation. *Progr. Theor. Phys*, 12:603–622, 1954.

[68] S.K. Bogner, R.J. Furnstahl, S. Ramanan, and A. Schwenk. Low-momentum interactions with smooth cutoffs. *Nuclear Physics A*, 784(1-4):79 – 103, 2007.

[69] Takaharu Otsuka, Toshio Suzuki, Michio Honma, Yutaka Utsuno, Naofumi Tsunoda, Koshiroh Tsukiyama, and Morten Hjorth-Jensen. Novel features of nuclear forces and shell evolution in exotic nuclei. *Phys. Rev. Lett.*, 104(1):012501, Jan 2010.

[70] Stanisław D. Głazek and Kenneth G. Wilson. Renormalization of hamiltonians. *Phys. Rev. D*, 48(12):5863–5872, Dec 1993.

[71] Franz J. Wegner. Flow-equations for hamiltonians. *Annalen der Physik*, 3:77 – 91, 1994. NON-PERTURBATIVE QCD AND HADRON PHENOMENOLOGY.

[72] S. Kehrein. *The flow equation approach to many-particle systems.* Springer Verlag, 2006.

[73] S.R. White. Numerical canonical transformation approach to quantum many-body problems. *The Journal of Chemical Physics*, 117:7472, 2002.

[74] H. Hergert and R. Roth. Unitary correlation operator method from a similarity renormalization group perspective. *Physical Review C (Nuclear Physics)*, 75(5):051001, 2007.

[75] J. Fujita and H. Miyazawa. Pion theory of three-body forces. *Prog. Theor. Phys*, 17(360):28, 1957.

[76] K. Tsukiyama, SK Bogner, and A. Schwenk. In-Medium Similarity Renormalization Group for Nuclei. *Arxiv preprint arXiv:1006.3639*, 2010.

[77] T. T. S. Kuo, J. Shurpin, K. C. Tam, E. Osnes, and P. J. Ellis. A simple method for evaluating Goldstone diagrams in an angular momentum coupled representation* 1. *Annals of Physics*, 132(2):237–276, 1981.

[78] C.P. Heidbrink and G.S. Uhrig. Renormalization by continuous unitary transformations: one-dimensional spinless fermions. *The European Physical Journal B-Condensed Matter and Complex Systems*, 30(4):443–459, 2002.

[79] A. Mielke. Flow equations for band-matrices. *The European Physical Journal B-Condensed Matter and Complex Systems*, 5(3):605–611, 1998.

[80] Murray Gell-Mann and Francis Low. Bound states in quantum field theory. *Phys. Rev.*, 84(2):350–354, Oct 1951.

[81] J. Goldstone. Derivation of the Brueckner many-body theory. *Proceedings of the Royal Society of London. Series A, Mathematical and Physical Sciences*, 239(1217):267–279, 1957.

[82] P. J. Ellis and E. Osnes. An introductory guide to effective operators in nuclei. *Rev. Mod. Phys.*, 49(4):777–832, Oct 1977.

[83] G. Hagen, T. Papenbrock, and D. J. Dean. Solution of the center-of-mass problem in nuclear structure calculations. *Phys. Rev. Lett.*, 103(6):062503, Aug 2009.

[84] E. R. Anderson, S. K. Bogner, R. J. Furnstahl, and R. J. Perry. Operator evolution via the similarity renormalization group: The deuteron. *Phys. Rev. C*, 82(5):054001, Nov 2010.

[85] P. Navrátil and E. Caurier. Nuclear structure with accurate chiral perturbation theory nucleon-nucleon potential: Application to ^{6}Li and ^{10}B. *Phys. Rev. C*, 69(1):014311, Jan 2004.

[86] D. R. Tilley, C. M. Cheves, J. L. Godwin, G. M. Hale, H. M. Hofmann, J. H. Kelley, C. G. Sheu, and H. R. Weller. Energy levels of light nuclei $A = 5, 6, 7$. *Nuclear Physics A*, 708(1-2):3 – 163, 2002.

[87] SK Bogner, RJ Furnstahl, P. Maris, RJ Perry, A. Schwenk, and JP Vary. Convergence in the no-core shell model with low-momentum two-nucleon interactions. *Nuclear Physics A*, 801(1-2):21 – 42, 2008.

[88] G. Hagen, T. Papenbrock, and M. Hjorth-Jensen. *Ab Initio* Computation of the ^{17}F Proton Halo State and Resonances in $A = 17$ Nuclei. *Phys. Rev. Lett.*, 104(18):182501, May 2010.

[89] Z. Elekes, Z. Dombrádi, N. Aoi, and S. Bishop et al. Spectroscopic Study of Neutron Shell Closures via Nucleon Transfer in the Near-Dripline Nucleus ^{23}O. *Phys. Rev. Lett.*, 98(10):102502, 2007.

[90] R. Álvarez-Rodríguez, A. S. Jensen, D. V. Fedorov, H. O. U. Fynbo, and E. Garrido. Energy distributions from three-body decaying many-body resonances. *Phys. Rev. Lett.*, 99(7):072503, Aug 2007.

[91] C. R. Hoffman, T. Baumann, D. Bazin, J. Brown, G. Christian, P. A. DeYoung, J. E. Finck, N. Frank, J. Hinnefeld, R. Howes, P. Mears, E. Mosby, S. Mosby, J. Reith, B. Rizzo, W. F. Rogers, G. Peaslee, W. A. Peters, A. Schiller, M. J. Scott, S. L. Tabor, M. Thoennessen, P. J. Voss, and T. Williams. Determination of the N = 16 Shell Closure at the Oxygen Drip Line. *Physical Review Letters*, 100(15):152502, 2008.

[92] Takaharu Otsuka, Toshio Suzuki, Jason D. Holt, Achim Schwenk, and Yoshinori Akaishi. Three-body forces and the limit of oxygen isotopes. *Phys. Rev. Lett.*, 105(3):032501, Jul 2010.

[93] K. Tsukiyama, M. Hjorth-Jensen, and G. Hagen. Gamow shell-model calculations of drip-line oxygen isotopes. *Phys. Rev. C*, 80(5):051301, Nov 2009.

[94] Alexander Volya and Vladimir Zelevinsky. Continuum shell model. *Phys. Rev. C*, 74(6):064314, Dec 2006.

[95] Alexander Volya. Time-dependent approach to the continuum shell model. *Phys. Rev. C*, 79(4):044308, Apr 2009.

[96] J. Rotureau, N. Michel, W. Nazarewicz, M. Płoszajczak, and J. Dukelsky. Density matrix renormalization group approach for many-body open quantum systems. *Phys. Rev. Lett.*, 97(11):110603, Sep 2006.

[97] R. B. Wiringa and Steven C. Pieper. Evolution of nuclear spectra with nuclear forces. *Phys. Rev. Lett.*, 89(18):182501, Oct 2002.

[98] P. Navrátil and W.E. Ormand. Ab Initio Shell Model Calculations with Three-Body Effective Interactions for p-Shell Nuclei. *Physical Review Letters*, 88(15):152502, 2002.

[99] PG Thirolf, BV Pritychenko, BA Brown, PD Cottle, M. Chromik, T. Glasmacher, G. Hackman, RW Ibbotson, KW Kemper, T. Otsuka, et al. Spectroscopy of the 2_1^+ state in ^{22}O and shell structure near the neutron drip line. *Physics Letters B*, 485(1-3):16–22, 2000.

[100] M. Stanoiu, F. Azaiez, Z. Dombrádi, and O. Sorlin et al. N= 14 and 16 shell gaps in neutron-rich oxygen isotopes. *Phys. Rev. C*, 69(3):34312, 2004.

[101] C.R. Hoffman, T. Baumann, D. Bazin, J. Brown, G. Christian, D.H. Denby, P.A. DeYoung, J.E. Finck, N. Frank, J. Hinnefeld, S. Mosby, W.A. Peters, W.F. Rogers, A. Schiller, A. Spyrou, M.J. Scott, S.L. Tabor, M. Thoennessen, and P. Voss. Evidence for a doubly magic ^{24}O. *Physics Letters B*, 672(1):17 – 21, 2009.

[102] B.A. Brown and W.A. Richter. Magic numbers in the neutron-rich oxygen isotopes. *Physical Review C*, 72(5):57301, 2005.

[103] B.A. Brown and W.A. Richter. New "USD" Hamiltonians for the sd shell. *Physical Review C*, 74(3):34315, 2006.

[104] L. Coraggio, A. Covello, A. Gargano, N. Itaco, D. R. Entem, T. T. S. Kuo, and R. Machleidt. Low-momentum nucleon-nucleon interactions and shell-model calculations. *Phys. Rev. C*, 75(2):024311, Feb 2007.

[105] G. Hagen, T. Papenbrock, D. J. Dean, M. Hjorth-Jensen, and B. Velamur Asokan. Ab initio computation of neutron-rich oxygen isotopes. *Phys. Rev. C*, 80(2):021306, Aug 2009.

[106] Sofia Quaglioni and Petr Navrátil. Ab Initio Many-Body Calculations of n-^{3}H, n-^{4}He, p-^{3,4}He, and n-^{10}Be Scattering. *Phys. Rev. Lett.*, 101(9):092501, Aug 2008.

[107] T. Berggren. Use of resonant states in eigenfunction expansions of scattering and reaction amplitudes. *Nuclear Physics A*, 109:265, 1968.

[108] Tore Berggren. On the treatment of resonant final states in direct reactions. *Nuclear Physics A*, 169(2):353 – 362, 1971.

[109] Tore Berggren. On the interpretation of complex cross sections for production of resonant final states. *Physics Letters B*, 73(4-5):389 – 392, 1978.

[110] Tore Berggren. Expectation value of an operator in a resonant state. *Physics Letters B*, 373(1-3):1 – 4, 1996.

[111] Patric Lind. Completeness relations and resonant state expansions. *Phys. Rev. C*, 47(5):1903–1920, May 1993.

[112] N. Michel, W. Nazarewicz, M. Płoszajczak, and J. Okołowicz. Gamow shell model description of weakly bound nuclei and unbound nuclear states. *Phys. Rev. C*, 67(5):054311, May 2003.

[113] G. Hagen, M. Hjorth-Jensen, and N. Michel. Gamow shell model and realistic nucleon-nucleon interactions. *Phys. Rev. C*, 73(6):64307, 2006.

[114] R. Machleidt D. R. Entem. Accurate nucleon-nucleon potential based upon chiral perturbation theory. *Physics Letters B*, 524:1, 2002.

[115] G. Audi, A. H. Wapstra, and C. Thibault. The 2003 atomic mass evaluation: (ii). tables, graphs and references. *Nuclear Physics A*, 729(1):337 – 676, 2003. The 2003 NUBASE and Atomic Mass Evaluations.

[116] R. Kanungo, C. Nociforo, A. Prochazka, T. Aumann, D. Boutin, D. Cortina-Gil, B. Davids, M. Diakaki, F. Farinon, H. Geissel, R. Gernhäuser, J. Gerl, R. Janik, B. Jonson, B. Kindler, R. Knöbel, R. Krücken, M. Lantz, H. Lenske, Y. Litvinov, B. Lommel, K. Mahata, P. Maierbeck, A. Musumarra, T. Nilsson, T. Otsuka, C. Perro, C. Scheidenberger, B. Sitar, P. Strmen, B. Sun, I. Szarka, I. Tanihata, Y. Utsuno, H. Weick, and M. Winkler. One-Neutron Removal Measurement Reveals ^{24}O as a New Doubly Magic Nucleus. *Phys. Rev. Lett.*, 102(15):152501, Apr 2009.